Kamal D, 2017, Textural characteristics and chemical composition of chlorite from the Guichon Creek batholith, south-central British Columbia, BSc Thesis, UBC, BC, 62 p.

NSERC-CMIC Mineral Exploration Footprints Project Contribution 150.

Textural Characteristics and Chemical Composition of Chlorite from the Guichon Creek Batholith, South-Central British Columbia

by

Darius Kamal

A THESIS SUBMITTED IN PARTIAL FULFILLMENT OF THE REQUIREMENTS FOR THE DEGREE OF BACHELOR OF SCIENCE (HONOURS)

in

THE FACULTY OF SCIENCE

(Geological Sciences)

This thesis conforms to the required standard

……

Robert G. Lee

THE UNIVERSITY OF BRITISH COLUMBIA

(Vancouver)

April 2017

Abstract

The Upper Triassic Guichon Creek batholith (GCB) is located within the Canadian Cordillera as part of the Intermontane Belt. The batholith hosts the Highland Valley Copper (HVC) calc-alkaline porphyry district, which comprises five known mineralized centers: Bethlehem, Highmont, Lornex, and Valley. Chlorite forms as an alteration byproduct of the primary minerals in the granitic intrusions of the GCB both within and up to 25 km from the deposit. At Highland Valley, chlorite occurs either as part of the main and proximal sodic-calcic alteration assemblage (albite-chlorite-epidote ± actinolite ± diopside ± garnet) or with the generally more distal white mica-chlorite-prehnite assemblage. Petrographic observations and geochemical composition data of chlorite collected from the medial to distal areas of the GCB were conducted to evaluate the textural and chemical variations as a function of distance to mineralized centers within the different styles of alteration. Birefringence varies from deep brown in those samples found distally from the HVC district to a zoned brown-lilac colour within the Valley deposit. The pleochroism of chlorite grades from pale-green to moderate-green as you approach the Valley assemblage. Chlorite appears as needle-like aggregates within biotite, a fibrous habit in actinolite, and as patches within hornblende. Regionally metamorphosed samples have a higher Mg and Mn content, while samples from the mineralization center have higher levels of tetrahedral and octahedral aluminum and a Mg/Fe ratio near to one. Characterizing the textural characteristics, chemical content, and optical properties of chlorite provides a means to vector towards mineralization in large-scale porphyry deposits.

Table of Contents

List of Figures

List of Tables

List of Appendices

Acknowledgements

The completion of this thesis is part of the NSERC-CMIC Footprints Project and represents almost a year of work in collaboration with Mineral Deposit Research Unit and Teck Resources Limited (Teck). I would like to thank members of the CMIC Footprints Projects and NSERC for funding this project and providing valuable edits to my poster presentation at Round Up. Teck is thanked for their ongoing support and access to data.

Special thanks go to my supervisor, Robert Lee, for always being there to teach and guide me in my research and his tireless efforts to answer the multitude of questions and concerns I came up with. Guillaume Lesage and Kevin Byrne are thanked for their valuable role as mentors and providing thin sections for this study. Their advice and critique was invaluable. I would like to thank Greg Dipple for numerous conversations on the mechanics of chlorite, leading me in the right direction for a literature review, and helping with the normalization of microprobe data. Edith Czech is thanked for teaching and helping me with using the Electron Microprobe. Lucas Marshall of Teck is thanked for valuable critique and edits.

Above all, I would like to thank my friends and family for staying by my side through this project. Their encouragement, understanding, love, and support made this project possible and kept me driven when it mattered. They pushed me to work my hardest, but also kept me grounded and reminded me to enjoy my last year as a student at UBC.

Chapter 1 – Introduction, Geologic History and Setting, and Regional Metallogeny

1.1 Introduction

The Natural Sciences and Engineering Research Council of Canada (NSERC) and the Canadian Mining Innovative Council (CMIC) Footprints initiative is a multi-collaborative effort to identify lithogeochemical, mineralogical, petrophysical, and geophysical signatures related to an economic ore deposit from the core of the system to the distal edge to beyond current known or observed limits of an ore body. The project was implemented to develop more effective methods in mineral exploration through improved vectoring models of economic mineral deposits as well as providing new innovative techniques and integration within the Canadian mining industry and academia. One of the ore deposits in the study includes the Highland Valley Copper Deposit (HVC) located in south-central British Columbia which is fully owned and operated by Teck Resources Limited (Teck, 2017). The system is one of the largest porphyry copper deposits in Canada (McMillan, 1985; Byrne et al., 2013) and is hosted in the Guichon Creek batholith (GCB) providing a large-scale region in which to study features associated with porphyry Cu (±Mo) mineralization.

The HVC calc-alkaline porphyry district is located 54 km southeast of Kamloops in south-central British Columbia and comprises five known mineralized targets: Bethlehem, Highmont, J.A., Lornex, and Valley (McMillan, 1976; Casselman et al., 1995, Byrne et al., 2013). The deposits are emplaced within the Upper Triassic GCB which has a surface area of approximately 1000 km^2 (McMillan, 1976). On a larger tectonic scale, the porphyry Cu-Mo systems is located within the Intermontane Belt of the Canadian Cordillera (Byrne et al., 2013; Fig. 1) which comprises the Stikine Terrane, Quesnellia Terrane, and Cache Creek Terrane (Mihalynuk, et al., 1994). These terranes are believed to have been amalgamated by the late

Triassic (Mihalynuk, et al., 1994). Rocks in the HVC region show extensive epigenetic alteration, including abundant chloritization of primary and hydrothermal minerals.

The Highland Valley district has a long history of Cu and Mo production dating back to 1962. Total recorded production from 1962 to 2013 is 1615.16 million tonnes grading 0.40% Cu and 0.010% Mo (Byrne et al., 2013). As of December 31st, 2016, proven and probable mineral reserves, exclusive of resources at Highland Valley Copper were 546,600,000 tonnes at 0.29% Cu and 0.008% Mo, measured mineral resources are 517,400,000 tonnes at 0.31% Cu and 0.008% Mo, indicated mineral resources are 953,700,000 tonnes at 0.23% Cu and 0.010% Mo, and inferred mineral resources are 501,200,000 tonnes at 0.24% Cu and 0.008% Mo (Teck 2016 AIF, March 2017).

In silicate-rich rocks chlorite, commonly forms as an alteration byproduct of primary minerals through hydrothermal fluid flow as a hypogene alteration mineral, or as a retrograde product of other minerals that may include large-tonnage mineral deposition (Berger et al., 2008). However, chlorite can also form during regional metamorphism, such as that associated with the amalgamation of the Intermontane Belt (Bailey, 1988; Berger et al., 2008). Chlorite characteristics, such as colour, chemical composition, and structural composition can vary due to cation substitution, which is directly affected by pressure, temperature and bulk rock composition (Deer et al., 2009).

This study aims to present an improved understanding of the texture and composition of chlorite through petrographic observations and geochemical analysis of chlorite from the medial to distal areas of the GCB relative to the HVC deposits. The analysis will focus on how the chemistry and texture of chlorite varies through different alteration facies with distance from the center of the Valley deposit. These observations can then be used to interpret whether

the primary driving mechanism behind chlorite alteration was through hypogene hydrothermal processes or through regional metamorphism and whether this is consistent throughout the study area. This could be used as another tool in exploration geology and provide a more detailed geological understanding of the studied area. The gradational change in textural and chemical variations can potentially be used to vector back to the source of the alteration fluids.

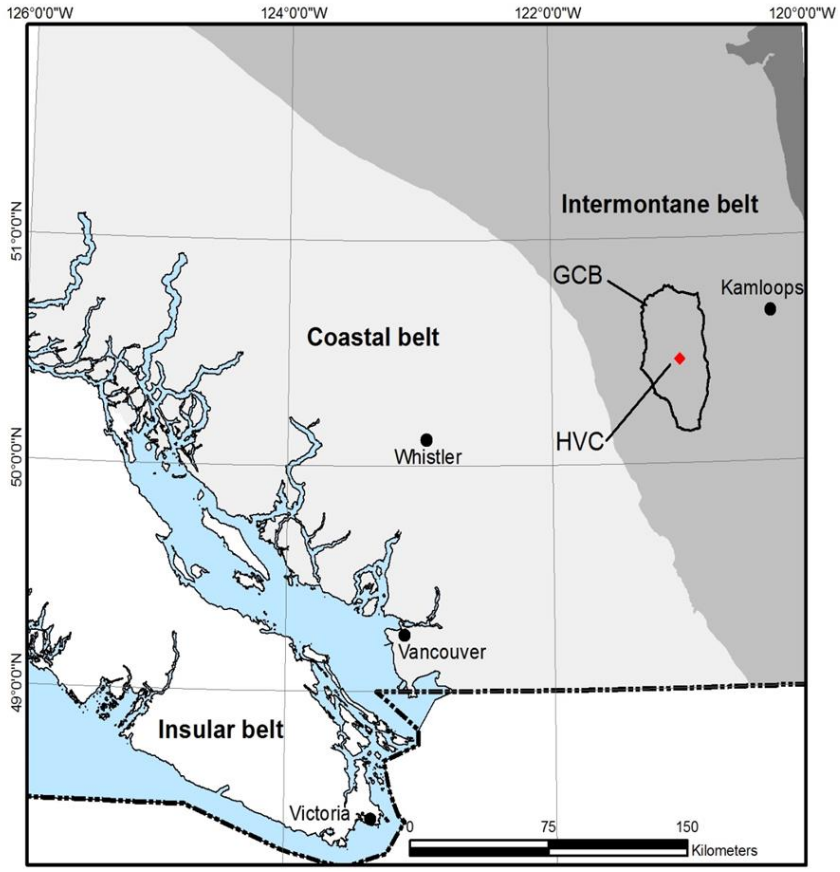

Figure 1: Location of the Intermontane Belt with its proximity to the Coastal and Insular Belt. Highland Valley Copper is shown in red within the outlined Guichon Creek batholith (modified after Lee et al., 2015)

1.2 Geologic History and Setting

Regional Setting

The GCB lies within the southern portion of the Intermontane Belt that extends from southwestern Yukon Territory into British Columbia (McMillan, 1976). The Intermontane Belt is comprised of several different tectonic terranes that were amalgamated by the late Triassic period, these terranes are: Stikinia, Quesnellia, Cache Creek, and the Yukon-Tanana terrane (Mihalynuk et al., 1994). The Stikinia and Quesnellia terranes are identified as an offshore island-arc terrane. The HVC district is contained within the southern portion of Quesnellia, bounded to the west by Stikinia, and bounded to the east by the Kootenay-Yukon-Tanana terranes (Fig. 2).

The Quesnellia arc contains clastic rocks that are shown to be part of the Kootenay Terrane, which indicates that the terrane was ancestrally part of North America (Wernicke and Klepacki, 1988). Nelson and Mihalynuk (1993) provide possible linkages between the Quesnellia and Yukon-Tanana Terrane. These include, but are not limited to: pericratonic assemblages within Slide Mountain being part of the basement that makes up Quesnellia; Quesnellian Jurassic plutons intruding the Yukon-Tanana Terrane; and upper Paleozoic quartzite clasts in northern Quesnellia. Throughout its history there has been evidence for extensive volcanism, both alkalic and calc-alkalic, throughout much of the Triassic and Jurassic (Nelson and Mihalynuk, 1993). Locally, Quesnellia consists of the Early Triassic to Early Jurassic Nicola group that are unconformably overlain by the Early to Middle Jurassic Ashcroft Formation (Frebold and Tipper, 1969).

District Geology

The GCB is one of many plutons associated with the late Upper Triassic volcanic rocks extending along the Intermontane Belt in a northwest-trending zone (McMillan, 1976). The volcanic rocks and associated plutons are thought to be products of island-arc volcanism derived from partial melting and subduction of oceanic crust (Monger et al., 1973; Monger and Price, 1979). Within the GCB region, Cache Creek and Nicola groups are either in fault contact or have ambiguous with each other (McMillan, 1976). Furthermore, there is evidence of Cache Creek rocks being deformed and metamorphosed prior to Triassic time by the presence of

metamorphosed blue schists within the oceanic terrane (Nelson and Mihalynuk, 1993). The batholith is a Late Triassic calc-alkaline, I-type intrusion that hosts the Cu-Mo deposit (McMillan, 1985; Casselman et al., 1995). The batholith intruded andesitic rocks of the Nicola Group in the late Triassic and crystallization ages from Uranium-lead zircon dating yield dates of emplacement from 213 to 207 Ma (D'Angelo et al., 2017)

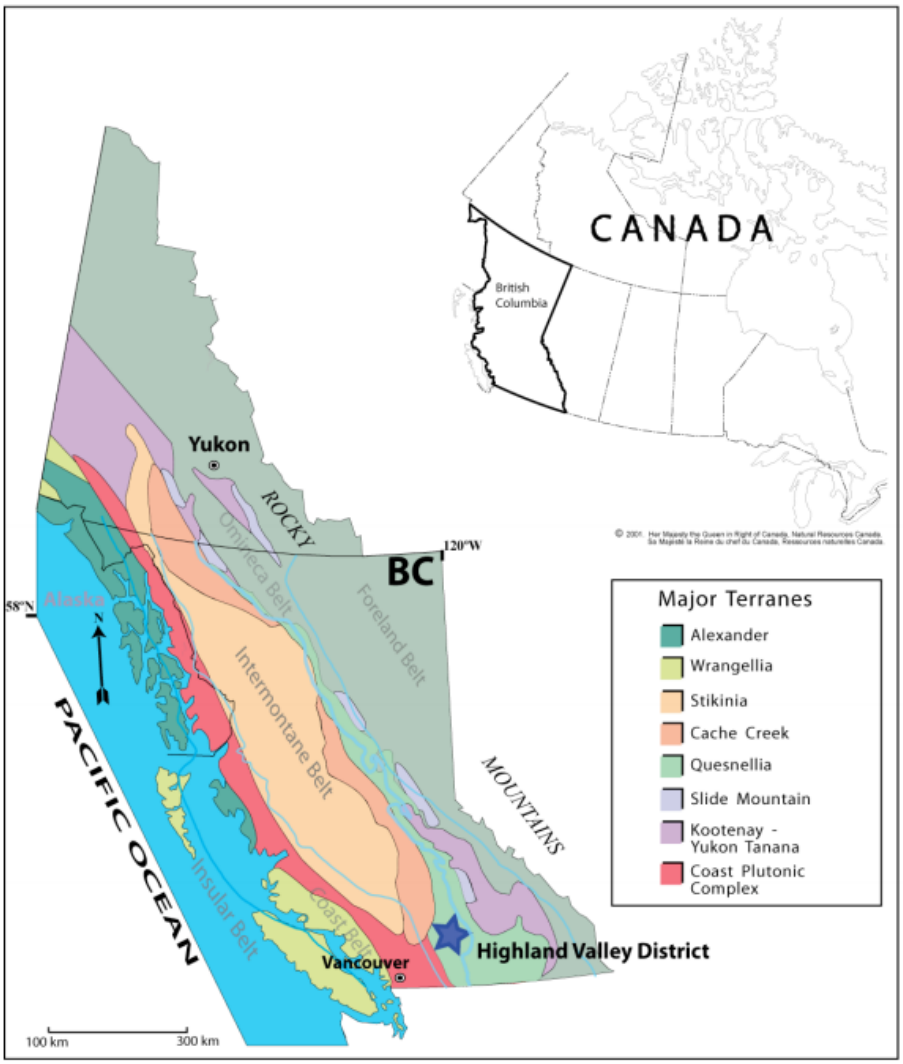

Figure 2. Regional locations of the different terranes found within British Columbia with HVC marked within Quesnellia. After Monger and Price, 1979

Since its formation, the GCB has been subject to Cretaceous shortening and Tertiary extensional deformation (Byrne et al., 2013). It is semi-concordant and approximately 65 km

by 30km wide (Byrne et al., 2013). Geologically, the facies young inwards with the older, more mafic composition residing on the outer margin, compared to younger, more felsic composition at the center (McMillan, 1985; Figure 3).

The geology of the concentrically zoned GCB has been described in detail over the last fifty years by mine-site and research geologists (Northcote, 1969; McMillan, 1976; Byrne et al., 2013). The oldest rocks along the margin of the batholith include the Border phase, which contains country-rock xenoliths, the Highland Valley facies which includes the Guichon and Chataway sub-facies. Next, the Bethlehem phase intruded and includes the Skeena variety. Finally, the last intrusive phase into the batholith is the Bethsaida phase which forms as a stock and post-dates Skeena, and later forms small dikes and plugs within the Bethlehem phase. There are two separate dykes, one associated with the Bethlehem phase and the other unit with the Bethsaida phase (McMillan, 1976).

Intrusive facies	Sub-facies	Primary mineral abundances							Al/Ti$_{molar}$ ratio range	Identifying Characteristics
		plag	ksp	qtz	bio	hbl	pyx	opa		
Border		52.2	3.7	19.6	7.8	11.3	2.7	2.5	20-40	Melanocratic, medium-grained diorite and quartz diorite (tonalite). Mafic-enriched, amphibole, biotite, and local pyroxene as cores in amphiboles, commonly displays strong seriate texture. ~20% hornblende and biotite.
Highland Valley	Guichon granodiorite	48.7	12.8	18.9	7.2	9.8	0.6	1.5	30-50	Quartz diorite to granodiorite, medium-grained, equigranular to seriate texture. Hornblende predominates and the facies is distinguished by conspicuous primary K-feldspar. 15% hornblende and biotite. (Fig. 5A)
	Chataway granodiorite	54.3	10.9	20.6	5.2	6.7	-	-	-	Granodiorite, hypidiomorphic granular and seriate texture. Abundances of biotite and hornblende are roughly equal. Anhedral quartz grains, and unevenly distributed clusters of hornblende and biotite (12%).
Bethlehem	Bethlehem granodiorite	59.0	9.9	20.8	3.2	4.3	-	2.3	60-85	Medium-grained inequigranular but grades into plagioclase and quartz – phyric phanerocrystalline facies. Distinguished by 1 cm poikilitic hornblende and locally coarse poikilitic potassic feldspar, in groundmass of evenly distributed fine- to medium-grained mafic minerals. Quartz is ameboid. 8% hornblende and biotite. (Figs. 5B and C)
	Skeena granodiorite	50	10	20	7.5	7.5	n/a	0.5	80-110	Contact zone of Bethlehem granodiorite and Bethsaida granodiorite, similar in texture to Bethlehem but grain size is larger, mafic content is lower, and quartz is coarse-grained and subhedral to anhedral. Biotite is subhedral to euhedral and hornblende is irregular, anhedral, and commonly poikilitic. ~6% hornblende and biotite. (Fig. 5E)
Bethsaida	Bethsaida granodiorite to quartz monzonite	52.1	10.6	29.4	6.3	0.4	-	1	110-150	Varies from granodiorite to quartz monzonite. Medium- to coarse-grained with coarse phenocrysts of quartz and biotite, average 0.5-1.0 cm. Distinct, euhedral biotite books (~1 cm). 1% accessory minerals of hornblende, magnetite, hematite, sphene, apatite and zircon. 6% biotite. (Fig. 8A)
	Salt and Pepper granodiorite	60	trc	20	7.5	-	-	9	-	Slightly porphyritic and medium-grained, plagioclase displays oscillatory zoning, quartz anhedral interstitial grain aggregates, orthoclase is interstitial and perthitic. Distinct, approximately 3-15% (but average >12%) disseminated 1mm biotite and magnetite crystals. (Fig. 8B)
	Feldspar-phyric inequigranular granodiorite	63	12	22	2	-	-	0.5	-	Medium- to coarse-grained plagioclase and quartz phenocrysts, mafic (biotite) phenocrysts average <0.3 cm and <2%. Trace magnetite and hematite. Similar to "salt and pepper" facies, but with distinct feldspar phenocrysts (0.5 cm) and sparse biotite. (Fig. 8D)
	Biotite and magnetite-rich cumulate	15	5	20	45	-	-	15	-	Mafic-cumulate facies with 25-60% euhedral, coarse-grained biotite (0.5 cm average). Locally 5-30% fine-grained disseminated magnetite clusters and veins. Commonly associated with stronger K-feldspar alteration. (Fig. 8C)

TABLE 1: Intrusive facies of the Guichon Creek batholith in chronological order. From Byrne et al., (2013) and McMillan (1985). Abbreviations: bio = biotite; hbl = hornblende; ksp = K- feldspar; opa = opaque minerals; plag = plagioclase; qtz = quartz; pyx = pyroxene.

Following the formation of the GCB, there was a period of erosion and deposition of Jurassic sedimentary rocks, represented by the Ashcroft Formation (Frebold and Tipper, 1969), followed by Cretaceous volcanic and sedimentary rocks of the Spences Bridge Group and Kingsvale group, and finally Tertiary volcanic and sedimentary rocks of the Kamloops group (McMillan, 1985; Alva Jimenez, 2011).

Two mineralization events are evident in the GCB and both occur as vein fill, disseminations in vein and fracture halos, breccia infill and disseminations, and as fault hosted mineralization (Byrne et al., 2013). The oldest mineralizing event coincides with dike intrusion and breccia formation after the emplacement of the Bethlehem phase and composes the orebodies: South Seas, Krain, and Bethlehem (Casselman et al., 1995; Byrne et al., 2013). The second, most important, mineralization event occurred after the Bethsaida phase and includes four major mineralization centers: Valley, Lornex, Highmont, and J.A (McMillan, 1976; Casselman et al., 1995).

The GCB is cut by the north-trending Lornex fault, the northwest trending Highland Valley fault, the Barnes Creek fault, and the Skuhun Creek fault (Byrne et al., 2013; Fig. 3). The Lornex fault truncates the Lornex and Valley porphyry systems and is inferred to have segmented a single porphyry centre (McMillan, 1985; Byrne et al., 2013). The Lornex fault has a strike-slip movement and, while there is a post-mineral component, it is undetermined if there was a pre or syn-mineral component to slip in addition. McMillan (1985) speculates that Valley formed at deeper conditions and higher temperature than Lornex.

Across the northern part of the district, a west-northwest trending basin is filled with Tertiary fluvial and lacustrine, and Quaternary lacustrine, glaciofluvial, and till deposits (Bobrowsky et al., 1993; Byrne et al., 2013).

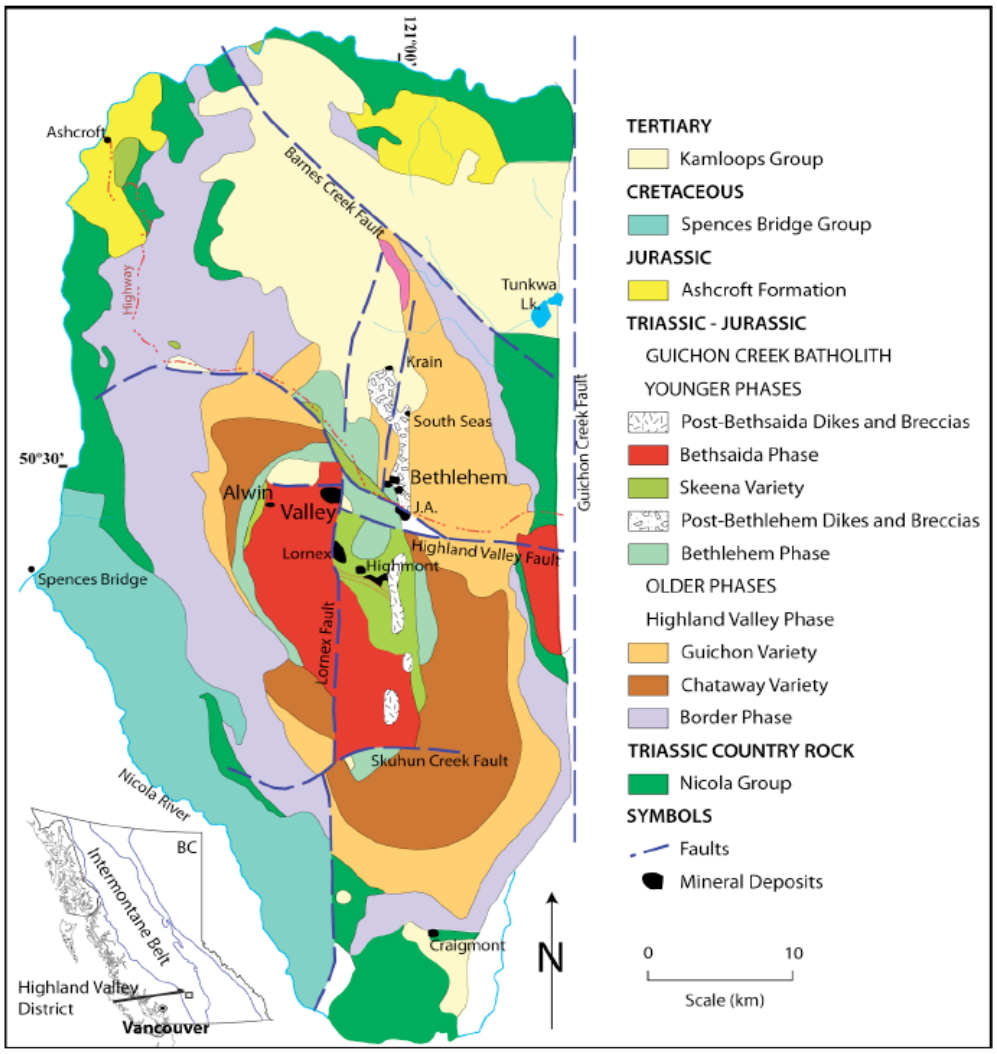

Figure 3. Geology of the Guichon Creek batholith with the various phases separated by age. Faults and Mineral deposits are highlighted and the GCB's location within the Intermontane belt is shown. From Alva Jimenez, 2011; from McMillan et al., 2009.

1.3 Exploration History

Mineral exploration of the Highland Valley district began in 1896 at the, then named, OK deposit (later renamed Alwin) (Casselman et al., 1995; Byrne et al., 2013). Production was steady from the early 1900s until the 1920s as mining was focused on high grade veins in OK, Snowstorm, Iona, Bethsaida, and Aberdeen targets (McMillan, 1985; Casselman et al., 1995). From 1920 to 1953 main-ore production ceased, with only brief periods of staking, trenching, and drilling. In 1955, exploration efforts increased as the focus was shifted away from high

grade veins, towards low grade, high tonnage mineralization, which is characteristic of the system today (McMillan, 1985; McMillan et al., 2009). Lornex was discovered in 1964 and production began in 1972. Valley was discovered in 1967 and entered production in that same year. J.A. was discovered in 1971 and remains an exploration target. (McMillan, 1976; McMillan, 1985; Alva Jimenez, 2011).

Low grade-high tonnage production was conducted by the Bethlehem Copper Corporation in 1962 with production beginning in the Bethlehem pit (Briskey, 1981). Production continued until 1980 when the Bethlehem pit was shut due to low copper prices (Alva Jimenez, 2011). Highmont was briefly active from 1980 to 1984 when production ceased; however, the east pit has since reopened in 2005 (Alva Jimenez, 2011). Current mining is focused in the Valley, Lornex, and Highmont pits, whereas the J.A. target remains undeveloped (Byrne et al., 2013).

Chapter 2 – Chlorite Structure and Chemistry, and Methodology

2.1 Chlorite Occurrence and Structure

The chlorite group of minerals comprises a series of phyllosilicates that derive their name from the characteristic green colour that most varieties exhibit (Bailey et al., 1988; Deer et al., 2009). The mineral colour varies widely depending on its composition and has been known to show shades of green primary colours, and black, brown, orange, red, pink, purple, blue, yellow, grey, and white secondary colours (Bailey, 1988). They are often found in large crystalline blocks as flexible basal laminae, but also occur as fine-grained scaly or massive aggregates (Deer et al., 1966)

Chlorite commonly occurs in low-grade metamorphic zones and may be the most abundant mineral in rocks found in the metamorphic zone represented by chlorite (Hey, 1954; Deer et al., 2009). It also forms in igneous rocks, usually forming secondarily by hydrothermal processes and is commonly found in hydrothermal alteration zones surrounding ore bodies (Bailey et al., 1988; Sillitoe, 2010).

Chlorite usually forms as fine-grained scaly or massive aggregates and shows perfect cleavage (Deer et al., 2009). The structure of chlorite consists of a negatively charged tetrahedral-octahedral-tetrahedral (T-O-T) that mimic talc-like layers with a positively charged brucite-like interlayer (Fig. 4; Deer et al., 2009; Alva Jimenez, 2011).

Bailey (1988) shows that chlorite's true crystal morphology is triclinic, yet it approximates rhombohedral or hexagonal geometry and its cleavage is parallel to (001). It is often a dull luster, but can occasionally be vitreous and pearly. It has a hardness of 2.5.

In thin section, chlorite exhibits weak pleochroism from colourless to pale green (although it is stronger in Fe-rich samples). Its birefringence varies depending on the major and trace elements within its chemical composition (Bailey, 1988; Deer et al., 2009; Alva Jimenez, 2011)

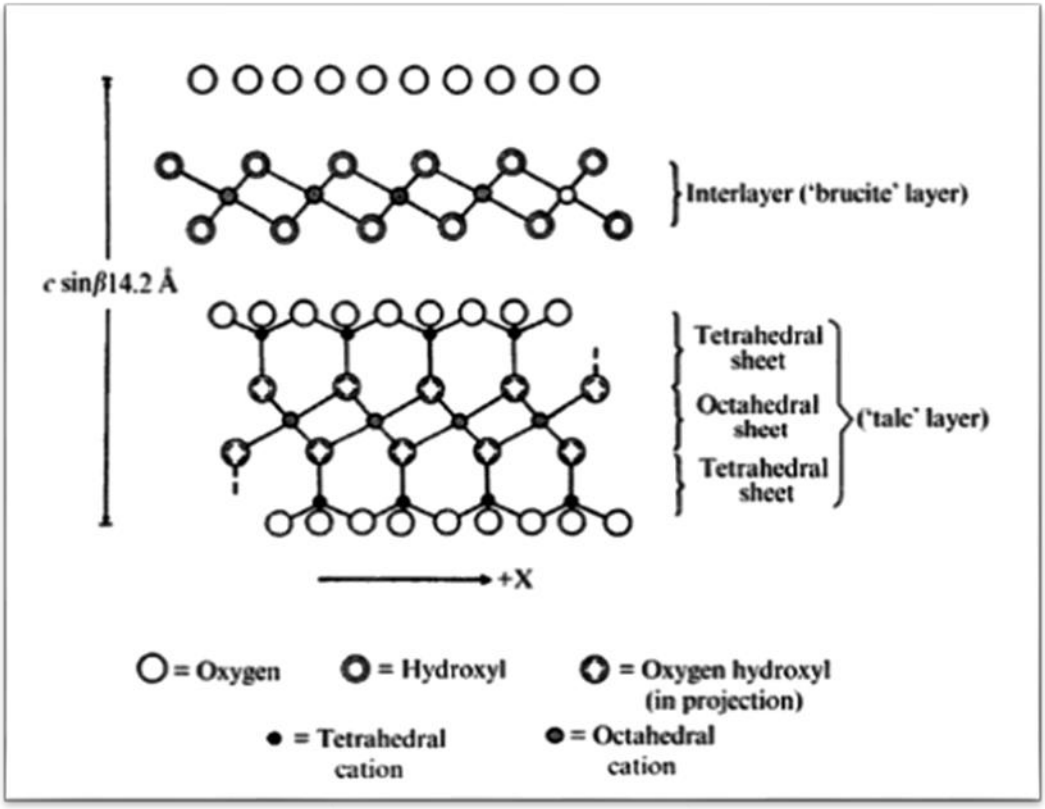

Figure 4. Chlorite structure illustrating T-O-T layers with alternating brucite, from Bailey, 1988.

2.2 Chlorite Chemistry

Chlorite is a hydrous silicate that allows for cation substitution which is affected by temperature, pressure, and bulk-rock composition at the time of formation (Alva Jimenez, 2011). The most common medium-sized octahedral cations are Mg, Al and Fe; however, Cr, Mn, Ni, V, Cu, Zn, and Li can also be present (Bailey, 1988). There is a solid solution between two end members of the chlorite group with the Mg-rich clinochlore on one end, and the Fe (ferroan)-rich chamosite on the other. Most chlorites belong to this solid solution series and are considered tri-octahedral (Bailey, 1988).

Trioctahedral chlorites have all three octahedral sites occupied, whereas the less common dioctahedral chlorite has only two of the three octahedral sites occupied, while one remains vacant (Deer et al., 2009). Di-trioctahedral chlorite is dioctahedral in the T-O-T layer, and trioctahedral in the brucite-like interlayer (Bailey, 1988; Alva Jimenez, 2011).

Bailey (1988) gives a generalized composition of trioctahedral chlorite which is as follows:

$(R^{2+}, R^{3+})_3(Si_{4-x}Al_x)O_{10}(OH)_2$ for the tetrahedral sheet that alternates with an octahedral sheet of ideal composition: $(R^{2+}, R^{3+})_3(OH)_6$.

For dioctahedral chlorite, generally Al substitutes for Si and Bailey (1988) gives a generalized formula of $Al_{4+x/3}(Si_{4-x}Al_x)O_{10}(OH)_8$

Finally, an example composition for di-trioctahedral chlorite is as follows for an Li rich chlorite: $(LiAl_4)(Si_3Al)O_{10}(OH)_8$ (Bailey, 1988).

Due to a high degree of substitution and various mechanisms of formation, it is hard to constrain a general formula for chlorite. Caritat et al., (1993) gives a generalized formula as follows: $(R_u^{2+}R_y^{3+}\square_z)^{VI}(Si_{4-x}Al_x)^{IV}O_{10+w}(OH)_{8-w}$; where $u+y+z = 6$, $z= (y-w-x)/2$, w is 0 or a small number, R^{2+} generally represents Mg^{2+} or Fe^{2+}, R^{3+} generally represents Al^{3+} or Fe^{3+}, and $\square$ is a structural vacancy. Octahedral sites are shown by the superscript VI and tetrahedral sites are shown by the superscript IV.

The compositional variations of chlorite are primarily affected by the Fe/Mg ratio, the Tschermak exchange, and the dioctahedral substitution between Al^{3+} and Mg^{2+} (Alva Jimenez, 2011). The Tschermak exchange refers to the most common type of substitution in chlorite where:

$$Mg^{2+(VI)}+Si^{4+(IV)} \leftrightarrow Al^{3+(VI)}Al^{3+(VI)}$$ (Caritat et al., 1993; Bailey, 1988)

This exchange is responsible for most of the substitution experienced by chlorite in solid solution between clinochore and chamosite. The extent of the Tschermak exchange can be determined using electron microprobe work, which can also give insight into the Mg/Fe ratio, and the di-tri exchange reactions (Caritat et al., 1993).

2.3 Methodology

Samples were collected by CMIC researchers in the 2013, 2014, and 2015 field seasons from the distal to medial areas of the batholith pertaining to the various projects undertaken around the region. A week of training and instruction in the area was provided by Teck and CMIC and included looking at the geology of the open pits, geological outcrops surrounding

the pits, drill core, and roadcuts and till samples distal to the mine site but still part of the batholith.

Samples of interest were chosen from a detailed database created by CMIC researchers categorizing all samples collected during the 2013, 2014, 2015, and 2016 field seasons respectively (Fig. 5).

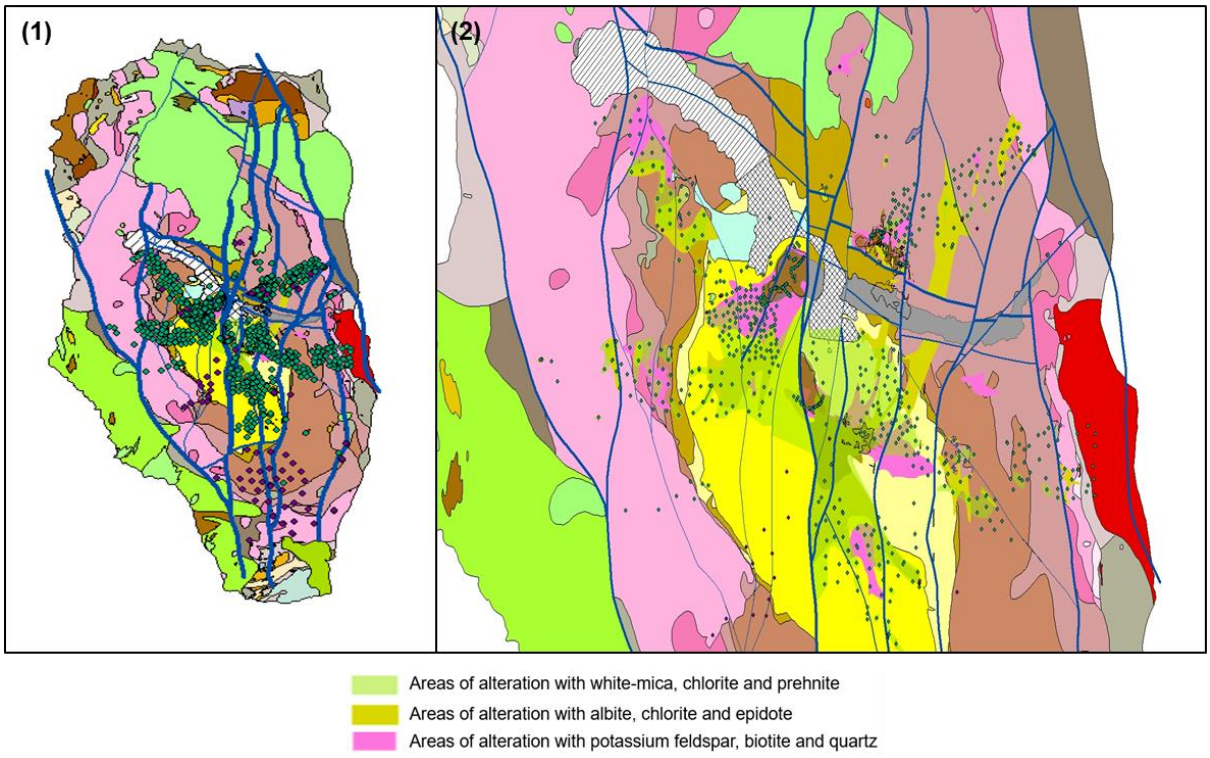

Figure 5. ARC GIS image of the GCB shown at different scales. (1) The GCB at a scale of 1:500,000. Faults are outlined in blue. 2014 and 2015 samples are shown with green circles, and 2016 samples are shown in purple diamonds. (2) The GCB shown at a scale of 1:100,000, showing a more detailed scope of the project site. (Modified after Lesage et al., 2017)

For this project, samples were chosen from different areas of the GCB associated with different mineral assemblages that contain chlorite (Byrne et al., 2013; D'Angelo, 2017; Lesage et al., 2017; Fig. 6). The first area of interest was chosen to be outside of the alteration facies, due to the chlorite occurrence assumed to be from regional metamorphism. These were considered as the 'distal' samples of the GCB as they were furthest away from the

mineralization centers. Samples were also chosen from within the sodic-calcic and propylitic mineral assemblage facies as they extend from just outside the mineralization centers and the chlorite alteration is the result of hydrothermal fluids. Finally, samples were chosen from within the Valley pit, as it is directly above and within the mineralization center, where the hydrothermal fluids entered the system. In total, 24 samples were selected for this project.

Petrography

A total of 24 thin sections were chosen to be assessed at the Mineral Deposit Research Unit (MDRU). They were provided by CMIC researchers. Additional thin sections were assessed but did not have a significant presence of chlorite. Analysis was conducted on two microscopes, a Nikon H600L with an attached Canon EOS Rebel T2I to record digital photos at different scales and a Nikon H550L with an attached Nikon D5200 camera.

The samples were assessed and classified through detailed descriptions of their texture, host, intensity, and accessory minerals, as well as their various optical properties such as their pleochroism and birefringence. Most analysis was done using transmitted light microscopy utilizing plane-polarized light (PPL) and cross-polarized light (XPL). Reflected light microscopy was only used to confirm the presence of sulfide minerals. Chlorite samples were split into transects A through E with three select samples outside of the transects but grouped with A (Fig. 6). A complete overview of petrographic descriptions of the samples can be found in Appendix A.

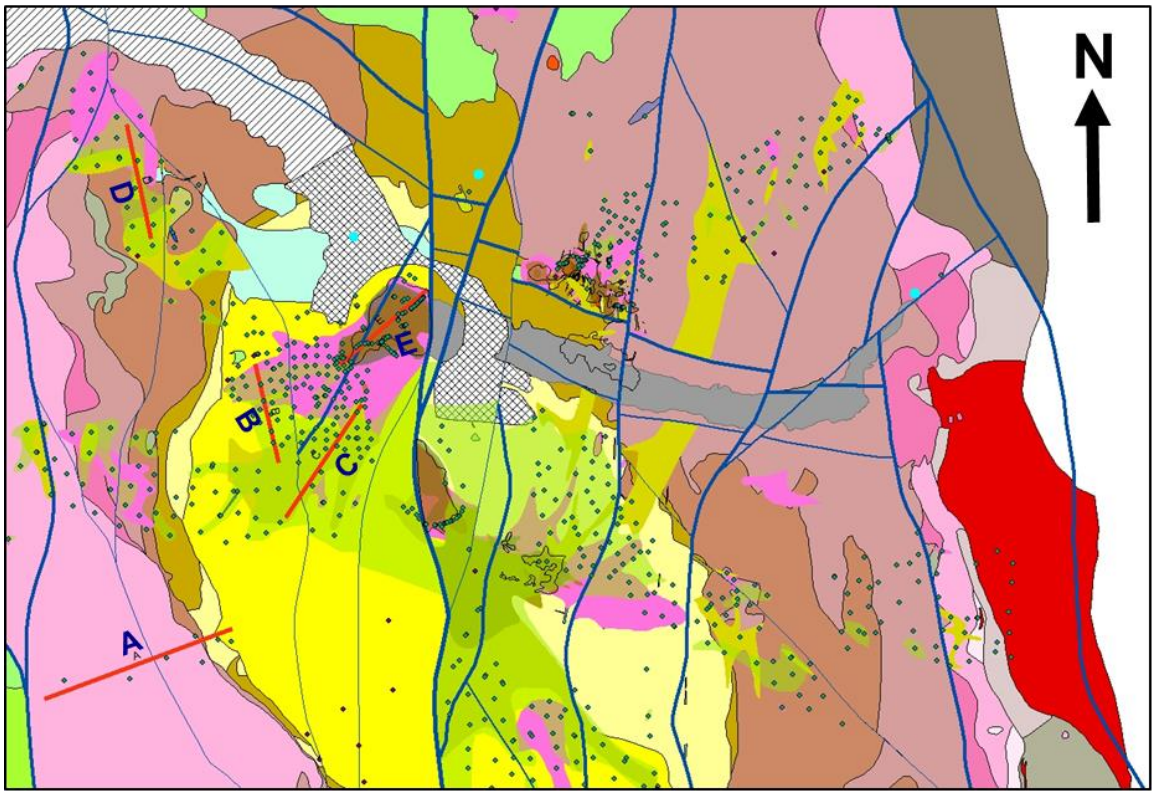

Figure 6. 1:80,000 scale image of the GCB taken from ARC GIS. Transects A through E are shown with red lines. Samples of interest were chosen on availability proximal to transect lines. Three more samples chosen are shown in light blue circles. Geology and alteration assemblages after Lesage et al., 2017.

Electron Microprobe Analysis

Eight thin sections were chosen to be analyzed by the electron microprobe (EMP) at the University of British Columbia. Carbon coating was done at the MDRU to prepare them for analysis. Two to three specific chlorite grains were outlined prior to the use of EMP and five points per grain were measured for a better representation and to consider error in the analysis. Scanning Electron Microscopy (SEM) at UBC was used to obtain backscatter images for reference but no actual analysis was done on the machine. Backscatter images can be found in Appendix B.

Electron-probe micro-analyses of chlorite were done on a fully automated CAMECA SX-50 instrument, operating in the wavelength-dispersion mode with the following operating conditions: excitation voltage, 15 kV; beam current, 10 nA; peak count time, 20 s; background

count-time, 10 s; spot diameter, 10 μm. Data reduction was done using the 'PAP' $\phi(\rho Z)$ method (Pouchou & Pichoir, 1985). For the elements considered, the following standards, X-ray lines and crystals were used: albite, Na$K\alpha$, TAP; synthetic phlogopite, Mg$K\alpha$, TAP; synthetic phlogopite, Si$K\alpha$, TAP; PET; synthetic phlogopite, K$K\alpha$, PET; kyanite, Al$K\alpha$, TAP; diopside, Ca$K\alpha$, PET; rutile, Ti$K\alpha$, PET; synthetic magnesiochromite, Cr$K\alpha$, LIF; synthetic rhodonite, Mn$K\alpha$, LIF; synthetic fayalite, Fe$K\alpha$, LIF. Data was reported as wt% oxide and exported into an excel spreadsheet. Analysis was done by normalizing to 14 anhydrous oxygens. The water content was not measured, and instead was calculated using mineral stoichiometry. All reported iron was assumed to be FeO and all occupancy of the water site was by OH, with no Cl or F substitution. Data filtering and calculation of the final chlorite formula was found using the following parameters listed in Table 2.

Chlorites:
Sum Oct. site = Al^{VI}+Ti+Fe+Mn+Mg+Cr+Ca+K+Na, Sum: 5.8-6.10 pfu A **K site = (Ca+K+Na) < 0.2 pfu B** **Oct. site = (Al+Ti+Fe+Mn+Mg+Cr)**
Sum cations: (Tet. site + Oct. site + K site) **Sum: 9.80-10.1 pfu C**
Sum Tet. Site (Si+Al^{IV}): 4 pfu
Sum anion site: OH = 8
Total summation Ox%: 98-102 wt% (oxide total + w%H2O) D

TABLE 2: Chlorite parameters for formula standardization. Octahedral (Oct.), tetrahedral (Tet.), oxide (Ox), ions per formula unit (pfu). The data was filtered according to four rules labelled in red A through D.

Chapter 3 – Petrography Results

Chlorite grain sizes are reported as very fine-grained (<0.25mm), fine-grained (0.25-1mm), medium-grained (1-2mm), or coarse-grained (2-5mm).

3.1 Transect A with Outliers

Transect A (Fig. 6) with additional outliers comprises five samples chosen for their location outside of the mapped alteration facies. As there is a lack of interaction with hydrothermal fluids due to their location outside the alteration facies, chlorite alteration can be assumed to be driven by regional metamorphism after the emplacement of the lithological facies. The samples are fresh based on petrographic evidence. The five samples are found within the Border, Skeena, and Bethsaida facies (Table 2).

Two of the samples (MD003A and MD004) are more distal to the mineralization center, being located more south-west in the GCB. MD057 is to the far east of the GCB, away from the mineralization centers. Finally, MD035 and MD060 are located to the north of Valley, outside of the alteration facies, but close to the copper deposits.

Thin Section ID	UTM Easting	UTM Northing	Transect	Facies
MD003A	633013	5586244	A	Border
MD004	634574	5586650	A	Bethsaida
MD035	637545.1	5596507	A	Skeena
MD057	651124	5595137	A	Border
MD060	640557	5598038	A	Skeena

TABLE 3: Transect A details showing thin section ID, location, transect, and lithological facies.

Optical properties of chlorite were generally uniform across the samples that were regionally metamorphosed. Despite being from different intrusive facies, the accessory minerals remained similar throughout. The thin sections were predominantly composed of plagioclase and quartz, with interstitial K-feldspar and biotite and actinolite (D'Angelo, 2016). Other minerals found with the chlorite grains were fine-grained epidote, trace amounts of

titanite, and very rarely zircon. Aside from chlorite, other alteration products included sericite and minor clay alteration. There was no significant presence of coarse muscovite.

As an alteration product, chlorite comprises a low modal abundance of the overall sample, from a few percent to ten percent. However, chloritization of the host mineral varies from trace to almost complete replacement, resulting in an almost complete pseudomorph (Fig.7).

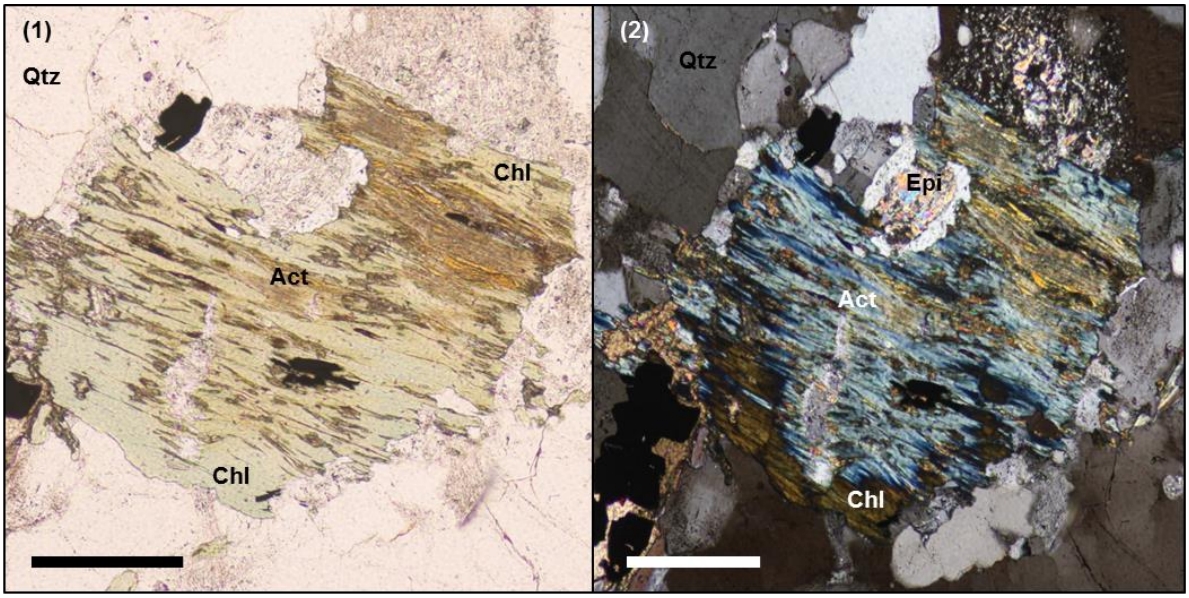

Figure 7. Chloritization of Actinolite. (1) shows sample in PPL and (2) in XPL. Chlorite (Chl), actinolite (Act), quartz (Qtz), epidote (Epi). Chlorite has replaced >50% of the original host crystal showing a pseudomorph. Chlorite is fine to medium-grained and fibrous, showing replacement from the cleavage planes and rims. Actinolite has first altered to biotite in places. Scale bar shows 0.5mm.

The pleochroism of the samples varied depending on the host mineral, but all were colorless to light green, with biotite alteration exhibiting slightly deeper pleochroism, and actinolite showing a lighter green in PPL. Pleochroism of chlorite samples can be used to estimate Fe and Mg ratios, with a deeper, more intense pleochroism signifying a more iron rich sample (Deer et al., 2009).

The host of the chlorite was found to differ from sample to sample based on location. In the Border phase lithology, chlorite was found to be an alteration product of both actinolite

and biotite; however, biotite itself was formed through the breakdown of hydrous actinolite (Fig 8).

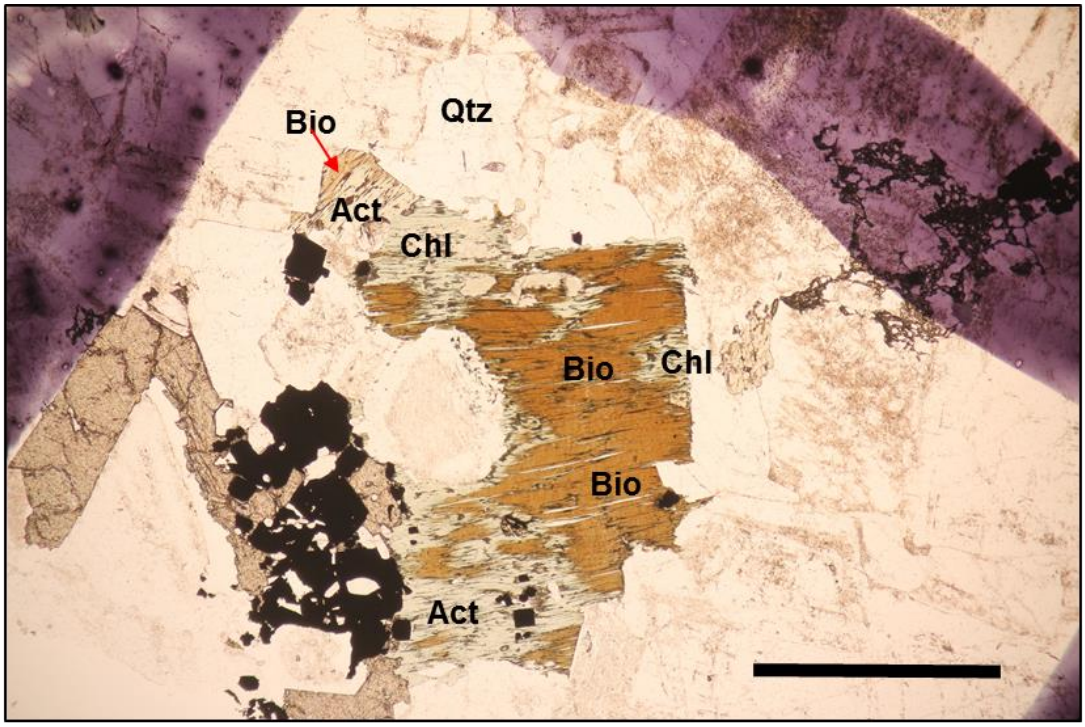

Figure 8. Anhedral actinolite almost completely replaced by retrograde biotite. Parts of the cleavage planes and rims of the biotite are being replaced by very fine-grained chlorite. Scale bar shows 1mm.

In the Bethlehem and Skeena facies, the host mineral is biotite and igneous hornblende. Although appearing in both minerals, chlorite appears to be more pervasive in biotite and has replaced more of the host mineral. When replacing biotite, chlorite forms along the cleavage planes and on the outer rims of the mineral, utilizing the anhedral, weak points within the mineral grain. In hornblende and actinolite, chlorite is seen to form only along the cleavage planes.

Texturally, chlorite forms needle-like aggregates in the cleavage planes of biotite and is generally fibrous and fine-to medium-grained depending on the degree of replacement. In actinolite, chlorite can appear as sinuous waves (Fig. 7), whereas in igneous hornblende it is patchier and block-like depending on the degree of chloritization. Crystals of secondary chlorite generally have high relief, but this can be influenced by the mineral it replaces.

In cross-polarized light (XPL), chlorite birefringence is distinctly brown first-second order birefringence in the Bethsaida facies. In the Skeena facies and Border phase, chlorite predominantly shows brown first-second order colours, but also shows a very minor amount of lilac birefringence often within the same crystal, showing a form of zoning (Fig. 9). This is less common in the Border phase.

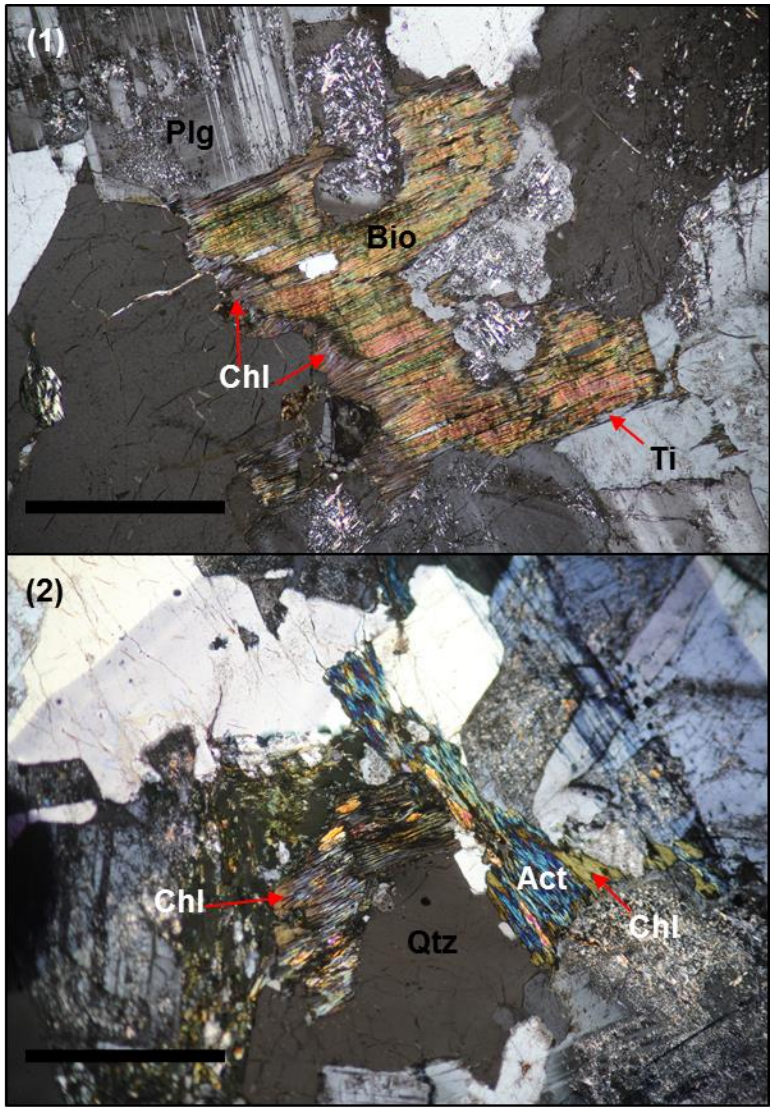

Figure 9. Ti (titanite), Plg (plagioclase). Variable birefringence in chlorite shown in XPL for (1) and (2). More common very fine-grained brown chlorite interspersed with rare anomalous blue (lilac) birefringence causing zoning. (1) shows a biotite altering to chlorite on the rims with small titanite. (2) shows actinolite altering to biotite which in turn has been chloritized. Scale bar shows 1mm.

3.2 Transect B

Transect B is made up of four samples shown within Table 4. The samples were chosen for their proximity to the mineralization center, and because of their location within the propylitic alteration facies (Fig. 6). Lithologically, they are found within the Bethsaida facies. Being part of the propylitic alteration assemblage, any alteration would be caused due to the interaction with hydrothermal fluids, rather than regional metamorphism.

Thin Section ID	UTM Easting	UTM Northing	Transect	Facies
BC14184G	635279.387	5592310.353	B	Bethsaida
BC14185G	635305.605	5592915.365	B	Bethsaida
BC14187A	635527.784	5593019.647	B	Bethsaida
BC14202H	635690.666	5592915.365	B	Bethsaida

TABLE 4: Transect D details showing ID, location, transect, and lithological facies.

McMillan (1976, 1985) defined the propylitic alteration facies at HVC as consisting of predominantly feldspars altering to sericite (fine-grained white mica), carbonate, and some clay minerals; whereas mafic minerals commonly alter to chlorite and carbonate with associated epidote. For this study, the mineral assemblage white mica ± chlorite ± prehnite as observed by Lesage et al., (2017) is included in the propylitic alteration.

Samples from transect B were predominantly made up of a K-feldspar and quartz dominated system, with intergrown plagioclase. There is a minor amount of opaques (primarily sulfide), and amphibole altering to biotite. There are inclusions of carbonate, shown by its very high birefringence, forming as part of the alteration assemblage. Much of the feldspar shows a high degree of sericite alteration showing replacement throughout the minerals. Muscovite (defined as a coarse-grained white mica) is present in needle-like aggregates, forming in the cleavage planes and identifiable due to its high birefringence and radiating texture. Chlorite forms as a replacement mineral and is often intergrown with muscovite crystals.

Characteristic of this alteration assemblage is the breakdown of actinolite to biotite, (Fig. 10). Therefore, chlorite appears to be hosted in actinolite grains, but also replaces the hydrothermal biotite that has formed due to the degradation of actinolite. Chlorite either infills the cleavage planes or along the rims of both actinolite and biotite expanding within the structural weak points of the phenocrysts (Fig. 11). In some places, chlorite has been overprinted by white mica.

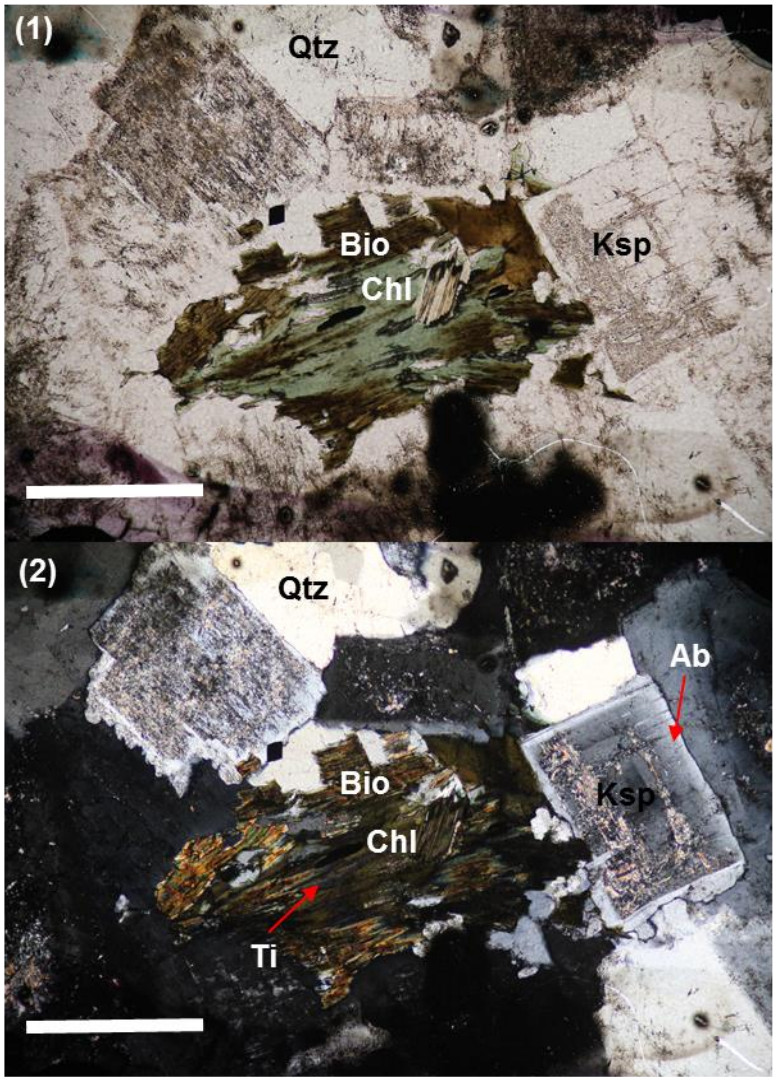

Figure 10. Ksp (K-feldspar), Ab (Albite). In this sample, we see the breakdown of actinolite to biotite on the rims of the crystal. (1) shows the sample in PPL where the green region indicates remnant actinolite overprinted by fine-grained chlorite. (2) shows the same image in XPL where we can see fine-grained chlorite (shown by brown birefringence) with small amounts of titanite. K-feldspar shows rims altering to albite. Scale bar shows 0.5mm.

Pleochroism from the four samples is uniform: colourless to pale green. The pleochroism is weak, but slightly deeper than the previous transect, indicating a slightly higher iron content (Deer et al., 2009). The minerals show moderate to high relief. Chlorite appears in various stages of intensity, from <10% of the host altered (Fig. 11), to >50%. In this transect, there is very strong brown birefringence and little to none of the lilac birefringence previously seen, with no evidence of zoning.

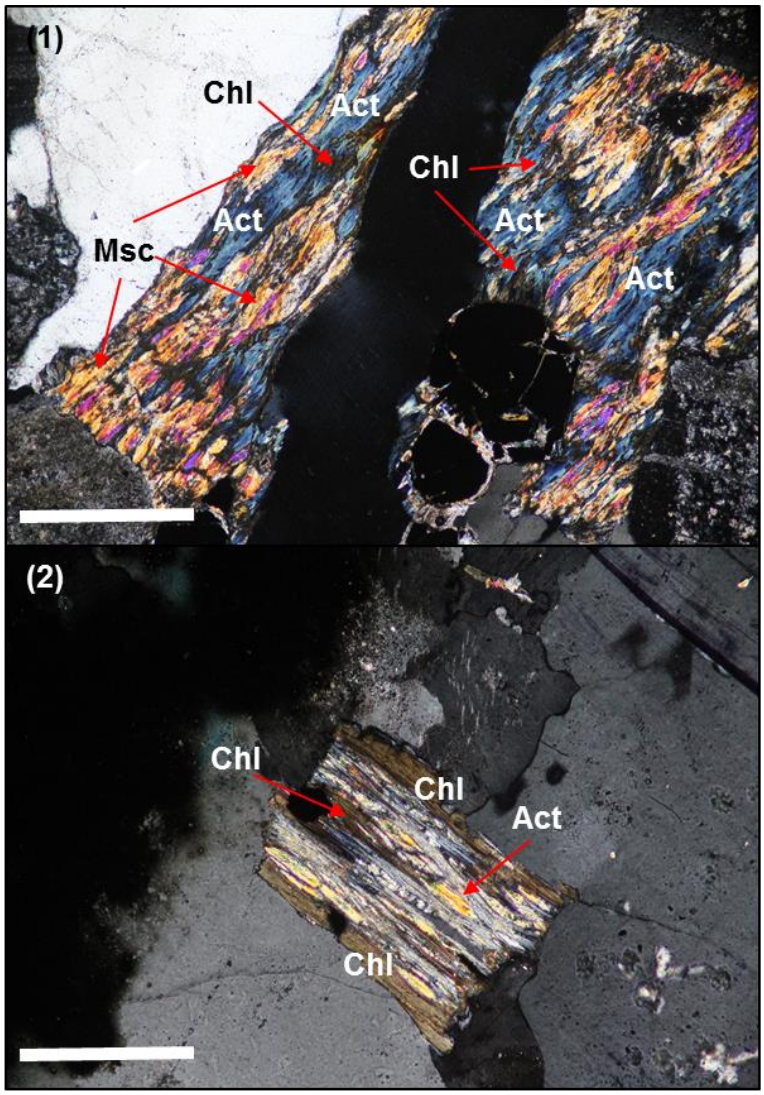

Figure 11. Msc (Muscovite). (1) actinolite is shown altering to chlorite. The blue birefringence is the host actinolite, while the brown chlorite is shown to infill cleavage planes of the amphibole. Muscovite is also indicated. (2) actinolite has first altered to biotite which has been chloritized significantly on the rim of the crystal. Chlorite also infills the cleavage planes. Scale bar indicates 0.5mm.

Characteristic of this assemblage is the lack of hornblende hosts when compared with transect A. In no sample was there any evidence of remnant igneous hornblende; every amphibole seen was actinolite being replaced by chlorite. Chlorite's habit differed depending on the host. In actinolite crystals, chlorite infilled the cleavage planes and were concentrated along them, identifiable due their birefringence. In biotite hosts, chlorite also appears in the cleavage planes, but is concentrated heavily along the rims of the biotite. However, it should be noted that biotite themselves first appear on the rims of the actinolite (Fig. 10). Chlorite grain size varies from very fine-grained in actinolite, to fine-grained in biotite, depending on the pervasiveness of the sample. In actinolite, it shows a felty texture in PPL.

3.3 Transect C

Transect C comprises two samples chosen for their location within the sodic-calcic alteration facies (Fig.6). They were both located inside the Bethsaida facies, as shown in Table 5. The two samples are found within the sodic-calcic alteration assemblage found within the GCB. Sodic-calcic assemblage typically denotes interaction with a non-magmatic fluid ~400°C (Jiminez, 2011). Dilles and Enaudi (1992) outline the typical mineral composition of the sodic-calcic assemblage as: albite, actinolite, and titanite as the primary minerals, followed by chlorite, epidote, diopside and calcite. Spatially, the samples are located south of the main ore body at Valley.

Thin Section ID	UTM Easting	UTM Northing	Transect	Facies
BC14213B	636570.248	5591263.248	C	Bethsaida
BC14124A	637058.544	5591933.769	C	Bethsaida

TABLE 5: Transect C details showing ID, location, transect, and lithological facies.

Petrographic studies of the two thin sections revealed uniform similarities between the two. Both consisted of predominantly equigranular quartz with plagioclase and K-feldspar with 5% opaques representing the sulfides in the thin section. Metamorphic minerals found within

the samples were chlorite, sericite replacement of feldspar grains, and muscovite found within small veinlets. The modal abundance of muscovite was very small compared to other samples, such as those found within the Valley Pit. It is very fine-grained and shows characteristic high birefringence.

Inclusions found within, or proximal to the chlorite were very fine-grained epidote, identifiable due to its extremely high birefringence, and intergrown titanite, showing first order grey colours.

Chlorite alteration varies in its intensity depending on the degree of replacement. Its host is predominantly subhedral to euhedral biotite, as opposed to actinolite found within other transects (Fig. 12).

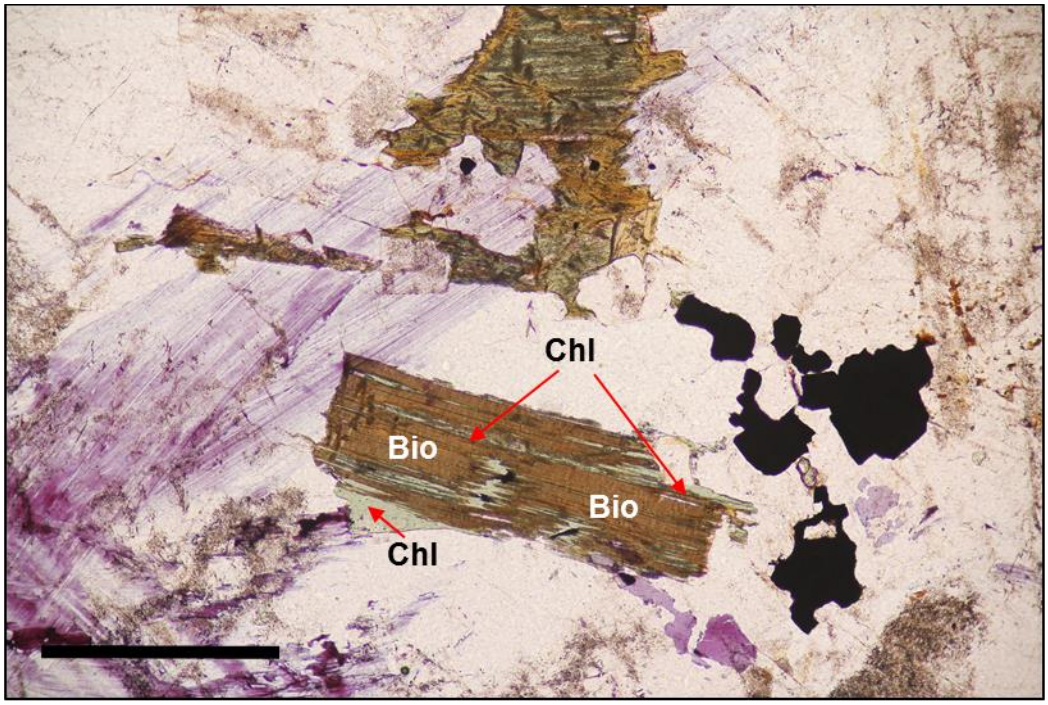

Figure 12. Euhedral biotite showing chlorite alteration throughout the cleavage planes and rims. Chlorite is very fine-grained and shows non-pervasive replacement. Shown in PPL. Scale bar shows 0.5mm.

As with other hosts, chlorite is found predominantly from within the cleavage planes of the biotite and around the rims, and replaces the weakest parts of the mineral. Intensity

varies between phenocrysts and various degrees of replacement are observed, from minor replacement around the rims, to an almost complete pseudomorph (Fig. 13)

Chlorite shows weak pleochroism, varying from colourless to pale green in PPL. Concerning birefringence, chlorite exhibits very strong brown birefringence, with little to none of the lilac birefringence that has previously been shown. Texturally, chlorite crystals are characteristic of their host, which in this case is the biotite crystal. Chlorite appears as very fine-grained (0.25mm) to fine-grained (0.25-1mm), with a minor amount of medium- grained chlorite (Fig. 13), and is subhedral. It appears as needle-like growths within the cleavage planes but does not display the sinuous pattern shown usually in actinolite hosts. It shows a felty texture when expanding pervasively from the actinolite crystal.

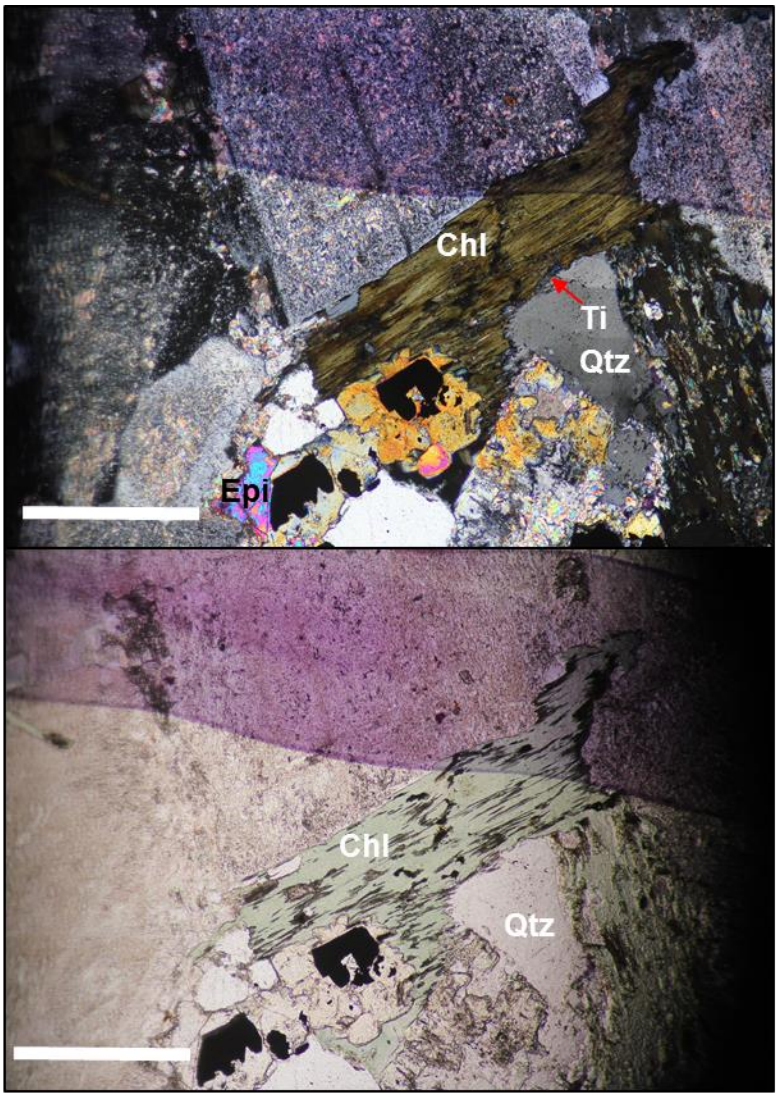

Figure 13. A nearly complete chlorite pseudomorph show in XPL with the same image in PPL. Chlorite shows very nearly complete replacement of an actinolite, having replaced >90% of the host. Inclusions include extremely fine-grained titanite and minor epidote. Sericite is seen on proximal phenocrysts. Scale bar indicates 0.5mm.

3.4 Transect D

Transect D comprises six samples distributed in the sodic-calcic/propylitic region of the GCB (Fig. 6). Details are shown in Table 6. They were chosen for their location due to the influence of hydrothermal fluids, such as in Transects B and C, but also because they are further away from the mineralization center in the Valley Pit. Therefore, we can see how the distance that the hydrothermal fluids had to travel plays a role within chlorite alteration, despite having similar mineral assemblages. They are located to the North-East of the Valley pit.

Thin Section ID	UTM Easting	UTM Northing	Transect	Facies
BC14318A	632722.5447	5597417.29	D	Chataway
BC14325H/G	632253.392	5597698.184	D	Chataway
BC14333A	631857.6325	5598423.301	D	Guichon
BC14334	632302.095	5598373.383	D	Chataway
BC14342H	631804.2965	5599444.828	D	Border

TABLE 6: Transect D details showing ID, location, transect, and lithological facies.

Samples BC14318A and BC14342H both are found in the sodic-calcic region of the GCB, whereas the rest are found in a sodic-calcic region overprinted by propylitic alteration. The samples were predominantly made up of feldspars and quartz, but with a higher percentage of amphibole than before, including primary hornblende and secondary actinolite. Within this transect, we also see the presence of fresh biotite, as well as biotite formed from the breakdown of actinolite. There are minor amounts of opaques, representing primarily sulfide minerals from within Valley. Intergrown with the chlorite is a large amount of muscovite, recognizable due to its habit and high birefringence. Additional accessory minerals are epidote and small

amounts of carbonate. Other metamorphic minerals include a large amount of sericite, occurring as dusting, and a minor amount of clay alteration.

Chlorite alteration appears in most actinolite crystals but varies in its intensity. Actinolite sometimes displays brown birefringence, which makes it difficult to pick out which sections have been chloritized. However, it should be noted that it is a possibility that the entire crystal has been chloritized, creating a pseudomorph (Fig. 14).

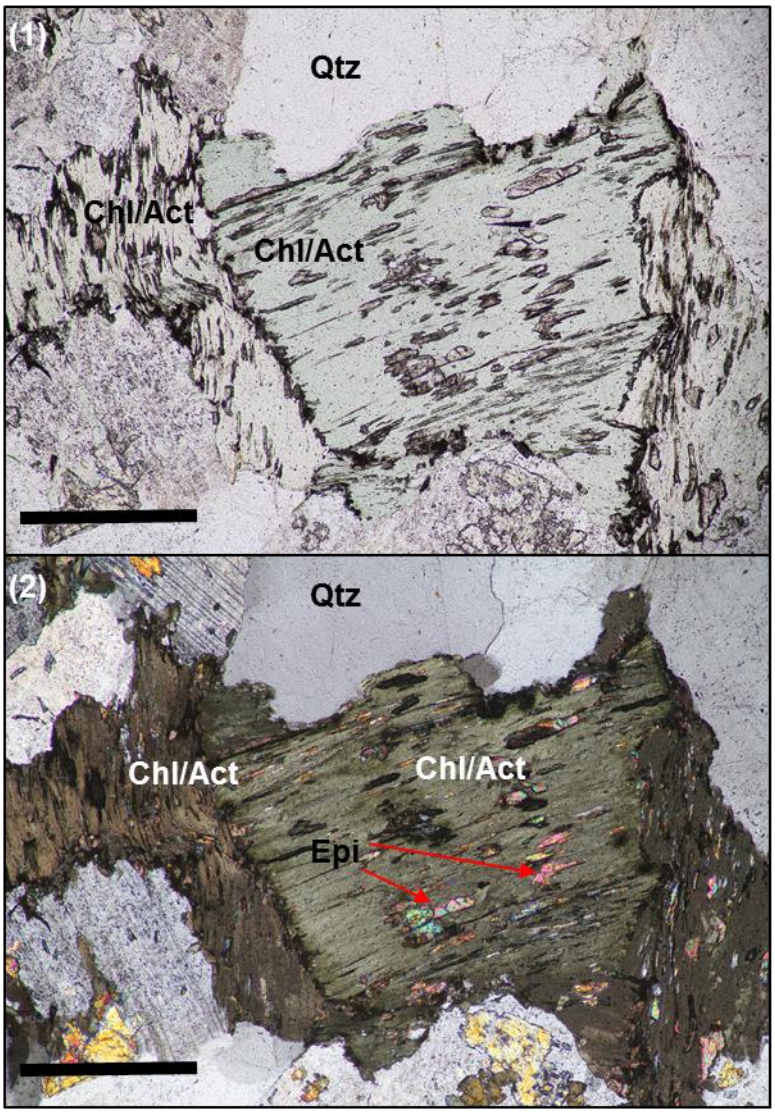

Figure 14. (1) image in PPL. (2) same image in XPL. Both images show two stages of actinolite, most likely formed from igneous hornblende. Actinolite displays brown

birefringence making it hard to distinguish the chlorite. It is possible that the whole grain has been chloritized. Epidote inclusions are shown. Scale bar indicates 0.5mm.

Pleochroism in the samples varies from weak to moderately strong depending on the host. It appears weaker in actinolite and stronger in biotite, although most chlorite alteration is contained within the altered biotite, not the fresh ones. In places, we see igneous hornblende breaking down to actinolite, which is then chloritized, although patches of the hornblende have been altered, specifically in the cleavage planes (Fig. 15).

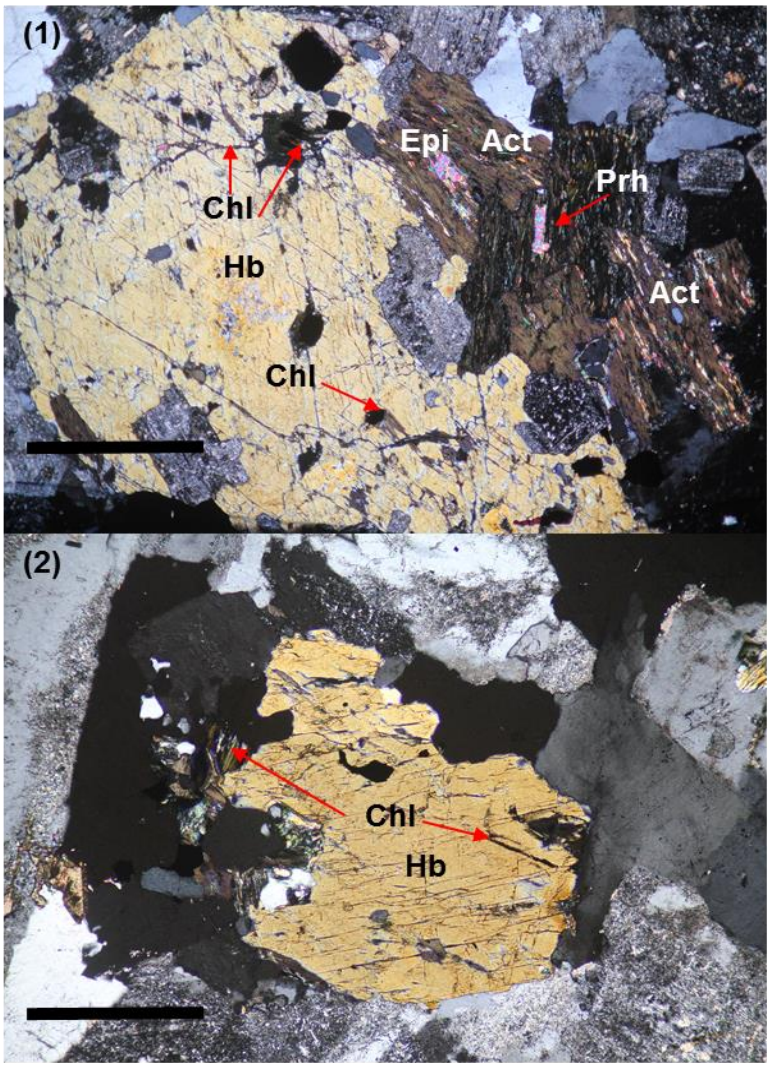

Figure 15. Hb (hornblende), Prh (prehnite). (1) hornblende altering to brown actinolite on its edge. Actinolite is infilled with epidote and prehnite. Chlorite is part of the brown crystal

shown. Chlorite also infills cleavage planes in hornblende, with one patchier section indicated. (2) hornblende altering to biotite on its rim, which has been minorly chloritized. Grain size varies from very fine-grained to medium-grained if the actinolite has been completely replaced. Scale bar indicates 1mm.

As actinolite is much higher in abundance then biotite, chlorite is confined to the sinuous pattern of the actinolite, leading it to take on a fibrous texture as it infills the weak points of the grain and pervasively extends into the groundmass (Fig. 16). Chlorite in biotite is somewhat fibrous, but less extensive, and chlorite in hornblende can form patchier sections as shown in Figure 15. Chlorite ranges in grain size from very fine-grained to medium-grained depending on the extent of the actinolite alteration.

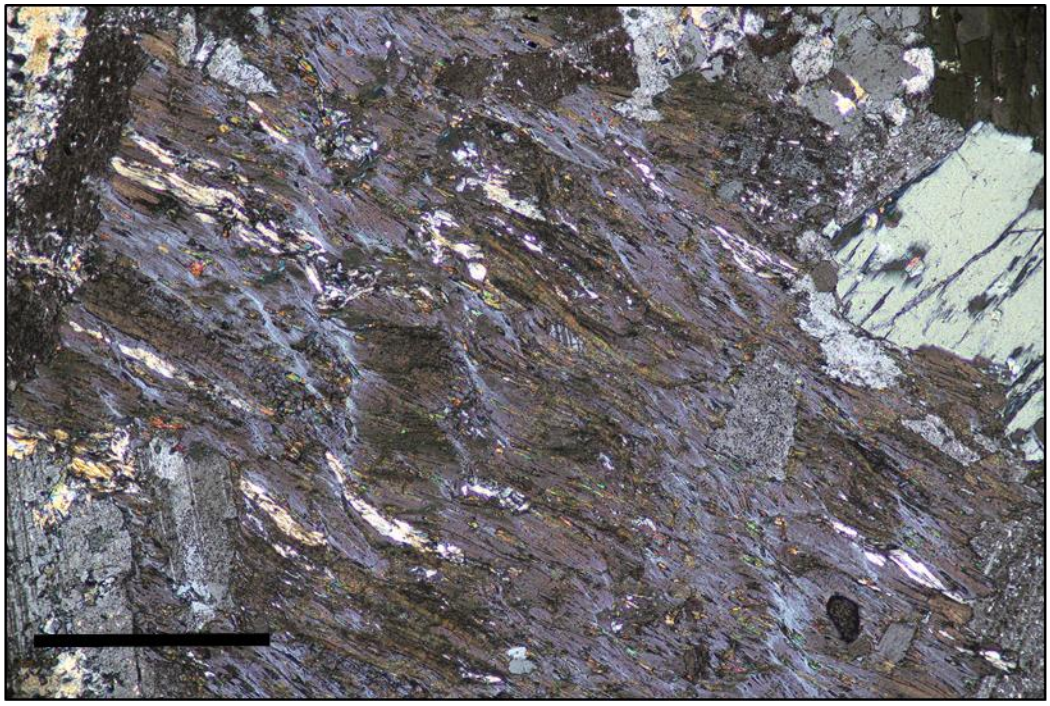

Figure 16. Large actinolite altering to chlorite. Image is shown in XPL for clarity. Lilac birefringence indicates remnant actinolite. Brown birefringence shows chlorite pervasively altering actinolite from the cleavage planes. Chlorite takes on a fibrous texture from its host. Chlorite ranges from very fine-grained to medium-grained. Scale bar indicates 1mm.

Chlorite birefringence is remarkably homogenous and is very intense brown across the actinolite and hornblende, similar to the other transects. In certain biotite grains traces of lilac

birefringence occur as observed in samples from the previously described transects. The lilac and brown birefringence is often found in the same grain and shows a form of zoning from one end to the other, however this is rare and confined to biotite (Fig. 17).

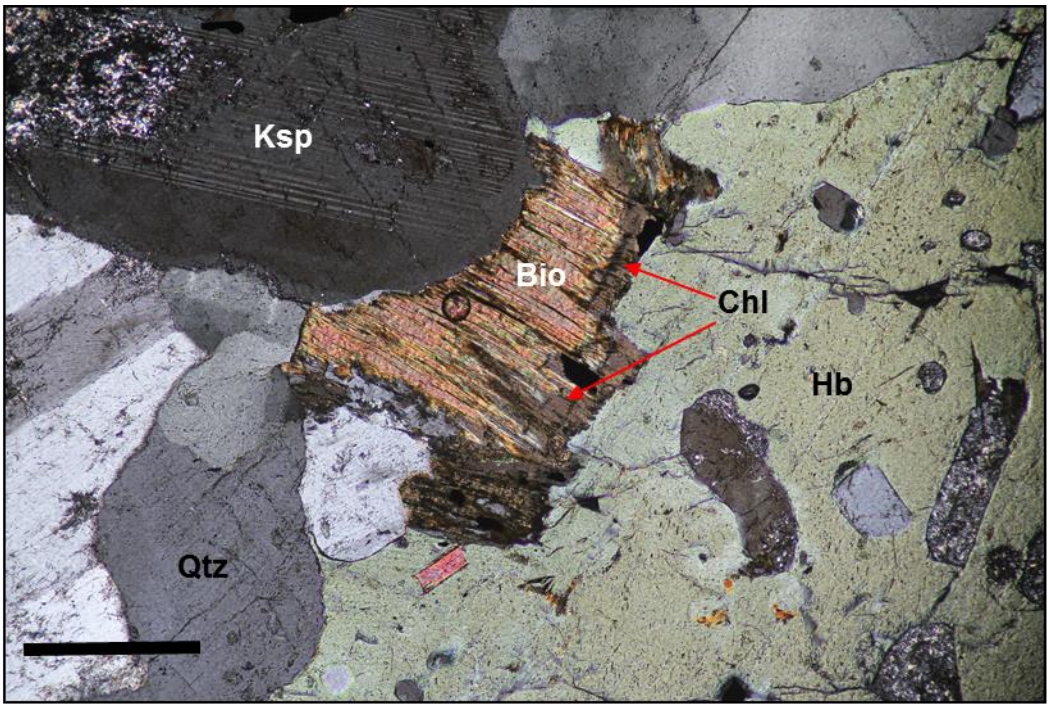

Figure 17. Biotite forming on the edge of a hornblende. Variable birefringence in chlorite is shown with both brown and lilac colours forming a zoning pattern. Scale bar indicates 0.5mm. Image shown in XPL.

3.5 Transect E

The final transect comprised six samples found either within, or directly proximal, to the Valley pit at HVC (Fig. 6). Details can be found in Table 7. The samples were chosen for their location within the Valley pit, an area mined for its high amounts of copper mineralization. They are within the alteration assemblage characterized by fracture controlled muscovite + quartz ± chalcopyrite ± bornite ± molybdenite; a high sulfide bearing assemblage. It should be noted that sample RL14HVC03 overlaps with the propylitic alteration assemblage.

The background of these samples is K-feldspar, quartz, and plagioclase, but there is a high amount of hornblende and actinolite, as well as pervasive biotite. Sulfides are easily identifiable as opaques, occurring anywhere from thick veins to sulfide stringers. Specific

sulfides were not identified and were left as opaques. Chlorite occurs primarily as part of the quartz-sulfide vein with muscovite assemblage, but also as part of the degradation of amphibole and biotite. Other metamorphic minerals included minor amounts of carbonate and sericite.

Thin Section ID	UTM Easting	UTM Northing	Transect	Facies
RL14HVC02	637290.171	5593546.717	E	Bethsaida
RL14HVC03	637304.901	5593388.657	E	Bethsaida
RL14HVC05	637469.922	5593321.973	E	Bethsaida
RL14HVC12	638760.660	5595432.454	E	Bethsaida
RL14HVC14	638891.750	5595584.773	E	Bethsaida
RL14HVC17	638225.506	5593954.038	E	Bethsaida

TABLE 7: Transect E details showing ID, location, transect, and lithological facies.

Chlorite characteristics vary depending on whether it is vein material, formed through fluid-wall rock interactions, or as the breakdown of amphibole/biotite hosts. This mainly affects grain size, but also the birefringence of the chlorites. Birefringence was found to vary between characteristic brown found within anhedral actinolite and biotite crystals (Fig. 18) and strong brown-lilac zoning found within vein material, intergrown with muscovite (Fig. 19a & 19b).

Pleochroism is strong when compared with other transects, going from colourless to a moderate green. Petrographically, this is indicative of an Fe-rich crystal when compared with other cations, or a lower Mg/Fe ratio concerning just those two specific cations (Deer et al., 1966). Chlorite forming within vein hosted material is hard to distinguish the primary host of grain as it is so degraded and anhedral. They were formed through fluid-wallrock interactions on a microscopic scale as hydrothermal fluids cooled and precipitated quartz and sulfides.

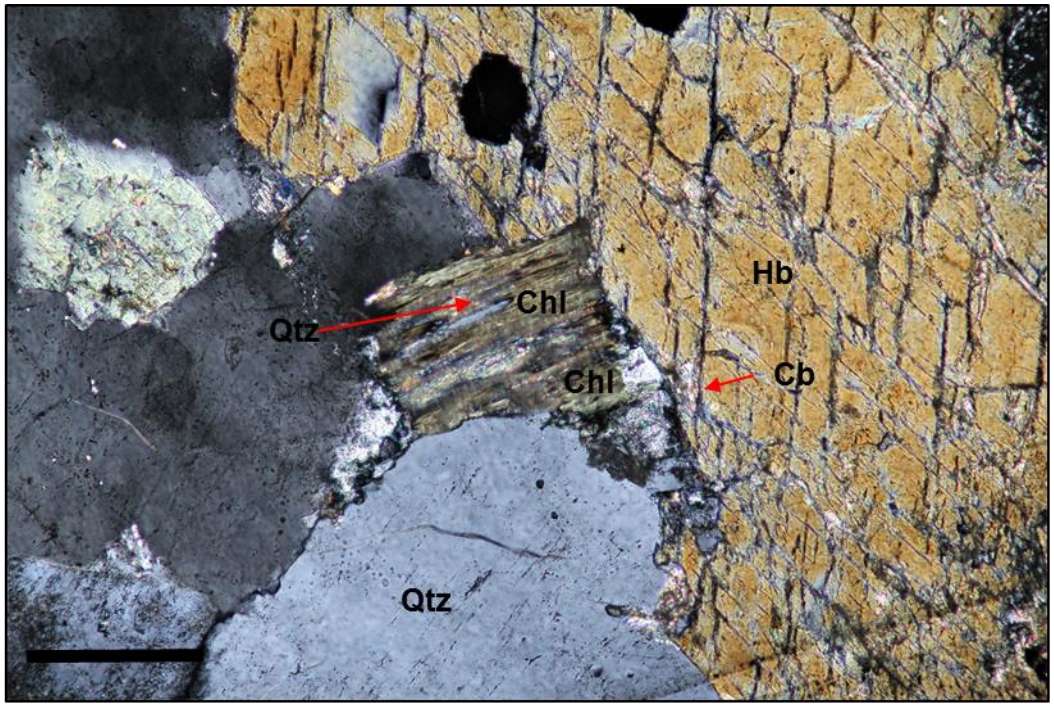

Figure 18. Cb (carbonate). Hornblende altering to a much smaller biotite on its rim. The biotite has been chloritized, as shown by brown birefringence. Grey striations indicate small quartz veins. Chlorite is fine-grained and sericite can be seen on top of the grain. Image shown in XPL. Scale bar indicates 1mm.

Chlorite grain size differs depending on the host. In amphibole and biotite hosts it is fine to medium-grained and appears as striations and pervasive infills of fracture planes. Unlike other transects, chlorite found within vein material shows a fan structure similar to the muscovite it is intergrown with. Vein hosted chlorite is also extremely fine-grained, being <0.1mm in size. The fan structures are radiating giving it an acicular appearance that generally grows towards the center of the vein. This acicular fan structure (Fig. 20) only occurs within transect E, and is a texture associated with extremely small grain size.

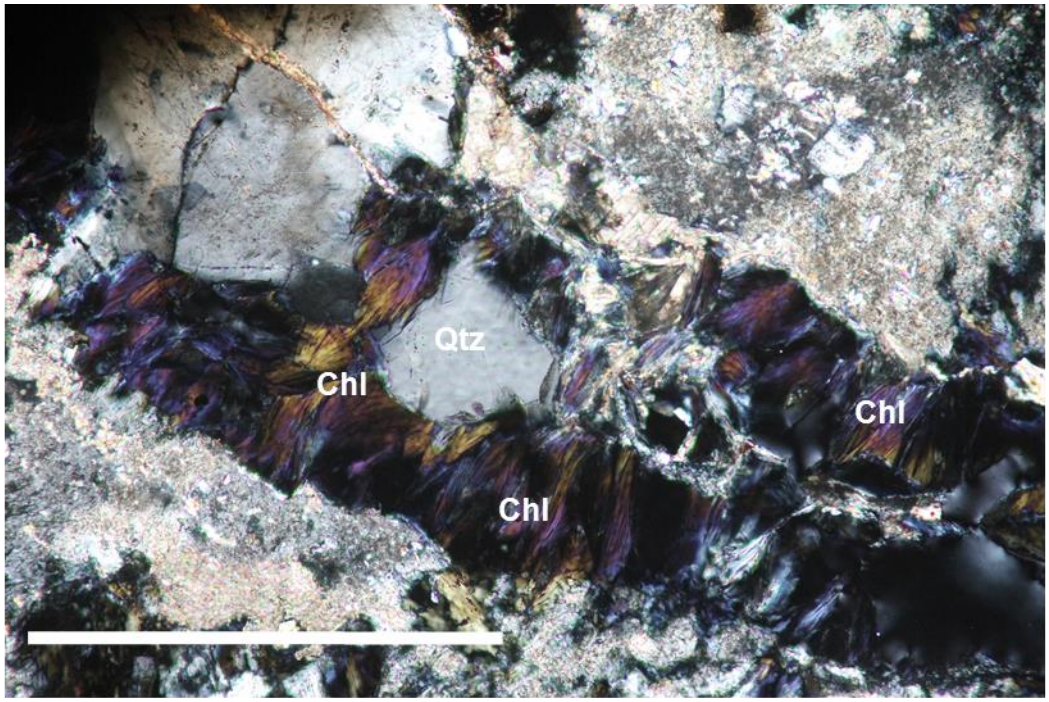

Figure 19a. Extremely fine-grained chlorite exhibiting strong birefringence zoning from brown to lilac. Scale bar indicates 0.5mm.

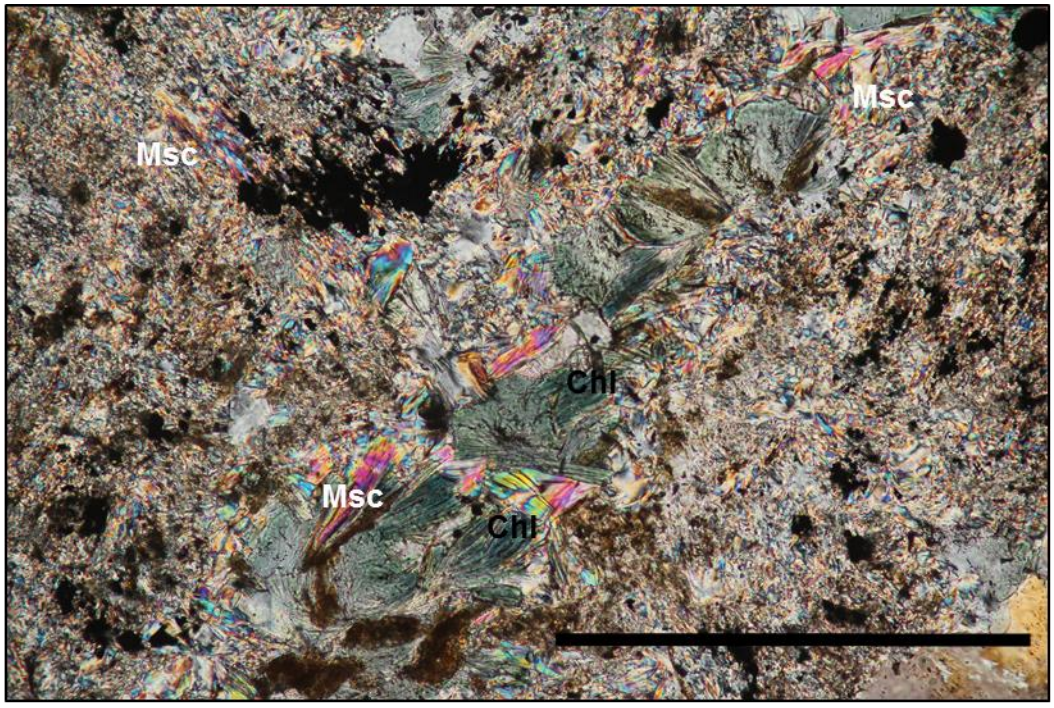

Figure 19b. Msc (Muscovite). Extremely fine-grained chlorite intergrown with muscovite and sericite groundmass. Chlorite also appears as replacing the edge of these acicular fan-structures. Larger muscovite are indicated. Scale bar indicates 0.5mm.

Chapter 4 – Geochemistry Results

4.1 Microprobe Results

Electron microprobe analysis was conducted on chlorite from eight samples selected from each of the transects and from representative regional, propylitic, sodic-calcic, and Valley mineral assemblages (Table 8). Sample BC13818A is of the same alteration as the other sodic-calcic region, but located further away from the mineralization center.

Thin Section ID	Transect	Alteration Type
BC1487A	B	Propylitic
BC14184G	B	Propylitic
BC14213B	C	Sodic-calcic
BC14124A	C	Sodic-calcic
MD004	A	Regional
MD060	A	Regional
BC14318A	D	Sodic-calcic
2758647	E	Valley Assemblage

TABLE 8. Thin sections chosen for Microprobe analysis. ID, transect, and alteration assemblage are indicated.

Samples were normalized according to the method described in Table 2. Chlorite formulas were calculated, along with %H_2O and total oxide%, and are reported in Table 9.1 and 9.2. Chlorite grains were carefully measured, data quality was assessed and those falling below threshold limits were not reported. Samples below detection limit are reported as zero.

	K site				Oct Site								Tet Site					
	Ca	K	Na	Sum K	Al (6)	Ti	Fe	Mn	Mg	Cr	Sum Oct	Si	Al (4)	Sum Tet	Sum total	wt% H2O	total Ox%
BC14187A-1-1	0.001156	0.000787	0.005899	0.007842	1.12868	0.002529	1.705335	0.085095	3.117235	0	6.038874	2.779516	1.220484	4	10.04672	11.66788	99.33708
BC14187A-1-2	0.007887	0.008014	0.013404	0.029306	1.144455	0.050134	1.643227	0.090112	3.00508	0.001916	5.934924	2.846318	1.153682	4	9.96423	11.77921	99.90631
BC14187A-1-4	0.009854	0.020574	0.014555	0.044983	1.122657	0.135621	1.63056	0.083398	2.856367	0.003816	5.832419	2.88261	1.11739	4	9.877402	11.85417	100.4678
BC14187A-1-5	0.009189	0.042387	0.016765	0.068341	1.13296	0.16005	1.593427	0.082598	2.834264	0.001587	5.804886	2.858051	1.141949	4	9.873227	11.88662	100.6647
BC14187A-1-6	0.00341	0.001405	0.021374	0.02619	1.151455	0.009289	1.656769	0.094427	3.086004	0.000951	5.998895	2.801625	1.198375	4	10.02508	11.86921	100.808
BC14187A-2-2	0.003156	0.0039	0.025996	0.033053	1.130617	0.004896	1.678412	0.092289	3.107939	0.00063	6.014783	2.793186	1.206814	4	10.04784	11.88773	101.1334
BC14187A-2-4	0.004111	0	0.030396	0.034508	1.174056	0.006808	1.624603	0.093682	3.07834	0	5.977489	2.81873	1.18127	4	10.012	11.68932	99.05592
BC14184G-1-4	0.021938	0.002215	0.020576	0.044729	1.117774	0.012327	1.635848	0.131403	3.082417	0.003208	5.982977	2.821742	1.178258	4	10.02771	11.67421	99.29891
BC14184G-1-5	0.121761	0.004528	0.022002	0.148292	1.154431	0.081687	1.540336	0.134461	2.896354	0.003512	5.810782	2.787065	1.212935	4	9.959074	11.82643	100.384
BC14184G-2-1	0.003477	0.005297	0.022795	0.03157	1.209402	0.001266	2.613853	0.187403	1.94112	0	5.953043	2.846932	1.153068	4	9.984613	10.97621	98.11251
BC14184G-2-2	0.002943	0.006169	0.00361	0.012722	1.214643	0.003692	1.844538	0.152825	2.771563	0.000952	5.988213	2.78493	1.21507	4	10.00094	11.65764	100.1806
BC14184G-2-3	0.004925	0.012343	0.01009	0.027357	1.216918	0.000599	2.098195	0.152967	2.479027	0	5.947706	2.85419	1.14581	4	9.975063	11.45426	99.62076
BC142138-1-1	0.005161	0.00207	0.021683	0.028914	1.136909	0.005482	1.799944	0.117048	2.922732	0.006423	5.988538	2.834554	1.165446	4	10.01745	11.60359	99.37639
BC142138-1-4	0.013278	0.004662	0.066738	0.084677	1.048035	0.019188	1.852936	0.102912	2.890551	0	5.913622	2.988391	1.011609	4	9.998299	11.48778	98.53708
BC142138-2-1	0.003328	0	0.032512	0.03584	1.12763	0.006045	1.692915	0.124573	3.022984	0	5.974148	2.872814	1.127186	4	10.00999	11.70104	99.63494
BC142138-2-2	0.0074	0.001575	0.023457	0.032432	1.129946	0.012118	1.657569	0.121544	3.047852	0.00096	5.96999	2.865047	1.134953	4	10.00242	11.75692	99.92722
BC142138-2-4	0.029189	0.007932	0.019912	0.057033	1.02117	0.033651	1.812872	0.11649	2.970808	0.000962	5.955953	2.912439	1.087561	4	10.01299	11.63133	99.78163
BC142138-3-2	0.020605	0.006358	0.017297	0.04426	1.068451	0.011513	2.017579	0.104322	2.740924	0	5.942791	2.958075	1.041925	4	9.987051	11.57498	100.0896
BC142138-3-3	0.010184	0.003018	0.025379	0.03858	1.144496	0.00377	1.837176	0.10952	2.884477	0	5.979439	2.840322	1.159678	4	10.01802	11.60903	99.56063
BC142138-3-4	0.001424	0.001126	0.007246	0.009795	1.178043	0.00289	1.77926	0.12859	2.919613	0.001289	6.009684	2.784304	1.215696	4	10.01948	11.55353	98.87513
BC142138-3-5	0.004568	0.049777	0.023577	0.077922	1.21128	0.004261	1.752987	0.112283	2.821337	0	5.902148	2.893413	1.106587	4	9.98007	11.81554	100.899
BC14124A-1-1	0.003619	0.000476	0.054382	0.058477	1.139558	0.001489	1.811758	0.117891	2.900637	0	5.971333	2.852701	1.147299	4	10.02981	11.57493	99.18923
BC14124A-1-2	0.002951	0.004427	0.027253	0.034631	1.221044	0.006701	1.736204	0.104342	2.907003	0.000639	5.975932	2.775469	1.224531	4	10.01056	11.71497	99.91637
BC14124A-1-3	0.008679	0.007357	0.043598	0.059634	1.137925	0.010987	1.824597	0.088957	2.896582	0	5.959048	2.853694	1.146306	4	10.01868	11.5633	99.0357
BC14124A-1-4	0.005282	0.007155	0.030289	0.042726	1.140732	0.000333	1.69627	0.118939	3.015914	0	5.972189	2.866217	1.133783	4	10.01491	11.65395	99.24785
BC14124A-2-1	0.004984	0	0.035004	0.039988	1.163593	0.005814	1.764254	0.09879	2.938296	0.001277	5.972024	2.834481	1.165519	4	10.01201	11.73167	100.1589
BC14124A-2-2	0.006313	0.00143	0.034309	0.042052	1.148147	0.005531	1.682398	0.104665	3.045701	0	5.986441	2.819545	1.180455	4	10.02849	11.66425	99.25015
BC14124A-2-3	0	0.005088	0.030911	0.035999	1.16931	0.003387	1.72719	0.107925	2.971114	0	5.978926	2.830064	1.169936	4	10.01493	11.66768	99.46708
BC14124A-2-4	0.119764	0.00794	0.004127	0.131831	1.058704	0.094638	1.741969	0.087867	2.848365	0.004119	5.835662	2.824982	1.175018	4	9.967493	11.83166	101.2965
BC14124A-2-5	0.002553	0.000792	0.024596	0.027941	1.208096	0.005545	1.67015	0.104214	2.972625	0	5.960631	2.829059	1.170941	4	9.988571	11.78006	100.0304
BC14124A-3-1	0.004577	0.002362	0.015915	0.022854	1.171336	0.005494	1.745509	0.100016	2.957433	0.001584	5.981372	2.825915	1.174085	4	10.00423	11.791	100.5546
BC14124A-3-2	0.002188	0.012068	0.031769	0.046025	1.180134	0.002786	1.66072	0.092856	3.033312	0	5.969808	2.826464	1.173536	4	10.01583	11.68938	99.26458
BC14124A-3-3	0.00167	0.002054	0.027813	0.031536	1.187877	0.004004	1.707418	0.110533	2.976231	0	5.986062	2.798786	1.201214	4	10.0176	11.69665	99.63875
BC14124A-3-4	0.003362	0.004306	0.027357	0.035025	1.18936	0.00021	1.68374	0.123576	2.993834	0	5.990719	2.790395	1.209605	4	10.02574	11.61951	98.95211
BC14124A-3-5	0.010445	0.00637	0.016782	0.033597	1.165157	0.004385	1.767239	0.120155	2.946609	0.002251	6.005796	2.768187	1.231813	4	10.03939	11.62564	99.50254

TABLE 9.1. Electron Microprobe results. Filtered chlorite data normalized to 14 anhydrous oxygens. Cations of the K, octahedral, and tetrahedral site are reported, as well as their sums and the wt% H_2O and total oxide%.

	K site					Oct Site							Tet Site				
	Ca	K	Na	Sum K	Al (6)	Ti	Fe	Mn	Mg	Cr	Sum Oct	Si	Al (4)	Sum Tet	Sum total	wt% H2O	total Ox%
MD004-C1-2	0.0127	0.01498	0.01791	0.04559	1.12969	0.00803	1.91155	0.18513	2.64412	0	5.87853	3.0389	0.9611	4	9.92412	11.4665	98.7972
MD004-C1-3	0.00051	0.00306	0.01117	0.01474	1.04987	0.00725	1.58397	0.23748	3.10658	0	5.98515	2.9501	1.0499	4	9.99988	11.6553	99.1991
MD004-C1-4	0.00179	0.00096	0.02069	0.02343	1.07263	0	1.64746	0.21931	3.03542	0.00256	5.97737	2.94486	1.05514	4	10.0008	11.6452	99.3388
MD004-C1-5	0.00567	0.00841	0.01333	0.02741	1.09606	0	1.81479	0.19146	2.79879	0	5.9011	3.06866	0.93134	4	9.92851	11.5648	99.1309
MD004-C2-1	0.00426	0.00503	0.02666	0.03595	1.11237	0	1.56655	0.24897	3.04777	0	5.97566	2.89611	1.10389	4	10.0116	11.5498	98.3158
MD004-C2-2	0.00711	0.00309	0.03558	0.04578	1.14157	0.00448	1.59005	0.22513	2.99553	0	5.95676	2.88306	1.11694	4	10.0025	11.5355	98.188
MD004-C2-3	0.00321	0	0.01601	0.01922	1.04739	0.00377	1.63829	0.22989	3.06172	0	5.98106	2.96051	1.03949	4	10.0003	11.6185	99.1118
MD004-C3-1	0.00329	0	0.00506	0.00835	1.13143	0.00148	1.32738	0.22896	3.29301	0	5.98227	2.88943	1.11057	4	9.99061	11.8652	99.5762
MD004-C3-2	0.00317	0.0035	0.00057	0.00724	1.24175	0.00648	1.36008	0.21474	3.06934	0	5.89238	2.95012	1.04988	4	9.89962	11.8412	99.1973
MD004-C3-3	0.00153	0.00032	0.00851	0.01036	1.11253	0.00331	1.3542	0.23089	3.27247	0.00545	5.97885	2.90581	1.09419	4	9.98921	11.7839	99.0583
MD004-C3-4	0.00574	0	0	0.00574	1.12036	0.00828	1.48233	0.2391	3.1519	0.0048	6.00677	2.83326	1.16674	4	10.0125	11.7257	99.3778
MD004-C3-5	0.00129	0.00258	0.00754	0.01141	1.12361	0.00619	1.48788	0.22777	3.13134	0	5.97679	2.89773	1.10227	4	9.9882	11.6878	98.9099
MD060-C1-1	0.06214	0.00391	0.0164	0.08246	1.13558	0.04936	1.58653	0.06137	3.04136	0.00375	5.87795	2.86145	1.13855	4	9.96041	12.0061	101.506
MD060-C1-3	0.0068	0.00285	0.01879	0.02845	1.20815	0.00431	1.6099	0.0565	3.04046	0	5.91931	2.90937	1.09063	4	9.94776	11.9038	100.389
MD060-C2-3	0.05195	0.03851	0.03079	0.12125	1.07525	0.05613	1.64326	0.04687	2.99498	0.00127	5.81776	3.0025	0.9975	4	9.939	11.752	99.5611
MD060-C2-4	0.04334	0.01241	0.02731	0.08306	1.07762	0.03076	1.68985	0.0597	2.99035	0.00127	5.84955	3.03409	0.96591	4	9.93261	11.81	100.156
MD060-C2-5	0.00817	0.04953	0.0912	0.14889	1.0941	0.02819	1.64673	0.04195	3.04963	0	5.8606	2.97125	1.02875	4	10.0095	11.925	101.091
MD060-C3-2	0.00129	0.00403	0.01162	0.01693	1.15576	0.00471	1.64509	0.05433	3.11526	0	5.97514	2.86633	1.13367	4	9.99207	11.6906	98.8963
MD060-C3-3	0.01398	0.00418	0.01234	0.0305	1.05959	0.00678	1.72208	0.05057	3.1025	0	5.94152	2.99932	1.00068	4	9.97202	11.6676	99.0203
MD060-C3-4	0.00834	0	0.01429	0.02263	1.14574	0.00508	1.62441	0.05635	3.11437	0	5.94596	2.92122	1.07878	4	9.96859	11.8619	100.169
MD060-C3-5	0.00265	0.00111	0.01197	0.01572	1.1871	0	1.62504	0.05371	3.1194	0	5.98524	2.82404	1.17596	4	10.001	11.8903	100.498
BCI4318A-1-1	0.05551	0.00113	0.02322	0.07986	1.14348	0.0348	1.8005	0.0443	2.86226	0.00127	5.88662	2.87701	1.12299	4	9.96648	11.6088	99.0894
BCI4318A-1-2	0.0086	0.0021	0.01431	0.02501	1.1565	0.00225	1.82601	0.05528	2.92106	0	5.96109	2.88319	1.11681	4	9.98611	11.5886	98.9398
BCI4318A-1-3	0.00634	0.00256	0.01709	0.02599	1.14851	0.00377	1.84314	0.03839	2.93038	0	5.9642	2.88322	1.11678	4	9.99019	11.729	100.155
BCI4318A-1-4	0.00265	0.00557	0.02821	0.03644	1.16626	0.00203	1.84341	0.04594	2.9018	0.00314	5.96259	2.86227	1.13773	4	9.99902	11.7615	100.514
BCI4318A-1-5	0.01105	0.00031	0.02129	0.03266	1.12193	0.00445	1.85006	0.05436	2.92277	0.00315	5.95671	2.90888	1.09112	4	9.98938	11.7176	100.186
BCI4318A-2-1	0.01006	0.0065	0.03229	0.04885	1.08267	0.00883	1.82002	0.03846	2.98822	0.00352	5.94172	2.95379	1.04621	4	9.99057	11.5421	98.4795
BCI4318A-2-3	0.01272	0.00323	0.02916	0.04511	1.06811	0.01881	1.8108	0.04087	2.96834	0.00191	5.90884	3.01687	0.98313	4	9.95395	11.6011	98.8398
BCI4318A-2-4	0.03019	0.00798	0.01765	0.05582	1.06927	0.05289	1.78559	0.03558	2.92084	0.00127	5.86543	3.0068	0.9932	4	9.92125	11.7381	99.9066
BCI4318A-2-5	0.01087	0.00846	0.04727	0.0666	1.06232	0.00272	1.82009	0.03595	3.04847	0	5.96955	2.91568	1.08432	4	10.0361	11.5261	98.4573
BCI4318A-3-1	0.03706	0.00286	0.01223	0.05215	1.07238	0.02423	1.74711	0.04993	3.03121	0	5.92486	2.94023	1.05977	4	9.97701	11.7861	100.29
BCI4318A-3-2	0.01344	0.00303	0.01461	0.03108	1.07959	0.00384	1.77431	0.04263	3.0094	0	5.90977	3.04866	0.95134	4	9.94085	11.7603	99.9143
BCI4318A-3-3	0.00872	0.00307	0.00946	0.02125	1.13305	0.00407	1.76767	0.04025	2.98395	0.00319	5.93217	2.96131	1.03869	4	9.95342	11.6255	98.7843
2758647-1-1	0.00651	0	0.04446	0.05097	1.14499	0.00642	1.64128	0.04178	3.13128	0	5.96575	2.85319	1.14681	4	10.0167	11.7217	99.171
2758647-1-3	0.00293	0.00016	0.01023	0.01332	1.02504	0.151	1.89333	0.03808	2.82732	0.00223	5.937	2.78048	1.21952	4	9.95032	11.6338	99.9254
2758647-1-4	0.01707	0.00752	0.01263	0.03722	1.1453	0.0216	1.60304	0.03912	3.15824	0	5.9673	2.82261	1.17739	4	10.0045	11.744	99.2063
2758647-1-5	0.00369	0.01102	0.00691	0.02163	1.18639	0.01039	1.64915	0.05241	3.05814	0	5.95648	2.85456	1.14544	4	9.97811	11.7703	99.5836
2758647-2-5	0.00604	0.00194	0.00685	0.01483	1.37615	0.00196	2.19381	0.03712	2.31343	0	5.92247	2.7541	1.2459	4	9.93731	11.509	99.8998
2758647-3-1	0.02391	0	0.02728	0.05119	1.35783	6.3E-05	2.14296	0.04202	2.3533	0	5.89617	2.77461	1.22539	4	9.94736	11.5073	99.7163
2758647-3-2	0.01805	0.00588	0.06979	0.09372	1.35295	0.00141	2.01841	0.03808	2.39653	0.00256	5.80995	2.90999	1.09001	4	9.90367	11.4255	98.2253
2758647-3-4	0.01588	0.00095	0.01555	0.03239	1.34434	0	1.94852	0.03328	2.54824	0.00126	5.87563	2.85487	1.14513	4	9.90802	11.7067	100.248
2758647-3-5	0.00381	0	0.03772	0.04153	1.41732	0.00331	2.08976	0.04147	2.32359	0	5.87545	2.77981	1.22019	4	9.91699	11.669	100.71

TABLE 9.2. Electron Microprobe results. Filtered chlorite data normalized to 14 anhydrous oxygens. Cations of the K, octahedral, and tetrahedral site are reported, as well as their sums and the wt% H_2O and total oxide%.

4.2 Chlorite Major Element Composition

Magnesium and iron concentration in chlorite samples show the highest Mg content occurs within the regionally metamorphosed samples, followed by the propylitic and sodic-calcic samples (Fig. 20). Samples from the Valley pit show the most Fe content, with a relatively equal Mg/Fe ratio. However, it should be noted that some samples from Valley cluster at a higher Mg value of ~3.0 pfu.

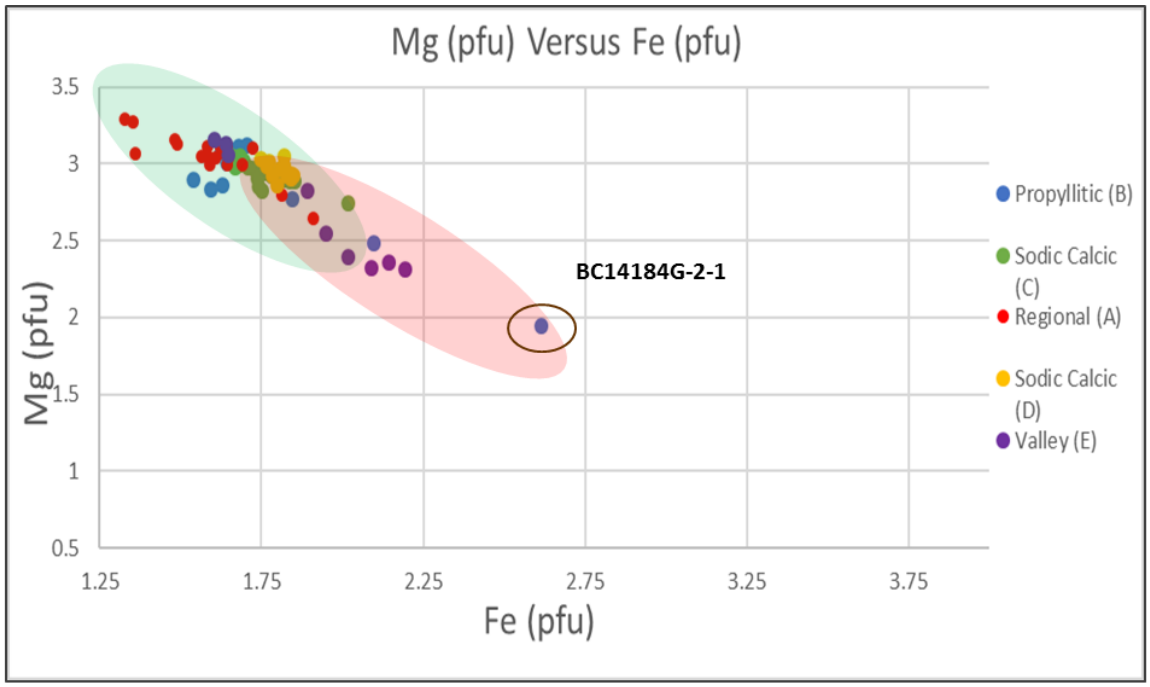

Figure 20. Major element Mg versus Fe in the octahedral site. Points are coloured according to alteration type and transect. Brown circle envelops a propylitic outlier which most likely shows a sample cut by a hematite grain (higher iron content). Green ellipse represents sodic-calcic samples and red ellipse represents phyllic chlorite data from Alva Jimenez (2011).

The outlier noted in Figure 20 represents a sample from the propylitic alteration assemblage with particularly high iron content. This could represent a specular hematite crystal as the trend is not observed within the other data points, and this would drastically affect the iron content of surrounding chlorites.

Samples from transect D plot very close to samples from transect C as they both belong to the sodic-calcic assemblage but transect D is further away. From the plot, it appears that they overlap one another and there is no major difference in their composition relative to the rest of the transects, despite their difference spatially.

Calcium levels in chlorite are generally low, with a total average of 0.0134 pfu across all the samples. They are typically <0.1 with two outliers showing just higher than 0.1 pfu. Potassium levels in the K site show an average of 0.00620 pfu for the ones that were above the detection limit. Potassium levels are slightly higher in samples affected by regional metamorphism and the lowest potassium content is found in the samples from Valley. Concerning sodium, the average across the samples is 0.0227 pfu (Tables 9.1 & 9.2) The highest sodium content is found in samples from the propylitic alteration facies, and those in the Valley pit; the lowest is found in the regionally metamorphosed samples.

Octahedral aluminum (Al^{VI}) has the same variation across the sodic-calcic and regionally metamorphosed samples as they have a high range with relatively equal magnesium ratios. It is slightly higher in the propylitic region as a percentage of the total octahedral site (Fig. 21). Al^{VI} is much higher in the samples from Valley with values clustered at 0.23 pfu (Fig. 21). The Mg/(Mg+Fe+Mn) value is quite uniform across the sodic-calcic, propylitic, and regional metamorphic samples with a few lower values found in the propylitic samples. The Valley samples have a higher iron content and a lower Mg/(Mg+Fe+Mn) relative to the other samples.

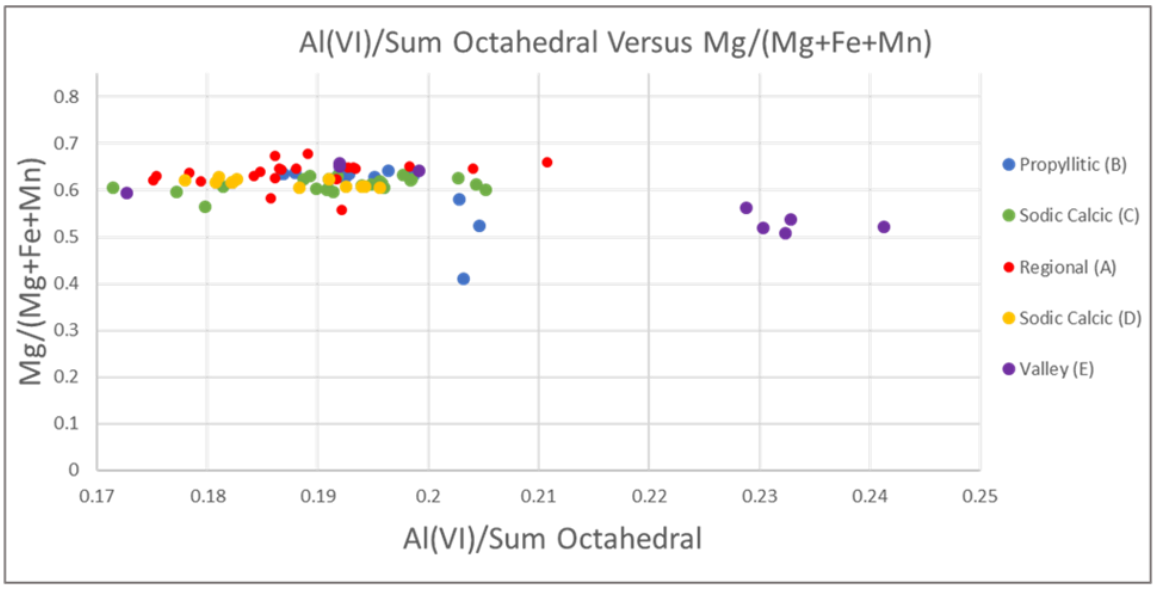

Figure 21. Mg/(Mg+Fe+Mn) versus Al^{VI} / Sum Octahedral of chlorite microprobe data according to alteration type. Sum octahedral represents (Al^{VI} + Ti +Fe + Mn + Mg + Cr). Outliers of Valley are clustered with other alteration regions.

Chromium levels are mainly below detection limits with a maximum value of 0.00642 pfu. Titanium values are typically less than 0.05 pfu, with a few outliers in the sodic-calcic and Valley samples showing a value >0.1 pfu.

Silica levels show an average of 2.88 pfu with the highest values occurring in the regionally metamorphosed samples. This is converse to the Al^{IV} values as the total tetrahedral site must sum to 4 pfu. All the silica values vary between 2.7 and 3.1 pfu.

When comparing the aluminum in the tetrahedral and octahedral sites, their ratios are relatively equal when normalized, with the regionally metamorphosed samples clustered around zero, while the rest trend towards a higher Al^{IV}-1 value (Fig. 22). Valley samples and two propylitic samples have the highest Al^{VI} + 2Ti +Cr -1 values, agreeing with trends shown in Figure 21. Samples from the sodic-calcic (C) have the same ratio as their transect D counterparts, but with slightly higher values of octahedral and tetrahedral aluminum.

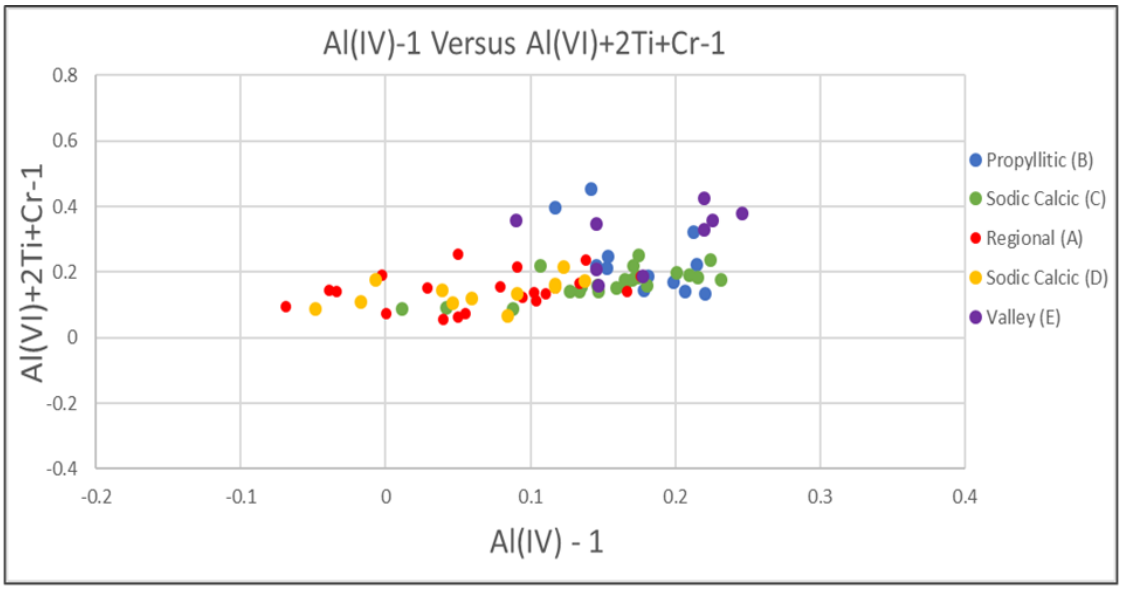

Figure 22. Al^{VI} + 2Ti +Cr -1 versus Al^{IV} – 1 for chlorite microprobe data according to alteration type. Normalization method after Bailey, 1988.

Similar trends are observed between normalized aluminum values versus the atomic ratio Mg/(Mg+Fe) (Fig. 23). Regionally metamorphosed samples have a higher magnesium content compared to iron and have lower values on average of octahedral and tetrahedral aluminum than Valley samples. Sodic-calcic samples from transects C and D have relatively similar levels of magnesium to iron ratios and the same levels of normalized octahedral aluminum. However, the sodic-calcic samples from transect C have slightly higher tetrahedral aluminum relative to samples from transect D. Propylitic samples are more erratic and show no discernable trend as their magnesium to iron ratios and levels of tetrahedral and octahedral aluminum vary greatly.

Manganese shows an average of 0.103 pfu across all the samples but is scattered across each sample. Values within the Valley assemblage are lowest with the sodic-calcic (D) samples. Highest values occur in the regionally metamorphosed samples, followed by the sodic-calcic (C) and propylitic samples (Fig. 24).

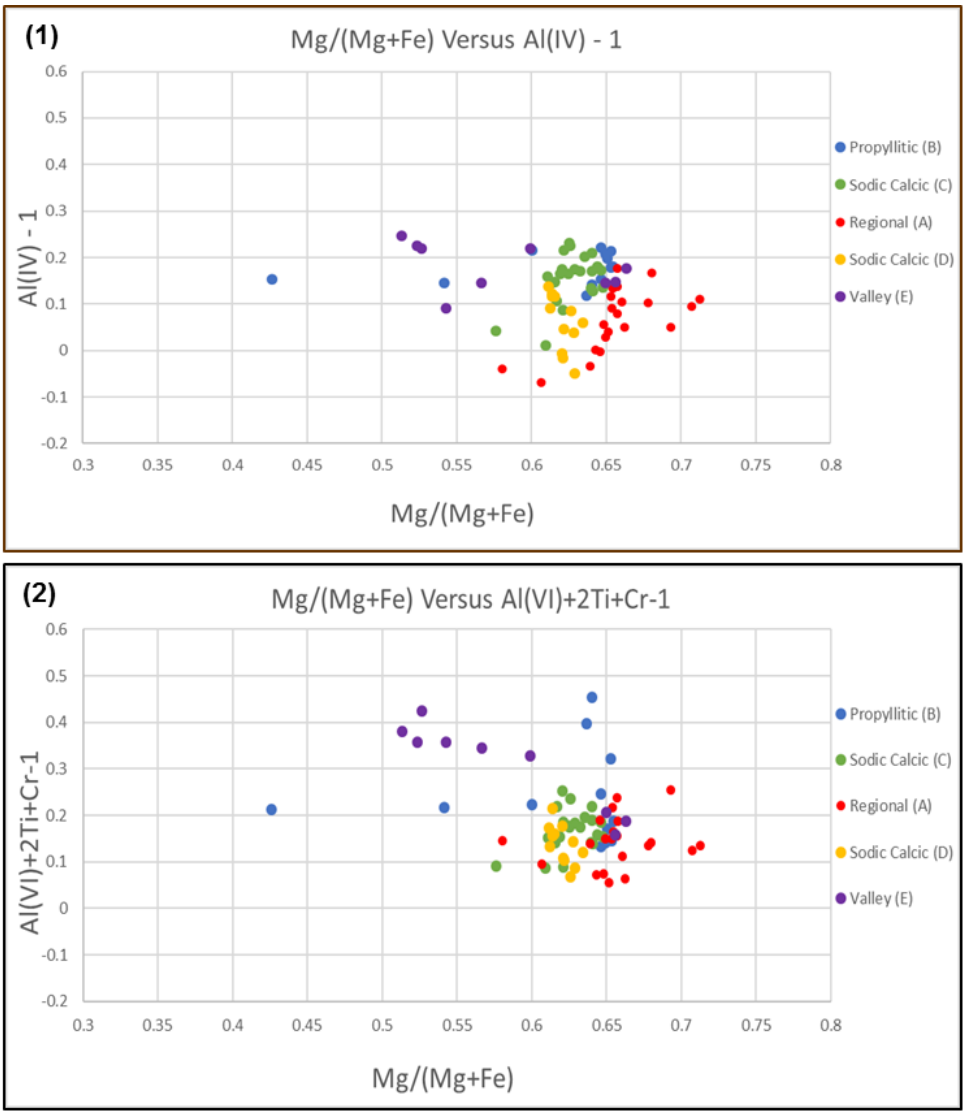

Figure 23. (1) chlorite composition (formula proportion $Al^{IV} - 1$ versus atomic ratio Mg/(Mg+Fe)) from microprobe data. (2) chlorite composition (formula proportion $Al^{VI} + 2\ Ti + Cr - 1$ versus atomic ratio Mg/(Mg+Fe)) from microprobe data.

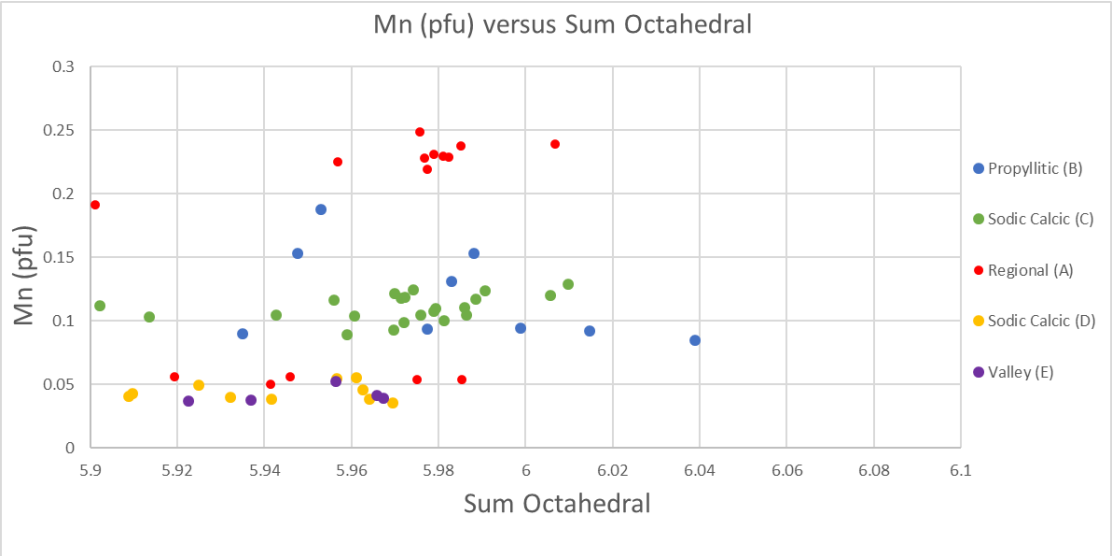

Figure 24. Plot of manganese content versus the sum of the octahedral content. Octahedral content represents (Al^{VI} + Ti +Fe + Mn + Mg + Cr).

Chapter 5 – Discussion and Exploration Implications

5.1 Discussion

Chlorite is present in regions throughout the GCB as both hydrothermally altered samples and as regionally metamorphosed samples (McMillan, 1985; Casselman et al., 1995). The hydrothermally altered samples were chosen in groups from the sodic-calcic mineral assemblage, propylitic assemblage, and from within the mineralization center in the Valley pit. Previous petrographic work has been done on the regionally metamorphosed samples, but without an emphasis on the chlorite alteration (D'Angelo, 2016). Concerning hydrothermal alteration, prior petrographic and geochemical work has been done on chlorite samples from the sodic-calcic, propylitic, and phyllic alteration assemblages, but without an emphasis on the Valley deposit (Alva Jimenez, 2011).

Petrographically, certain chlorite characteristics subtly alter throughout the five transects, while others do not seem to experience a significant change (Figs. 7; 14; 18; 19a; & 19b). Characteristics such as intensity and relief cannot be relied upon for vectoring towards the source of alteration as it appears to be erratic depending on the host of the mineral (actinolite, biotite, and hornblende). As these minerals differ in modal abundance from sample to sample, we can conclude that these characteristics are not indicative of the type of alteration, but are more based on the degree of alteration (Figs. 10; 11; 14; & 17).

Chlorite birefringence does alter throughout the samples, with the difference observed in chlorite from samples that have been altered by regional metamorphism versus those from within Valley pit (Figs. 7; 9; & 19a). Chlorite formed by regional metamorphism all exhibit deep brown birefringence which changes to light brown to lilac as you get closer to the mineralization center at Valley. Geochemically, these distal chlorites contain a higher Mg content as well as lower values of octahedral and tetrahedral aluminum (Figs. 20 & 23). Samples from the propylitic section show variable birefringence from brown to a lilac hue the closer to the center of the GCB. Kranidiotis and Maclean (1986) and Bailey (1988) demonstrate that the birefringence of chlorite grades from green to brown, to lilac, to deep blue as iron content increases. From Figure 20 and previous work done at HVC (Alva Jimenez, 2011),

Valley contains the highest iron content relative to magnesium, and shows the most lilac birefringence relative to the other samples. Transect B in the propylitic region also shows brown-lilac zoning of birefringence and is spatially close to the mineralization center. Conversely, samples from the sodic-calcic mineral assemblage, both adjacent to and distal from Valley, exhibit deep brown birefringence with little to no lilac colour. Samples from the sodic-calcic assemblage have a higher Mg content than the samples from Valley, as well some chlorite from the propylitic assemblage (Fig. 20). However, it should be noted that chlorite in Valley is not iron rich, but has more of a 1:1 Mg/Fe ratio relative to the other samples. As the alteration changes with distance, the iron content of the chlorites is dependent on the interaction of Fe-rich magmatic Cu-bearing fluids at the mineralization center with Mg-rich seawater, and as distance increases, the iron content decreases (Kranidiotis and Maclean, 1986; Byrne et al., 2017). From transect D, chlorite is highly pervasive, fully replacing many actinolite grains, but shows no evidence of lilac birefringence, indicating its iron content is not as high as in Valley. Furthermore, this is confirmed when looking at the pleochroism of the samples, with the deep shades of green exhibited in Valley absent from the regional metamorphic samples.

The host of the chlorite grains is of similar assemblage across the different transects, with a small difference within those samples from Valley. Both regional metamorphic and hydrothermally altered chlorite are found predominantly associated with actinolite and biotite, with small patches found in igneous hornblende. It is especially common for actinolite to alter to secondary biotite on its rims, which is then chloritized. Primary biotite, found with hornblende on the western side of Valley does not readily alter to chlorite, which was concentrated in amphibole. The only significant difference in the primary mineral were found within the Valley pit directly above the mineralization center. In these samples, chlorite was found in amphibole and biotite, but also within small veinlets, intergrown with muscovite, and proximal to sulfides. This chlorite formed through fluid-wall rock interactions, similar to that noted by Wilkinson et al., (2015) in Indonesia and in the petrographic sections from this study it is difficult to identify the original host due to the anhedral nature of the grains.

Grain size varies widely between transects, ranging from extremely fine-grained to medium-grained depending on the primary host for the chlorite. Grain size is a function of the mineral it is replacing and varies between the actinolite and biotite host depending on the

degree of replacement. However, within hornblende grain size is typically very fine-grained. This is consistent throughout every sample and shows that actinolite is much more readily replaced relative to hornblende. This could be due to actinolite being an alteration product of hornblende, or due to the thermodynamic stability of the crystal, but no evidence has been provided for this.

Chlorite grains exhibit different textures depending on their hosts. In actinolite, they show a fibrous, felty texture that infills the cleavage planes and appears sinuous under the microscope. It is far more common for chlorite to pervasively extend from the cleavage planes than replace the rims of amphibole. However, in biotite, chlorite appears as needle-like aggregates that are relatively linear in the cleavage planes, or begin to replace the rim of the biotite and move inwards. It should be noted that this can occur in both simultaneously, as biotite often appears as an alteration product on the amphibole rims. Replacement occurs in the biotite not the primary mineral grain. In hornblende, chlorite appears as far patchier and in blocks, and minorly infills the cleavage planes. It appears in small squares, as it replaces the structural weak points of the grain. Within the Valley pit, we see a unique texture within the extremely fine-grained chlorite occurring within veins. This is shown in the small fan structures that the chlorite adopt while intergrown with muscovite. As the chlorite forms from hot, hydrothermal fluids, this irregular structure could be a result of the rapidly cooling metal-bearing fluids, which reflect higher iron content (Inoue et al., 2010). Byrne et al., (2017) showed that the sodic-calcic fluid temperature was 370–500°C, but the other regions have yet to be determined. Texturally, it is hard to distinguish between chlorite from the regional metamorphic zones with those that occur within the sodic-calcic and propylitic assemblages. There are fine differences in the structure and size of the chlorite right above the mineralization center and those adjacent to the pit.

There are subtle differences in the composition of chlorite throughout the GCB and HVC district. Chlorite from Valley differs in octahedral aluminum content relative to the other areas of the GCB (Fig. 22). Regional metamorphic and sodic-calcic assemblage samples have a generally overlaying pattern concerning octahedral aluminum, whereas samples from the propylitic assemblage have slightly higher values (Figs. 21 & 23). Valley contains the highest percentage of octahedral aluminum, relative to other cations in the octahedral site. Cathelineau

and Nieva (1985) show that the occupancy of the tetrahedral and octahedral site by alumina is temperature controlled; therefore, the decreasing amount of aluminum in the tetrahedral and octahedral sites of chlorite found in the propylitic and sodic-calcic assemblage is consistent when compared to samples from the Valley pit which are associated with high-temperature quartz-kspar veins (Byrne et al., 2013; Lesage et al., 2017). The high iron bearing chlorite potentially represent a more acidic environment which accommodates a higher amount of octahedral aluminum than the surrounding Mg-rich chlorites (Alva Jimenez, 2011).

Tetrahedral chlorite Al^{IV} content increases with temperature (Cathelineau and Nieva, 1985), which agrees with our data that the Valley and propylitic assemblage samples have a higher tetrahedral aluminum content than other samples. Regional metamorphic samples have lower tetrahedral aluminum on average than other samples.

A graph of manganese content (Fig. 24) compared to the octahedral sum shows that manganese content is far higher in regionally metamorphosed rocks than hydrothermally altered rocks. Within the hydrothermal alteration zones, manganese is similar within regions that are close together, such as the propylitic and sodic-calcic (C) samples. The sodic-calcic (D) samples do not have as high manganese relative to the sodic-calcic (C) counterparts. Manganese in chlorite structure is not well studied, but it is suggested that the manganese content is related to the magmatic-hydrothermal fluids, or brines that have been enriched in manganese (Wilkinson et al., 2008; Wilkinson et al., 2015). However, from the high content of the regionally metamorphosed samples, it could be argued that the manganese content is remnant of the protolith, which would also be explained by the overlapping composition between samples that belong to different mineral assemblages, but are spatially close to each other. If this is the case, then the protoliths of the regionally metamorphosed samples would be high in manganese relative to rocks in the surrounding areas.

5.2 Exploration Implications

From these results, there are very subtle petrographic differences between regionally metamorphosed chlorite and direct hydrothermal chlorite; however, there is a grey area where the hydrothermal alteration assemblage show characteristics of both regionally metamorphosed rocks and those found directly above the mineralization center. Variations in

petrography and geochemistry of chlorite observed in this study suggest that birefringence, pleochroism, and Mg/Fe ratios can provide a vector toward core of the hydrothermal system. The occurrence of high octahedral and tetrahedral aluminum could also be used to look for zones of high temperature, potentially representing the highest temperature of the hydrothermal fluid. However, it should be noted that major assumptions were made for this study, which should be considered in further detail before using chlorite alteration in industry practices. Most importantly, how ferric and ferrous iron affect the results of iron-rich chlorite, as all iron was assumed to be Fe^{2+} in this study. Other assumptions would also be the substitution of F and Cl for OH^- in the chlorite structure, which was assumed to be negligible in this study. More detail should be spent on the chemistry of the amphibole hosts to see how replacement changed between hornblende and actinolite.

Chapter 6 – Conclusion

6.1 Conclusion

There are subtle petrographic variations between regional metamorphic chlorite of the GCB and chlorite associated with various mineral assemblages derived from the mineralizing HVC deposit. Birefringence varies as a function of iron content, from deep brown in those samples found distally from the HVC district to a zoned brown-lilac colour within the Valley pit. This is further highlighted in the pleochroism of the samples which varies from very light green to moderate green as you move closer to the Valley pit. Texturally, chlorite ranges in grain size around the batholith, but with the smallest grains found within veins and intergrown with muscovite in the Valley pit. Chlorite displays needle-like aggregates within biotite, a fibrous habit within actinolite, and a far less pervasive, patchy appearance within hornblende. Geochemically, regional metamorphic chlorite contains a higher magnesium content relative to samples associated with fluids potentially originating from the center of the HVC system. Chlorite associated with the sodic-calcic and propylitic assemblage have a higher Mg/Fe ratio relative to those chlorites from the Valley pit which have Mg/Fe ratios near to one. Both tetrahedral and octahedral aluminum are higher in the Valley samples while the regional metamorphic samples have the lowest aluminum content. Manganese levels are enriched in the regionally metamorphosed samples compared to other samples from this study.

References

Alva Jimenez, T.R., 2011, Variation in Hydrothermal Muscovite and Chlorite Composition in the Highland Valley Porphyry Cu-Mo District, British Columbia, Canada, University of British Columbia MSc Theses, 249p.

Bailey, S.W., 1988, Hydrous Phyllosilicates (exclusive of micas), Reviews of Mineralogy, v.19, p 405-453.

Berger, B.R., Ayuso, R.A., Wynn, J.C., and Seal, R.R., 2008, Preliminary model of porphyry copper deposits: U.S. Geological Survey Open-File Report 2008-1321, 55p.ob

Bobrowsky, P.T., Kerr, D.E., Sibbick, S.J., and Newman, K., 1993, Drift exploration studies, Valley copper pit, Highland Valley copper mine, British Columbia: Stratigraphy and sedimentology: Geological Fieldwork 1992, British Columbia Geological Survey, paper 1993-1, p. 427-437.

Briskey, J.A., 1981, Geology, petrology, and geochemistry of the Jersey, East Jersey, Huestis, and Iona Porphyry Copper-Molybdenum Deposits, Highland Valley, British Columbia, Ph.D. thesis, Oregon State University, Corvallis, Oregon, p.427.

Byrne, K., Stock, E., Ryan, J., Johnson, C., Nisenson., J., Alva Jimenez, T.R., Lapointe, M., Stewart, H., Grubisa, G., and Sykora, S., 2013, Porphyry Cu-(Mo) deposits in the Highland Valley district, south-central British Columbia, Porphyry systems of central and southern British Columbia: Tour of central British Columbia porphyry deposits from Prince George to Princeton. Society of Economic Geologists, Field Trip Guidebook, Series, 43, pp. 99-116.

Byrne, K., Lesage, G., Gleeson, S.A., and Lee, R.G., 2017, Large-scale sodic-calcic alteration around porphyry copper systems: examples from the Highland Valley Copper district, Guichon batholith, south-central British Columbia; in Geoscience BC Summary of Activities 2016, Geoscience BC, Report 2017-1, p. 213–222

Caritat, P.D., Hutcheon, I., and Walshe, J.L., 1993. Chlorite geothermometry: a review. Clays and Clay Minerals, 41.

Casselman, M.J., McMillan, W.J., and Newman, K.M., 1995, Highland Valley porphyry copper deposits near Kamloops, British Columbia: A review and update with emphasis on the Valley deposit: Porphyry Deposits of the Northwestern Cordillera of North America: The Canadian Institute of Mining and Metallurgy, Paper 8, p.161 191.

Cathelineau, M., and Nieva, D., 1985, A chlorite solid solution geothermometer the Los Azufres (Mexico) geothermal system. Contributions to Mineralogy and Petrology, 91(3), pp. 235-244.

D'Angelo, M., 2016, Geochemistry, petrography and mineral chemistry of the Guichon Creek and Nicola batholiths, southcentral British Columbia, Lakehead University, unpublished MS.c thesis, 435 p.

D'Angelo, M., Alfaro, M., Hollings, P., Byrne, K., Piercey, S., Creaser, R.A., 2017, Petrogenesis and magmatic evolution of the Guichon Creek Batholith: Implications for the Highland Valley porphyry Cu ± (Mo) district, southcentral British Columbia. Economic Geology (in press).

Deer, W.A., Howie, R.A, and Zussman, J., 1966, AN INTRODUCTION TO THE ROCK FORMING MINERALS, p. 231-241.

Deer, W.A., Howie, R.A., and Zussman, J., 2009, Rock-Forming Minerals, Layered Silicates Excluding Micas and Clay Minerals, v.3B, 2nd edition, p.81-156.

Dilles, J.H., and Einaudi, M.T., 1992, Wall-rock alteration and hydrothermal flow paths about the Ann-Mason porphyry copper deposit, Nevada - A 6-Km Reconstruction: Economic Geology, v.87, p.1963-2001.

Frebold, H., and Tipper, H.W., 1969. Lower Jurassic Rocks and Fauna Near Ashcroft, British Columbia and Their Relation to Some Granitic Plutons (92-I) (Report, 2 Figures and 1 Plate). Department of Energy, Mines and Resources.

Hey, M.H., 1954, A new review of the chlorite: The Mineralogical Magazine, v.30, p.277-292.

Kranidiotis, P., and Maclean, W.H., 1987, Systematics of chlorite alteration at the Phelps Dodge massive sulfide deposit, Matagami, Quebec. Economic Geology, 82(7), pp. 1898-1911.

Lee, Robert G., Lesage, Guillaume., Hart, Craig, J., D'Angelo, Mike., Hollings, Pete., Bryne, Kevin.,Gleeson, Sarah., Grenon, Christophe., Chouteau, Michel., 2015, Defining the 'Footprint' at the Highland Valley Copper deposits, BC; an overview of the CMIC NSERC porphyry Cu subproject: PDAC-SEG Abstracts with Programs.

Lesage, G., Byrne, K., Lee, R.G., Hart, C.J.R., 2017, District-scale porphyry-related hydrothermal alteration and the quantitative use of feldspar staining: the case of Highland Valley Copper, British Columbia, PDAC-SEG Abstracts with Programs.

McMillan, W.J., 1976, Geology and genesis of the Highland Valley ore deposits and the Guichon Creek batholith: In Porphyry Deposits of the Canadian Cordillera: The Canadian Institute of Mining and Metallurgy, Special Volume 15, p.85-104.

McMillan, W.J., 1985, Geology and ore deposits of the Highland Valley camp: Geological Association of Canada, Mineral Deposits Division, Field guide and reference manual series, Number 1, p.1-87.

Mihalynuk, M.G., Nelson, J., Diakow, L.J., 1994, Cache Creek Terrane Entrapment: Oroclinal Paradox Within The Canadian Cordillera. Tectonics 13.3, p. 575-595.

Monger, J.W.H., Price, R.A., and Tempelman-Kluit, D.J., 1982. Tectonic accretion and the origin of the two major metamorphic and plutonic welts in the Canadian Cordillera. Geology, 10(2), pp.70-75.

Monger, J.W.H., and Price, R.A., 1979. Geodynamic evolution of the Canadian Cordillera progress and problems. Canadian Journal of Earth Sciences, 16(3), pp.770-791.

Nelson, J., and Mihalynuk, M., 1993. Cache Creek ocean: Closure or enclosure?, Geology, 21(2), pp.173-176.

Pouchou, J.L., & Pichoir, F., 1985, PAP $\phi(\rho Z)$ procedure for improved quantitative microanalysis. Microbeam Analysis, 1985, 104-106.

Sillitoe, R.H., 2010, Porphyry Copper Systems: Economic Geology, v.105, p.3-41.

Teck Resources Limited (2016) Annual information form, 45 p.

Teck Resources Limited (2017) Annual information form, 117 p.

Wernicke, B., and Klepacki, D.W., 1988. Escape hypothesis for the Stikine block. Geology, 16(5), pp.461-464.

Wilkinson, J.J., Wilkinson, C.C., Vry, V.H., Rusk, B.G., Séguel, J., Zentilli, M. and Jeffries, T.E., 2008. Ore fluid chemistry in super-giant porphyry copper deposits. In Proceedings of the PACRIM 2008 Congress, pp. 295-298.

Wilkinson, J.J., Chang, Z., Cooke, D.R., Baker, M.J., Wilkinson, C.C., Inglis, S., Chen, H. and Gemmell, J.B., 2015. The chlorite proximitor: A new tool for detecting porphyry ore deposits. Journal of Geochemical Exploration, 152, pp.10-26.

Appendix A: Thin Section descriptions

Thin Section ID: MD003A	**UTM Easting: 633013 UTM Northing: 5586244**
Macroscopic Description: Border Phase lithology. White, crystalline background with darker biotite and amphibole **Accessory Minerals/Description** Dominantly plagioclase, K-spar, and amphibole with biotite and quartz. Rutile, apatite, and magnetite are also present. Biotite occurs along the rims of amphibole. Phaneritic, equigranular texture. **Metamorphic Minerals** Biotite alteration and chlorite alteration with light sericite dusting. **Type of Alteration:** Regional metamorphic	**Chlorite** **Texture/Habit** Anhedral linear formation among cleavage planes of biotite. Chlorite is fine-grained and forms as selvage along the cleavage planes after infilling them. Chlorite is fibrous and sinuous within actinolite crystals and needle-like within biotite. **Host** Forms replacement of actinolite and hornblende with minor biotite replacement. Biotite forms as amphibole replacement and is then altered to chlorite along its rims. **Colour** Chlorite is colourless to weak green in PPL. **Intensity** Chlorite intensity is very weak and not pervasive. It appears minorly in cleavage planes and on the rims of biotite. It makes up trace amounts of the total thin section. **Birefringence** Birefringence is deep brown with a trace amount of lilac.

Thin Section ID: MD004	**UTM Easting: 634574 UTM Northing: 5586650**
Macroscopic Description: Bethsaida – Monzogranite. Clear, white background with brown phenocrysts **Accessory Minerals/Description** Dominated by quartz and plagioclase with interstitial K-spar. Epidote occurs as aggregates parallel to cleavage planes of biotite crystals. There are minor zircon inclusions. **Metamorphic Minerals** Chlorite **Type of Alteration:** Regional Metamorphic	**Chlorite** **Texture/Habit** Chlorite is fine-grained to very fine-grained and fibrous within actinolite crystals. They are sub to anhedral and occur along cleavage planes. Within biotite they are thick and needle-like. **Host** Chlorite is pervasively replacing actinolite and includes very fine-grained inclusions of zircon. Chlorite also occurs within biotite on the edge of amphibole. There is no evidence of hornblende. **Colour** Chlorite is pleochroic light green. **Intensity** Chlorite shows a high degree of replacement of host mineral, sometimes having replaced >50% of the host. Replacement is identified through pleochroism **Birefringence** Chlorite shows deep birefringent brown colours.

Thin Section ID: MD035	**UTM Easting: 637545.1 UTM Northing: 5596507**
Macroscopic Description: Clear background showing biotite and hornblende crystals. Part of the Skeena facies. **Accessory Minerals/Description** Plagioclase, quartz, and K-spar dominant. Minor amphibole and biotite present. Chlorite is present with epidote and titanite in minor amounts. **Metamorphic Minerals** Chlorite **Type of Alteration:** Regional metamorphism	**Chlorite** **Texture/Habit** Chlorite is anhedral and fine to very-fine grained in biotite. It appears as needle aggregates and is somewhat fibrous. Chlorite is fine-grained in hornblende and shows a patchy, block-like texture. **Host** Chlorite predominantly replaces biotite and hornblende. In biotite, it appears in the cleavage planes and along the rims. In hornblende, it appears in cleavage planes and very rarely on the edge of the phenocryst. **Colour** Chlorite is colourless to weak green pleochroic with it being slightly stronger in biotite. **Intensity** Chlorite varies in intensity but is pervasive in most biotite crystals. It shows heavy alteration and almost complete replacement in some. It is less pervasive in hornblende. **Birefringence** Chlorite shows strong brown birefringence.

Thin Section ID: MD057	**UTM Easting: 651124 UTM Northing: 5595137**
Macroscopic Description: Composed of clear plagioclase, quartz, and K-spar with small amounts of amphibole and biotite. Border Phase. **Accessory Minerals/Description** Primarily euhedral plagioclase with hornblende and biotite. Minor amounts of K-spar with trace titanite and rutile. **Metamorphic Minerals** Chlorite with sericite dusting and minor clay alteration. **Type of Alteration** Regional Metamorphic.	**Chlorite** **Texture/Habit** Chlorite is not pervasive and is very fine-grained. It appears as needle-like aggregates in biotite and patchy within hornblende. It is subhedral to anhedral. **Host** Chlorite is hosted predominantly in biotite. There is a minor amount of hornblende alteration but mainly hornblende first alters to biotite and then to chlorite. It is concentrated on the rims of biotite. **Colour** Colourless to light green in PPL. **Intensity** Chlorite is not pervasive and appears as trace amounts through the sample. **Birefringence** Chlorite is birefringent brown and has very minor lilac alteration.

Thin Section ID: MD060	**UTM Easting: 640557 UTM Northing: 5598038**
Macroscopic Description: White background of plagioclase and quartz. Green mineral is high in abundance. Bethlehem phase. **Accessory Minerals/Description** Dominant plagioclase with interstitial quartz. K-spar is present throughout with minor amounts of hornblende and biotite. **Metamorphic Minerals** Chlorite with minor clay alteration **Type of Alteration:** Regional metamorphic	**Chlorite** **Texture/Habit** Chlorite is fine-grained within biotites and patchy within hornblende. In less altered crystals it appears somewhat fibrous, but grades into a patchy, block-like appearance in pseudomorphs or hornblende. It is fine-grained in hornblende. **Host** Chlorite appears in both hornblende and biotite crystals. Chlorite is associated with epidote and titanite. **Colour** Chlorite is colourless to pale green in PPL and shows slightly stronger pleochroism in biotite then hornblende. **Intensity** Chlorite is pervasive throughout the sample and ranges from a few percent replacement to almost complete replacement of biotite crystals. It is less pervasive in hornblende crystals. **Birefringence** Chlorite shows dominant brown birefringence with minor lilac colours showing zoning in the chlorite samples.

Thin Section ID: BC14185G	**UTM Easting: 635305.605 UTM Northing: 5592915**
Macroscopic Description: Bethsaida facies **Accessory Minerals/Description** Plagioclase and K-spar dominant. Minor amounts of amphibole shown. Small biotite replacing amphibole. **Metamorphic Minerals** Chlorite with sericite dusting and minor amounts of carbonate **Type of Alteration:** Propylitic	**Chlorite** **Texture/Habit** Needle like aggregates forming throughout biotite cleavage planes. Chlorite is very fine to fine-grained. Appears as needles throughout actinolite or blocky on the edge of the grain. **Host** Chlorite predominantly replaces actinolite. Chlorite also replaces biotite which is replacing amphibole. In some places, we can see all three stages of replacement. **Colour** Colourless to pale green, slightly stronger than previous samples **Intensity** Chlorite is pervasive throughout the sample and is highly visible due to pleochroism. Chlorite shows high relief on the edge of crystal. **Birefringence** Birefringent brown with minor amounts of anomalous lilac colours.

Thin Section ID: BC14202H	**UTM Easting: 635690.666 UTM Northing: 559215.365**
Macroscopic Description: Large portion of white feldspars and quartz background with 10% biotite and 5% amphibole. **Accessory Minerals/Description** Dominated by feldspars and quartz with a minor amount of amphibole and opaques **Metamorphic Minerals** Muscovite is present through the feldspars, which also show sericite dusting. Chlorite is present in amphibole and biotite. **Type of Alteration:** Propylitic	**Chlorite** **Texture/Habit** Chlorite is fine-grained and fibrous within amphibole and appears along needly muscovite. It appears as sinuous waves within amphibole. Within biotite, chlorite is linear and appears within the cleavage planes. **Host** Chlorite is replacing biotite and actinolite with no evidence of hornblende replacement. Chlorite is not appearing on the rims but is found exclusively within the cleavage planes. **Colour** Chlorite is pleochroic pale green and slightly weaker than in other samples from the same transect. **Intensity** Chlorite is less pronounced and is intergrown with muscovite. It is not pervasive in this sample and makes up a minor amount of the sample. **Birefringence** Chlorite is showing variable birefringence with deep brown and minor anomalous lilac colour.

Thin Section ID: BC14187A	**UTM Easting: 635527.784 UTM Northing: 559301.647**
Macroscopic Description: Predominantly made up of feldspar with green amphibole and biotite. Lighter green mineral could show chlorite. **Accessory Minerals/Description** K-spar, plagioclase, and quartz. Actinolite occurs as 10% and alters to biotite. **Metamorphic Minerals** Sericite dusting across feldspars and muscovite found along cleavage planes. Chlorite forms through alteration of actinolite. **Type of Alteration:** Propylitic	**Chlorite** **Texture/Habit** Texture is less fibrous than before. Grains are generally euhedral and chlorite is fine to very-fine grained. Chlorite appears in two stages of replacement, with one appearing more radiating than the other. **Host** Chlorite appears to be replacing actinolite along with biotite at the same time. Chlorite appears as blocks on the rims of amphibole. In biotite is it more striated and forms near K-spar and quartz crystals. **Colour** Colourless to pale green in PPL **Intensity** Chlorite is very intense and pervasive. Most amphiboles and biotites have been at least partially replaced by chlorite. **Birefringence** Birefringence is a deep brown colour.

Thin Section ID: BC1484G/H	**UTM Easting: 635279.387 UTM Northing: 5592310.353**
Macroscopic Description: Bethsaida facies – white crystalline background of feldspars and quartz **Accessory Minerals/Description** Large euhedral plagioclase and K-spar with amphibole. **Metamorphic Minerals** Sericite dusting with chlorite as replacement mineral. **Type of Alteration:** Propylitic	**Chlorite** **Texture/Habit** Fibrous to rectangular in different grains. Needle-like in cleavage planes but appears patchier in actinolite and hornblende. Shows almost completion of a chlorite pseudomorph making it range from very fine to medium-grained. **Host** Chlorite infills the cleavages of amphibole hosts and expands along fracture planes. It is found with some white mica over printing it. It predominantly replaces actinolite and hornblende, not biotite in this sample. **Colour** Chlorite is colourless to moderate green in this sample. **Intensity** Chlorite shows various stage of intensity ranging from a few percent to almost replacing a whole amphibole crystal. Relief is low. **Birefringence** Chlorite shows strong brown birefringence with minor amounts of lilac colour.

Thin Section ID: BC14213B	**UTM Easting: 636570.248 UTM Northing: 5591263.248**
Macroscopic Description: Equigranular feldspars, quartz, with minor black and green minerals. **Accessory Minerals/Description** Interlocking quartz and feldspars dominate. Small grains of carbonate can be seen. There are small opaques present. **Metamorphic Minerals** Pervasive sericite dusting with muscovite and chlorite. **Type of Alteration:** Sodic-calcic	**Chlorite** **Texture/Habit** Chlorite is fine-grained and present throughout the whole host. It shows sinuous habit in actinolite and pervasive replacement of biotite. **Host** Chlorite completely replaces a biotite crystal and shows minor amounts of actinolite alteration. It is associated with epidote inclusions in parts. **Colour** Chlorite shows weak pleochroism. **Intensity** Chlorite is pervasive throughout the whole sample and is present in all biotite crystals. **Birefringence** Chlorite shows deep brown birefringence.

Thin Section ID: BC14124A	**UTM Easting: 637058.544 UTM Northing: 5591933.769**
Macroscopic Description: Composed of dominantly feldspars with green and black amphibole inclusions. **Accessory Minerals/Description** ~90% quartz, Kspar, and plagioclase. Grains are interlocking with fine-grained fractures running through the system **Metamorphic Minerals** Muscovite, sericite, and chlorite. **Type of Alteration:** Sodic-calcic	**Chlorite** **Texture/Habit** Chlorite is fine-grained and subhedral. It is shown both in the cleavage planes of the host and pervasively replacing the grain. When replacing actinolite it shows a characteristic felty/fibrous texture. **Host** Chlorite is replacing biotite and actinolite throughout the section. It appears proximal to K-spar crystals, and has intergrown titanite with minor epidote. It appear son biotite rims and cleavage planes. **Colour** Chlorite is weak to colourless green in PPL **Intensity** Chlorite is replacing most of the original crystal in some phenocrysts and is always present to some degree, even in a euhedral biotite. Different stages of replacement show different intensity. **Birefringence** Chlorite is birefringent brown, with no anomalous lilac showing.

Thin Section ID: BC14318A	**UTM Easting: 632722.5447 UTM Northing: 5597417.29**
Macroscopic Description: White crystalline background of feldspars and quartz with 25% amphibole and minor black mineral inclusions. **Accessory Minerals/Description** Plagioclase interlocking with Kspar and quartz with hexagonal inclusions of rutile (?). Actinolite and subhedral biotite present. **Metamorphic Minerals** Sericite, chlorite, and hydrothermal muscovite **Type of Alteration:** Sodic-calcic	**Chlorite** **Texture/Habit** Chlorite is fine-grained and fibrous and sometimes radiating in needle-like habit. In actinolite is appears fibrous, whereas in hornblende it is patchy. **Host** Chlorite appears within both actinolite and hornblende, as well as on the edges of anhedral biotite grains. Hornblende can be seen altering to actinolite, which in turn alters to chlorite. We can also see some prehnite and epidote associated with the alteration. **Colour** Chlorite shows extremely weak to no pleochroism in this sample. **Intensity** Chlorite is pervasive throughout the sample but predominantly replaces actinolite to a high degree and minor amounts of hornblende **Birefringence** Chlorite shows dominant brown birefringence.

Thin Section ID: BC14334	**UTM Easting: 632302.095 UTM Northing: 5598373.383**
Macroscopic Description: Sample is composed of predominantly crystalline background of quartz and feldspars with minor amount of green mineral. **Accessory Minerals/Description** Dominantly Kspar with quartz and plagioclase with actinolite and minor biotite. **Metamorphic Minerals** Carbonate/sericite/chlorite **Type of Alteration:** Propylitic	**Chlorite** **Texture/Habit** Chlorite is very fine-grained and shows a fibrous habit within amphibole. **Host** Chlorite is predominantly replacing actinolite. It occurs with highly birefingent minerals such as prehnite and calcite. Small biotite grains show high amounts of chlorite alteration. **Colour** Chlorite shows weak to moderate green pleochroism in PPL. **Intensity** Chlorite is pervasive throughout the whole sample and shows varying intensity depending on the host; it is stronger in actinolite than biotite. **Birefringence** Chlorite shows strong brown birefringence

Thin Section ID: BC14325 H/G	**UTM Easting: 632253.392 UTM Northing: 5597698.184**
Macroscopic Description: White crystalline background with actinolite and brown biotite. Lighter green shows chlorite. **Accessory Minerals/Description** Dominantly plagioclase and kspar with quartz. Actinolite with some altered biotite but also fresh euhedral biotite that is unaltered. **Metamorphic Minerals** Chlorite and sericite dusting with hydrothermal muscovite and minor clay alteration. **Type of Alteration:** Sodic-calcic	**Chlorite** **Texture/Habit** Chlorite is fine-grained to extremely fine grained. Most chlorite is euhedral with light dusting on top. It appears in laths on the edge of altered biotite and fibrous within actinolite. In hornblende, it is as needle aggregates on the cleavage planes and not on the edge of the host. **Host** Chlorite is replacing actinolite that has also altered to biotite and appears on the edges and cleavage of the grain. Secondary biotite appears on the edge of hornblende as well and is altering to chlorite. **Colour** Colourless to pale green in PPL **Intensity** Not intense throughout the sample. It is not common and is often covered by sericite dusting. **Birefringence** Chlorite is deep brown in most crystals with very minor lilac in some biotite.

Thin Section ID: BC14333A	**UTM Easting: 631857.6325 UTM Northing: 5598423.301**
Macroscopic Description: Mainly composed of white feldspars/quartz with green and black phenocrysts. **Accessory Minerals/Description** Mainly quartz, Kspar and plagioclase with a large amount of actinolite and hornblende. **Metamorphic Minerals** Chlorite and sericite dusting with lots of clay alteration **Type of Alteration:** Sodic-calcic/Propylitic	**Chlorite** **Texture/Habit** Chlorite appears as sinuous habit within actinolite and is fibrous. It is very grained to fine-grained and shows patchy sections on the edge of hornblende with needle-like aggregates within the hornblende cleavage planes. **Host** Chlorite replaces both actinolite and hornblende with small evidence of biotite alteration. **Colour** Chlorite is faintly pleochroic from colourless to light green. **Intensity** Chlorite is pervasive throughout the sample varying in intensity. In some cases, chlorite has altered >50% of actinolite but shows minor amount of alteration in hornblende, making up only trace amounts of the crystal. **Birefringence** Chlorite is deep brown in actinolite and hornblende. It shows trace amounts of lilac in biotite.

Thin Section ID: BC14342H	**UTM Easting: 631804.2965 UTM Northing: 5599444.828**
Macroscopic Description: Background of white crystalline material mainly composed of feldspars and quartz with a high percentage of green amphibole and black opaques. **Accessory Minerals/Description** Interlocking plagioclase/Kspar/quartz. Kspar is altered. High percentage of amphibole present in high amounts. **Metamorphic Minerals** Lots of sericite and carbonate alterations. Hydrothermal muscovite and chlorite. **Type of Alteration:** Sodic-calcic/propylitic	**Chlorite** **Texture/Habit** Chlorite is fine-grained and fibrous within actinolite. In hornblende, appears as needle like aggregates in a few of the cleavage planes. **Host** Chlorite is replacing biotite, actinolite, and hornblende in this sample. However, it only replaces small portions of the grain and is not pervasive. It is not intergrown with muscovite and appears in early stages of alteration. **Colour** Chlorite shows weak pleochroism from colourless to pale green. **Intensity** Chlorite is not pervasive throughout the sample and grains show weak replacement. **Birefringence** Birefringence is deep brown.

Thin Section ID: RL14HVC02	**UTM Easting: 637290.171 UTM Northing: 5593546.717**
Macroscopic Description: Crystalline background with sulphide stringers. **Accessory Minerals/Description** Large quartz phenocrysts with muscovite. Small localized veins of quartz and muscovite with some K-spar. **Metamorphic Minerals** Muscovite and sericite alteration with chlorite **Type of Alteration:** Valley assemblage	**Chlorite** **Texture/Habit** Chlorite appears as fine-grained to extremely fine grained subhedral needle aggregates that form fan structures near muscovite. (20x) lens and has an irregular structure, growing in all directions **Host** Chlorite appears a secondary mineral directly from the hydrothermal fluid interaction with muscovite. It appears predominantly near sulfide grains/stringers and it is hard to tell what the host mineral is. **Colour** Chlorite is colourless to moderate green in PPL. **Intensity** Chlorite is present throughout the sample, mainly as part of the vein assemblage. **Birefringence** Chlorite is pale brown to anomalous lilac birefringence showing zoning.

Thin Section ID: RL14HVC03	**UTM Easting: 637304.901 UTM Northing: 5593546.717**
Macroscopic Description: White feldspar background with green phenocrysts and larger light green patches. **Accessory Minerals/Description** Hornblende being altered to actinolite with feldspars and muscovite also present. **Metamorphic Minerals** Sericite/chlorite/muscovite **Type of Alteration:** Valley assemblage	**Chlorite** **Texture/Habit** Chlorite is fine-grained and fibrous within actinolite and patchy within hornblende. It is not pervasive throughout the sample. **Host** Chlorite is mainly replacing actinolite but also directly replaces hornblende. It infills cleavage planes and replaces the rims of actinolite and on the edges of hornblende. **Colour** Colourless to pale green in PPL **Intensity** Weak replacement of hornblende crystals as well hydrothermal actinolite. Not pervasive throughout the sample. **Birefringence** Strong brown birefringence.

Thin Section ID: RL14HVC05	**UTM Easting: 637469.922 UTM Northing: 5593321.973**
Macroscopic Description: Quartz background with feldspars and light green minerals with ~15% sulfides **Accessory Minerals/Description** Quartz with sulfides, feldspars, actinolite, and some biotite with a degree of alteration. **Metamorphic Minerals** Muscovite, sericite, and chlorite **Type of Alteration:** Valley assemblage	**Chlorite** **Texture/Habit** Chlorite is fine-grained, blocky, and fibrous within actinolite. There is small needles within hornblende and biotite. **Host** Chlorite appears to predominantly replace biotite and actinolite with small replacement of hornblende. It is often intergrown with muscovite. **Colour** Colourless to moderate green in PPL. **Intensity** Chlorite is pervasive throughout the sample and most biotite is almost fully replaced. Intensity is less within hornblende. **Birefringence** Variable birefringence from light brown to anomalous lilac.

Thin Section ID: RL14HVC12	**UTM Easting: 638760.660 UTM Northing: 5595432.454**
Macroscopic Description: White quartz background with 30% sulfide veins and stringers **Accessory Minerals/Description** Mainly composed of quartz phenocrysts set in a muscovite groundmass. Muscovite is radiating with an irregular habit. Sulfide veins appear as opaques. Hornblende alters to actinolite. **Metamorphic Minerals** Muscovite/sericite/chlorite **Type of Alteration:** Valley assemblage	**Chlorite** **Texture/Habit** Chlorite is extremely fine-grained and needle like aggregates intergrown with muscovite. It is viewed with the 20x lens and makes up part of the groundmass. **Host** Chlorite, although not pervasive, appears form fluid interaction and makes up part of the groundmass. It appears on the edge of sulfide veins and is intergrown with muscovite. It is anhedral and the host cannot be determined. **Colour** Strong pleochroism from colourless to moderate green. **Intensity** Chlorite is present throughout the sample in minor amounts of the groundmass but is hard to identify due to small grain size. **Birefringence** Chlorite is light brown but also shows signs of speckled lilac colour.

Thin Section ID: RL14HVC17	**UTM Easting: 638225.506 UTM Northing: 5593954.038**
Macroscopic Description: Quartz and plagioclase background with minor sulfides and ~40% green mineral. **Accessory Minerals/Description** Quartz and plagioclase with remnant hornblende (identifiable due to cleavage). Large muscovite vein cross cuts sample. **Metamorphic Minerals** Muscovite, chlorite, sericite, with clay alteration **Type of Alteration:** Valley assemblage.	**Chlorite** **Texture/Habit** Chlorite is fine-grained and fibrous appearing in what appears to be actinolite. It shows a felty texture. Chlorite is anhedral. **Host** It is hard to tell what chlorite is replacing due to the anhedral nature of the grains but it appears to be actinolite. No evidence of hornblende alteration and no biotite appears present in this sample. Chlorite appears on actinolite rims. **Colour** Colourless to moderate green throughout. **Intensity** Chlorite is present throughout the sample in the high percentage of actinolite present. **Birefringence** Birefringence is brown with some minor amounts anomalous lilac.

Thin Section ID: RL14HVC14	**UTM Easting: 638225.506 UTM Northing: 5593954.038**
Macroscopic Description: White quartz, feldspar background with green minerals. Vein runs through thin section. **Accessory Minerals/Description** Quartz and plagioclase dominant with actinolite and biotite present with minor sulfides. **Metamorphic Minerals** Muscovite/sericite/chlorite **Type of Alteration:** Valley assemblage	**Chlorite** **Texture/Habit** Chlorite is extremely fine-grained to fine grained and fibrous within actinolite. It appears as needles within biotite, and shows an extremely fine grained fan structure when intergrown with vein material. **Host** Chlorite is hard to identify but is present in small amounts within actinolite and biotite as well as in vein material. **Colour** Colourless to moderate green in PPL. **Intensity** Chlorite is not pervasive and is hard to pick out in sample. **Birefringence** Chlorite shows brown birefringence with zoned lilac within vein material and in actinolite hosts.

Appendix B: Backscatter Images

MD004

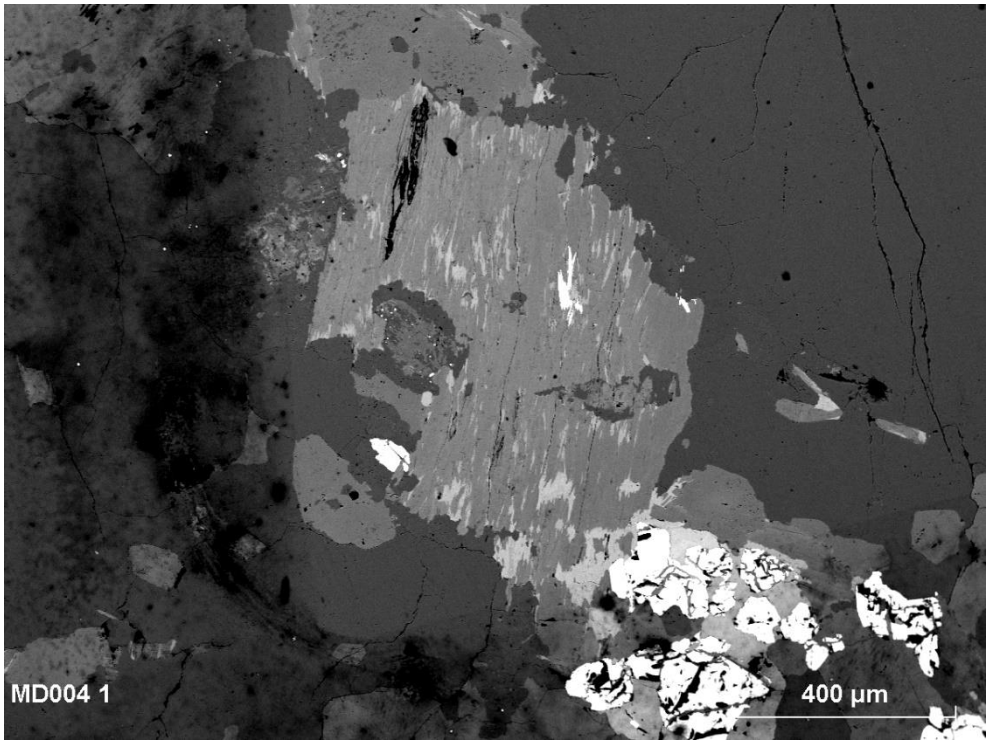

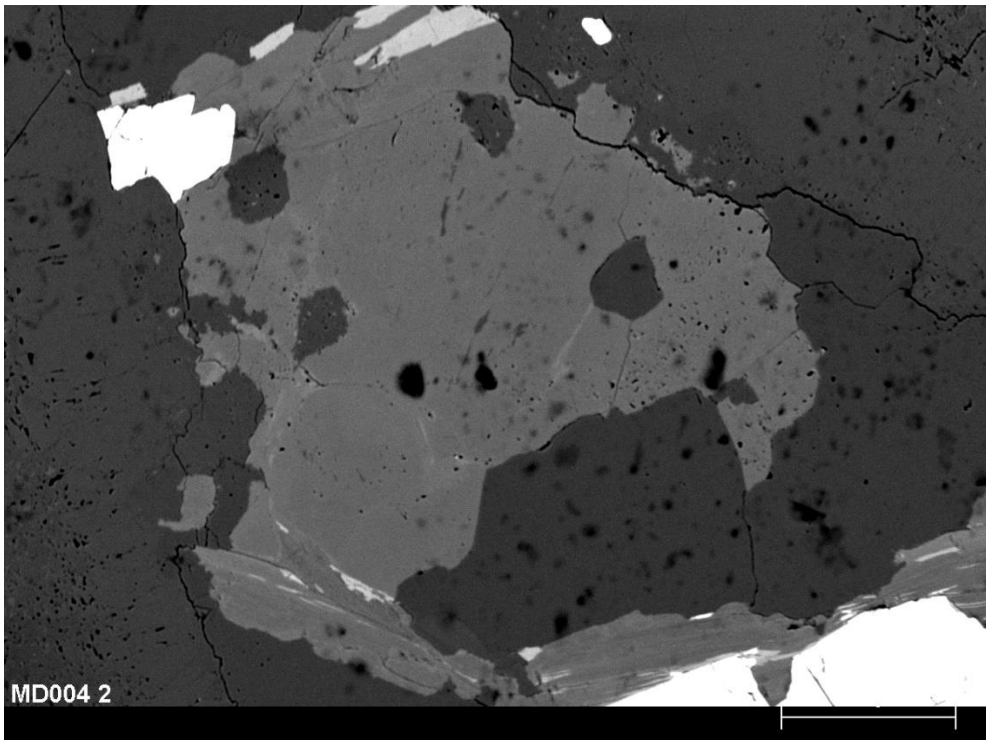

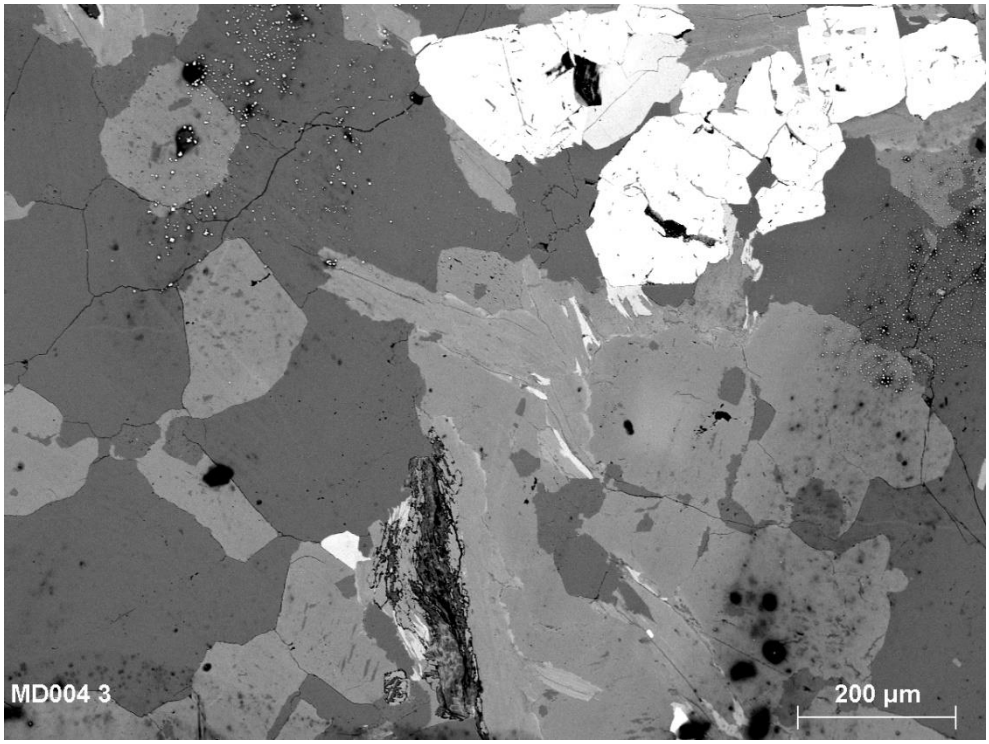
MD004 3
200 µm

MD060

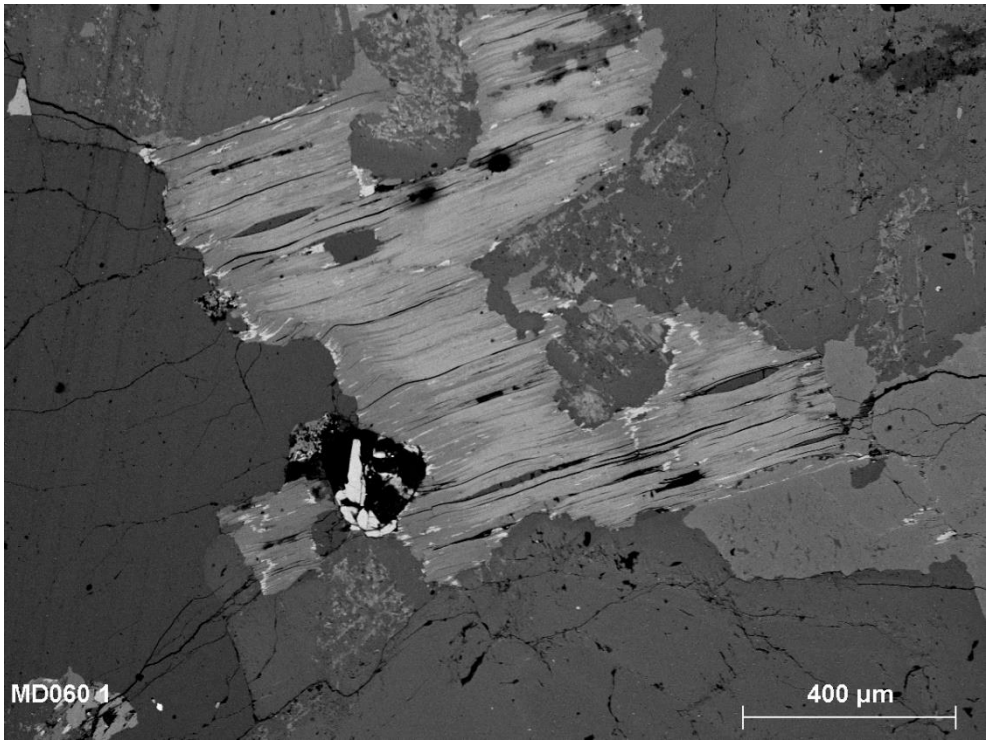

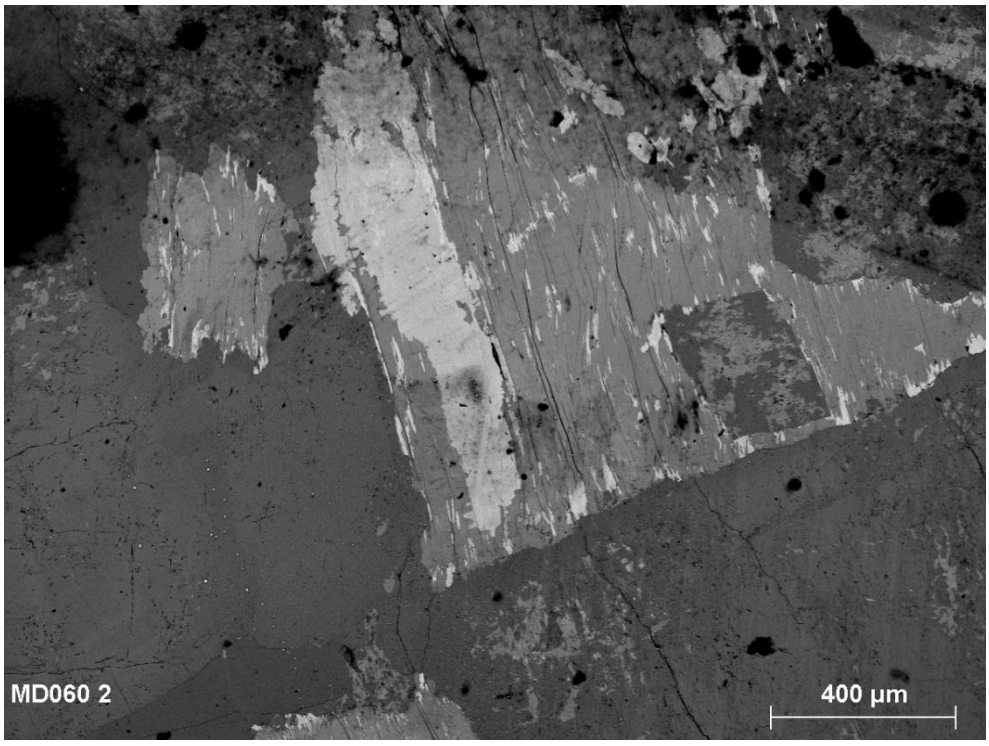

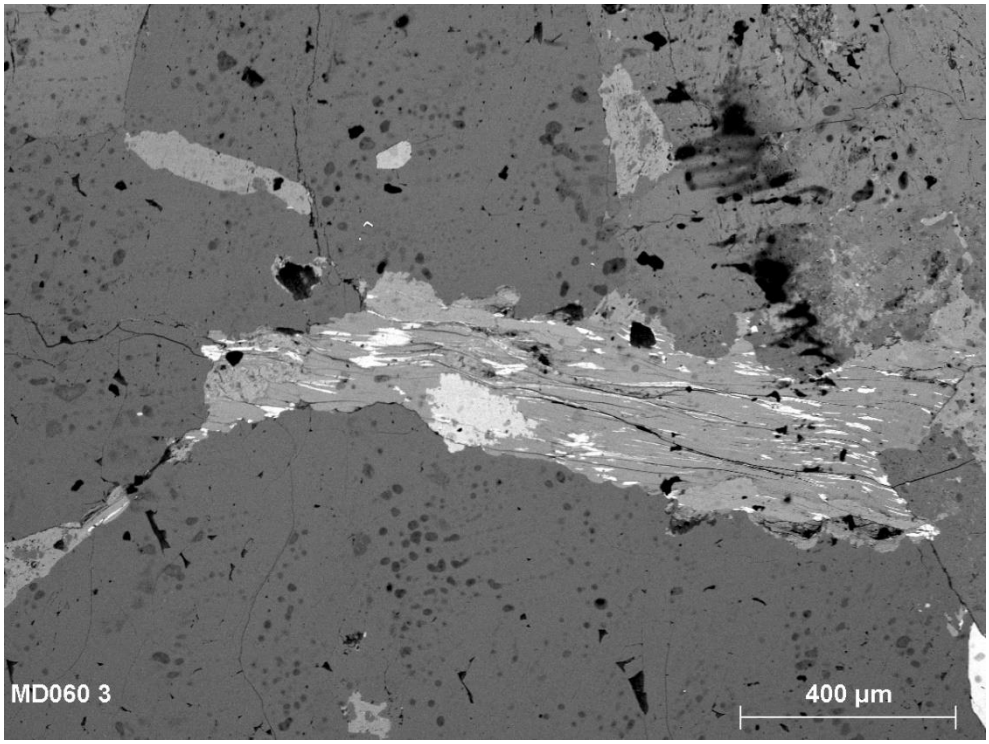
MD060 3
400 µm

BC14124A

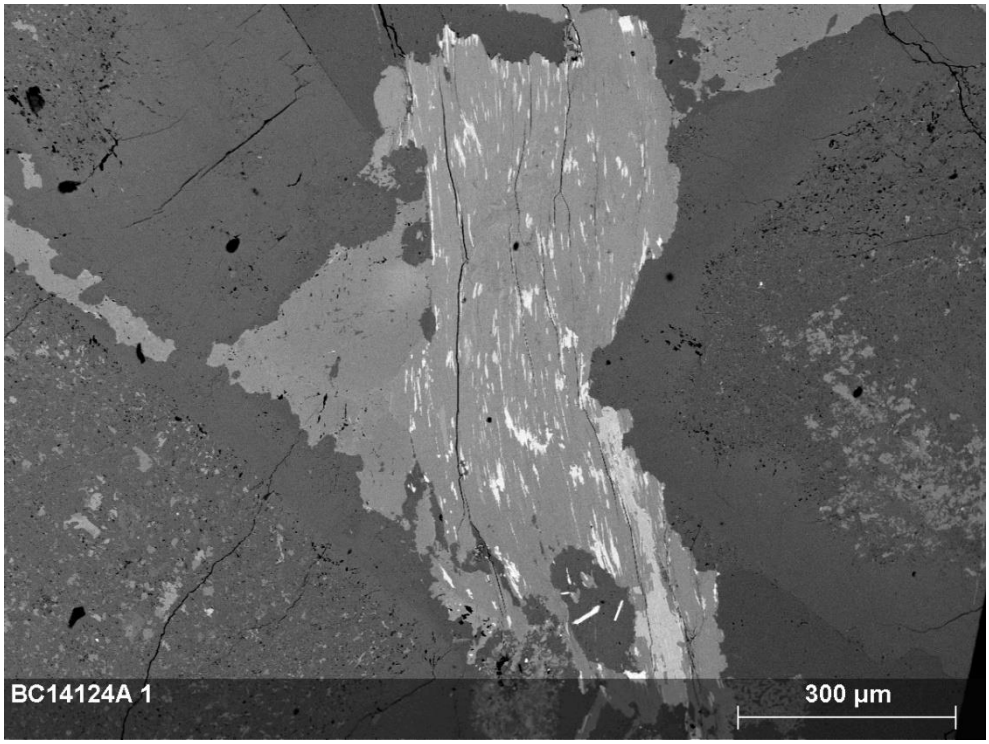

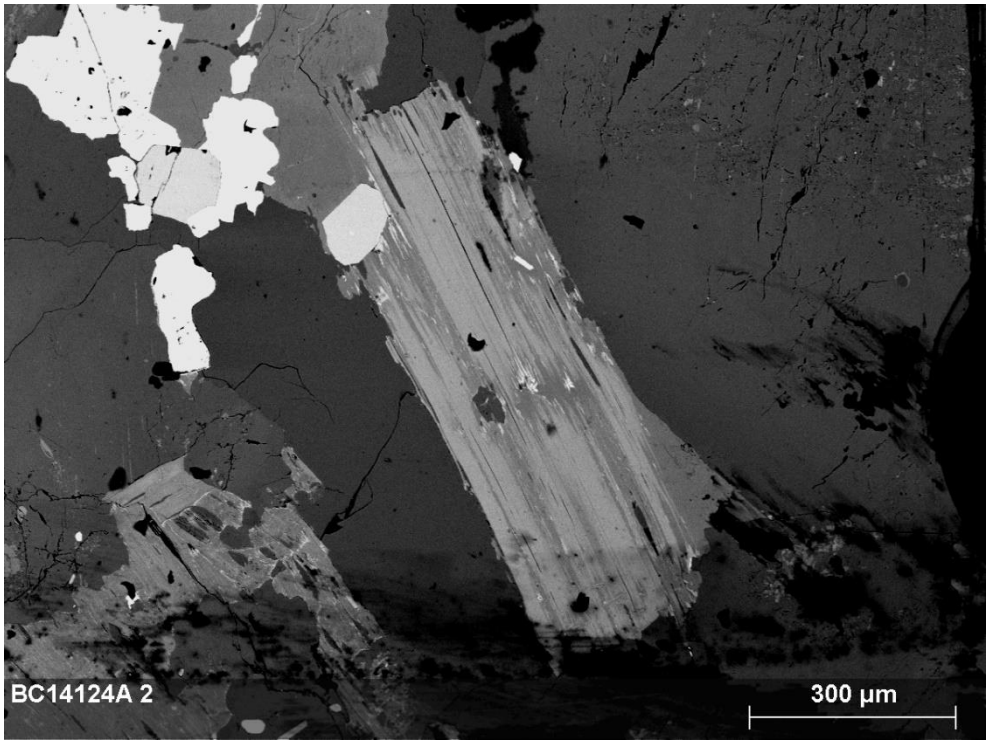

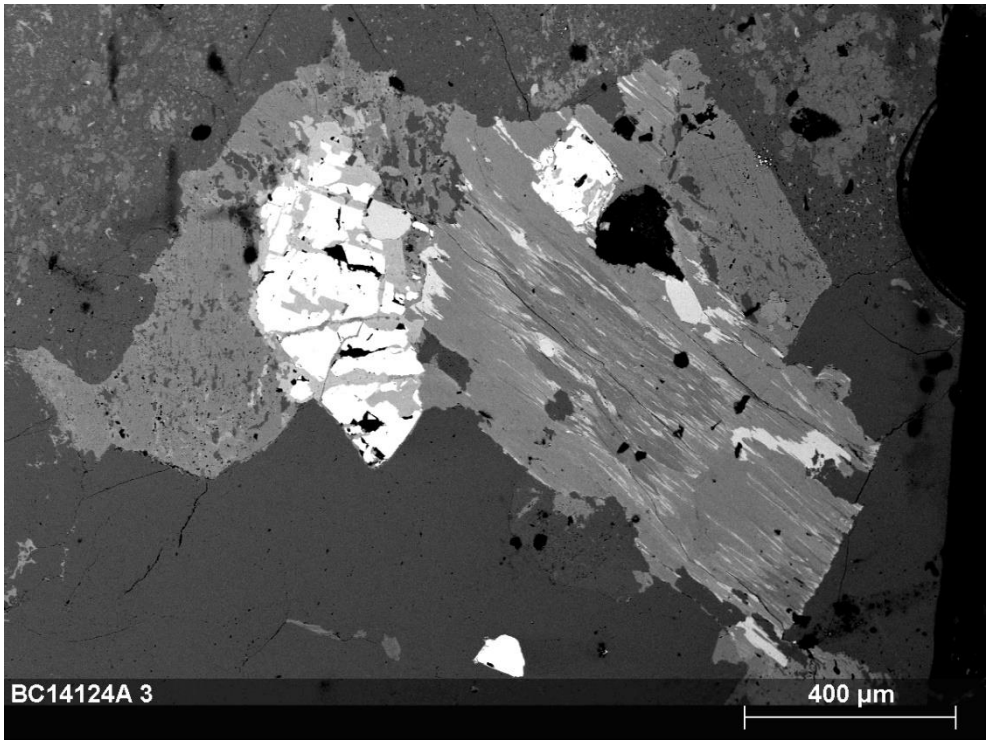
BC14124A 3
400 µm

BC14184G

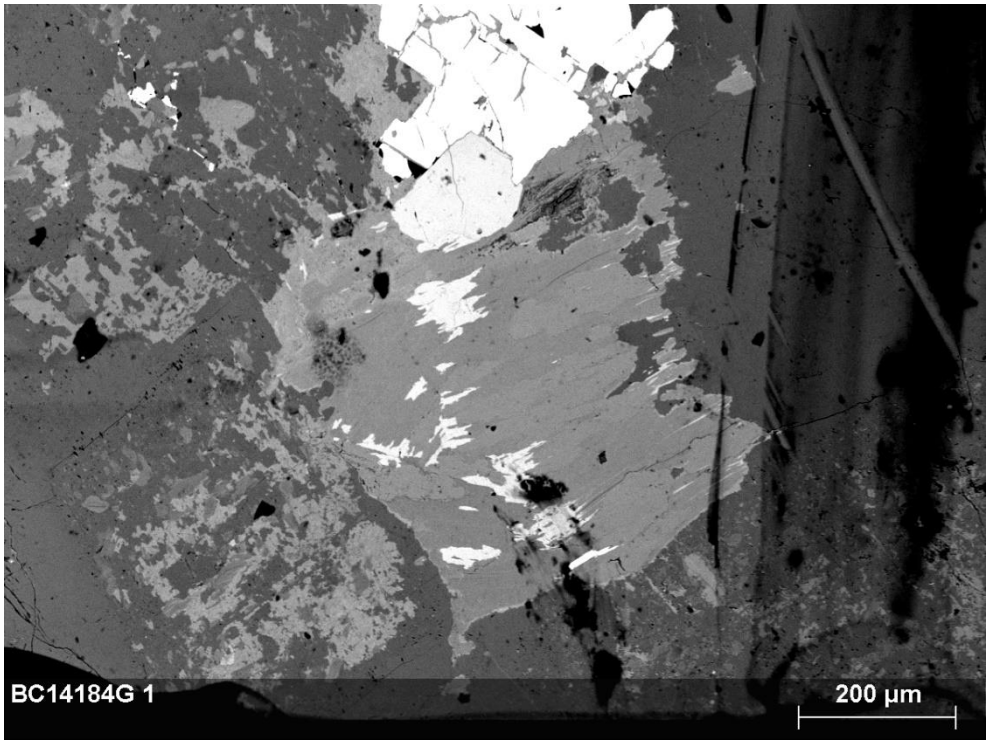

BC14187A

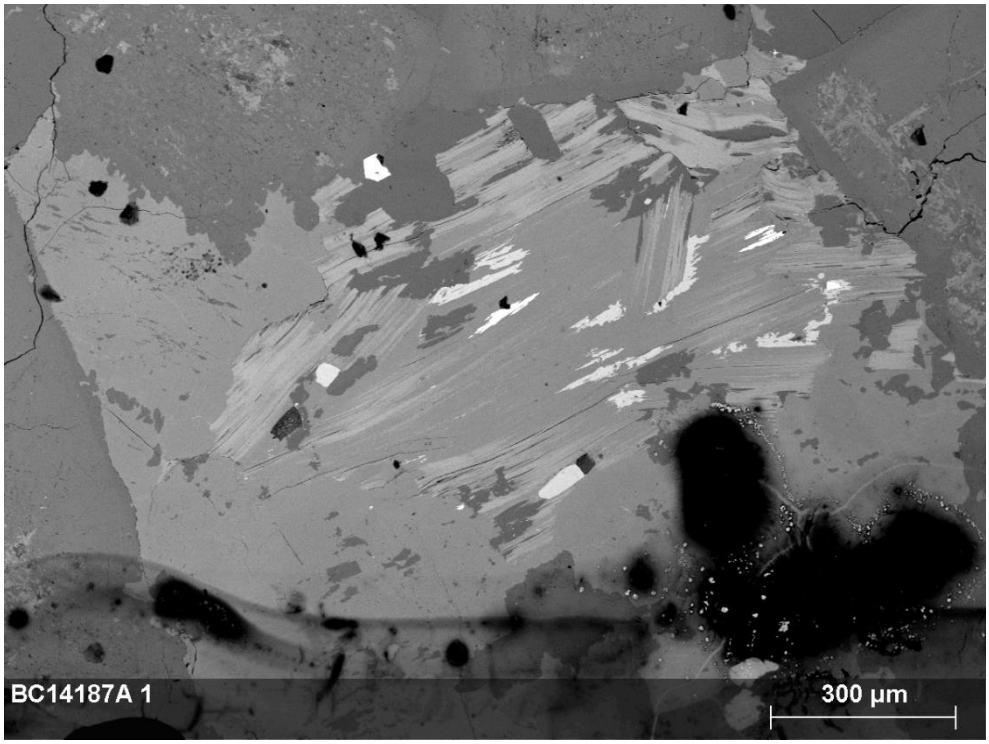

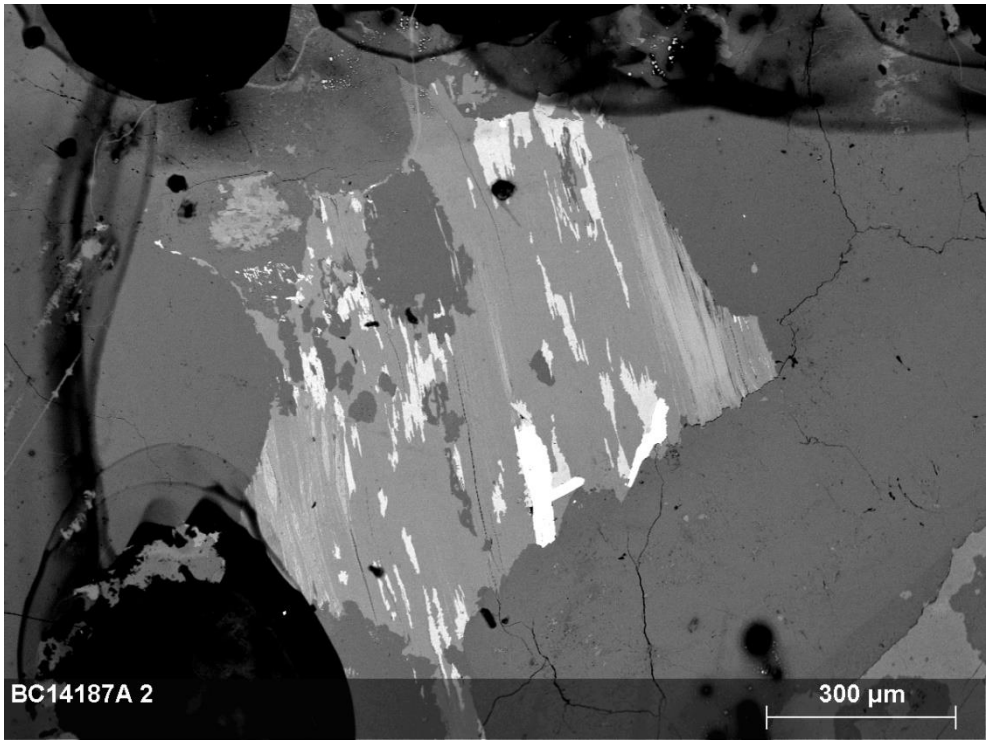

BC14318A

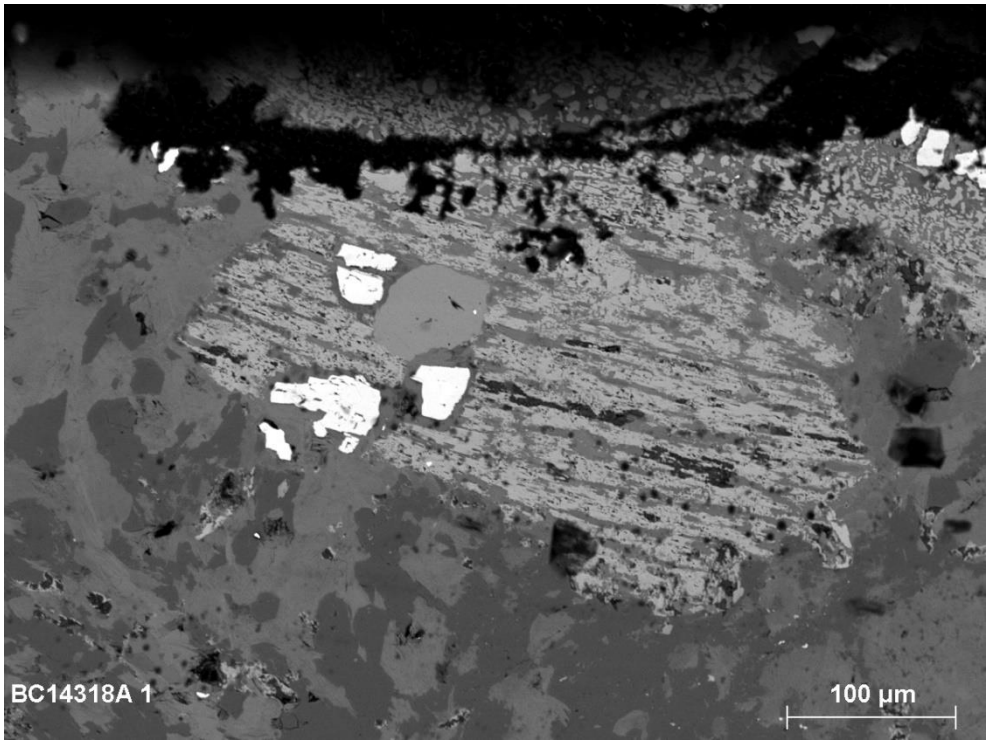

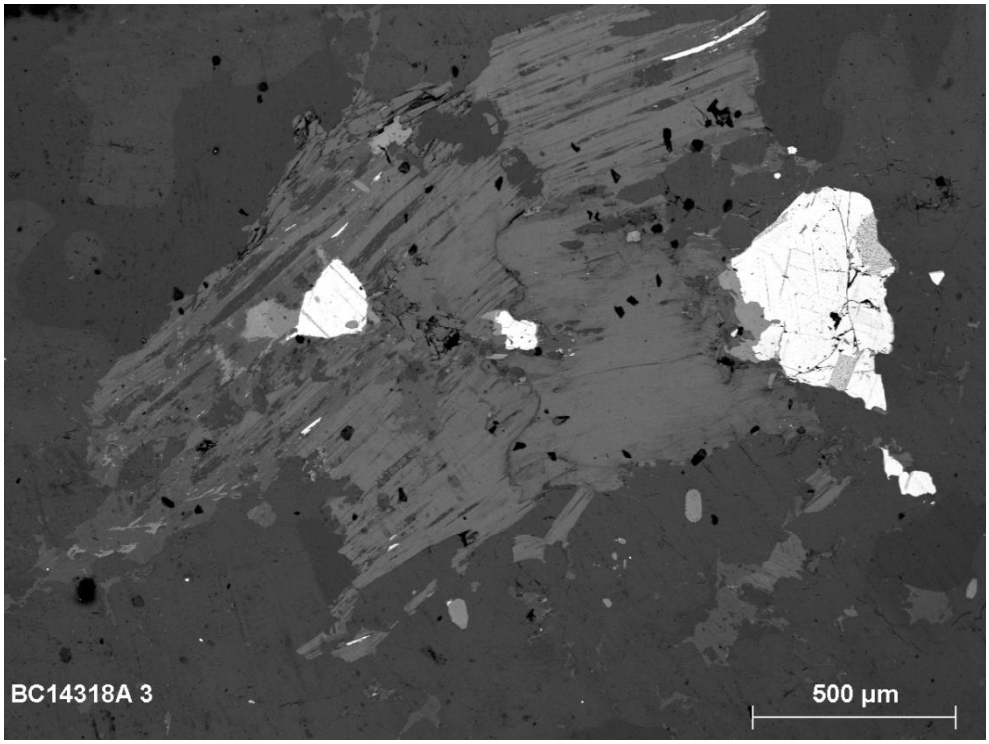

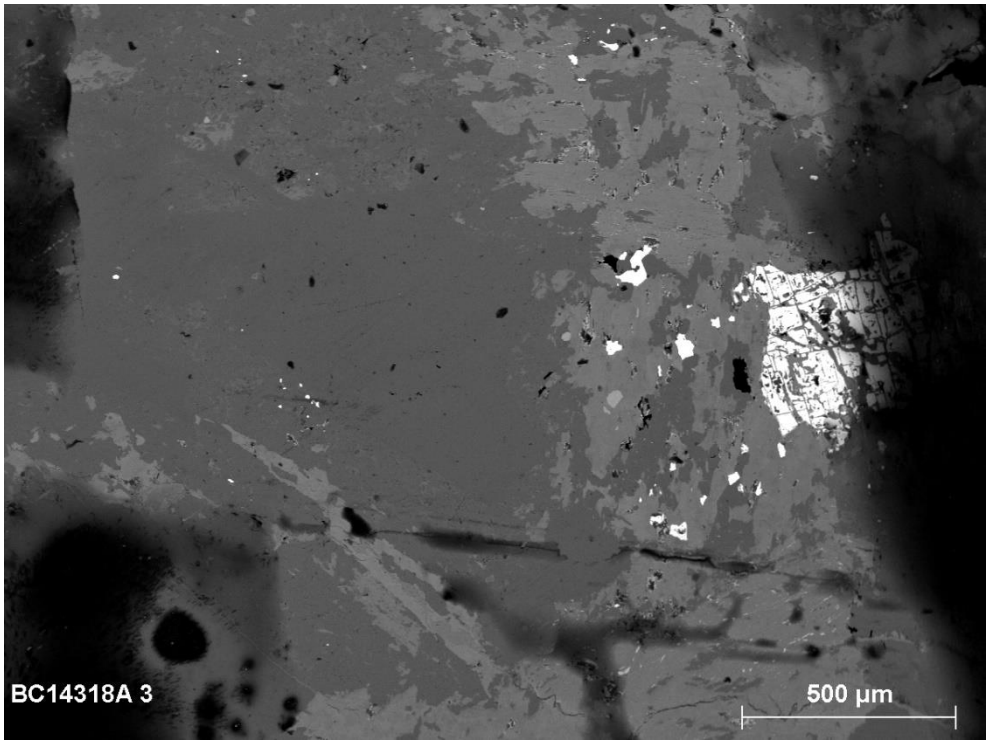
BC14318A 3
500 µm

BC14213B (2238783)

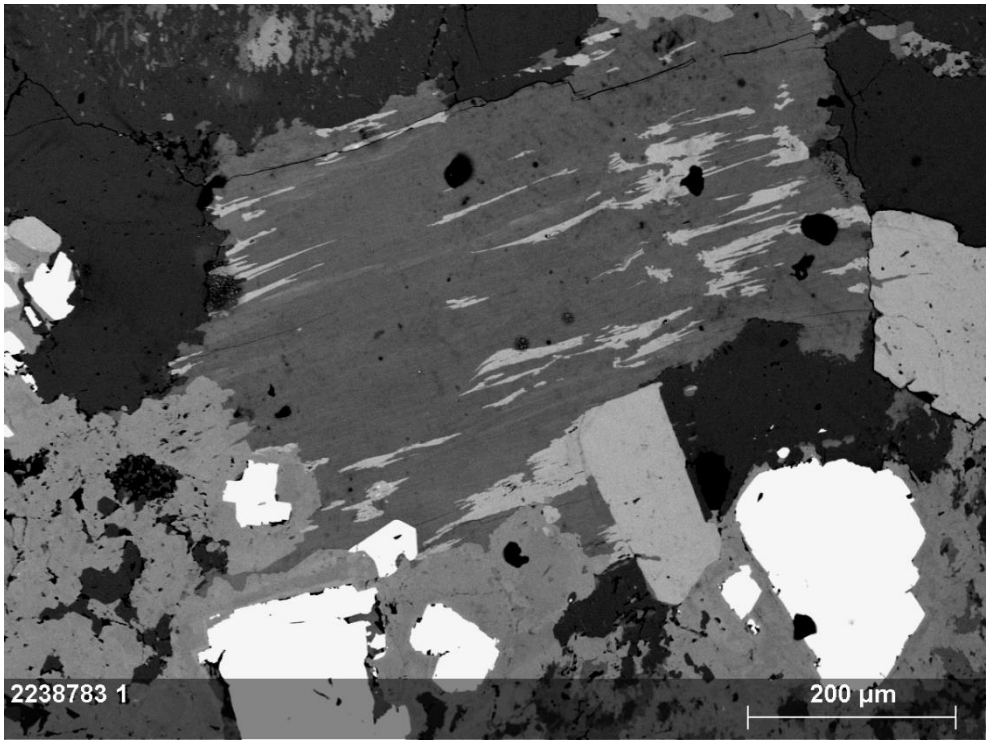

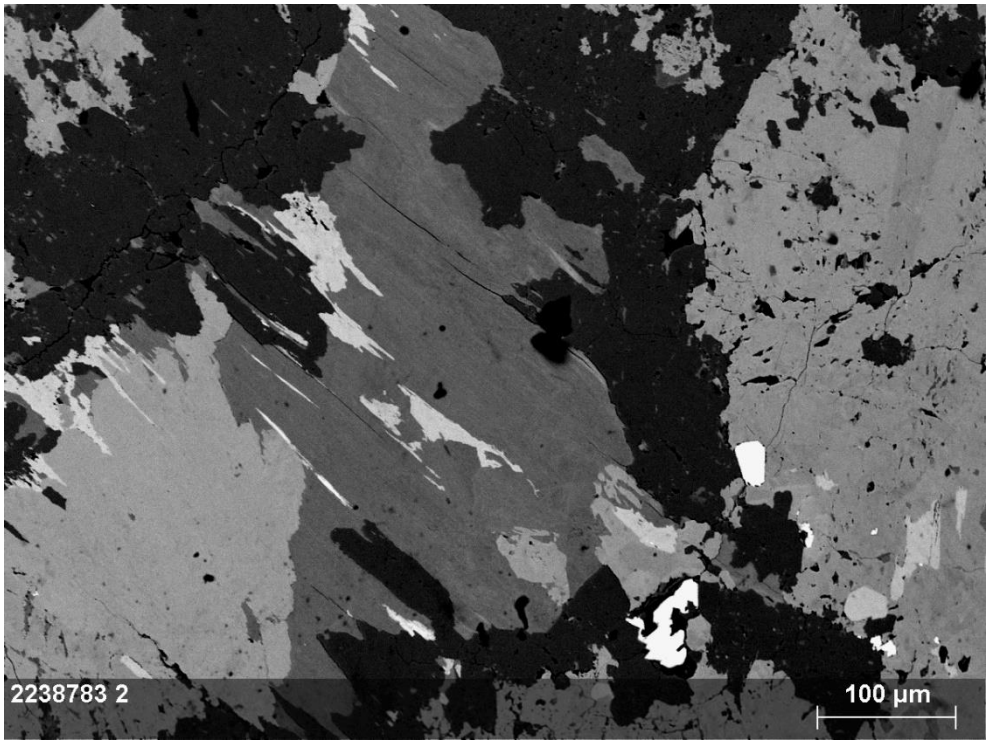

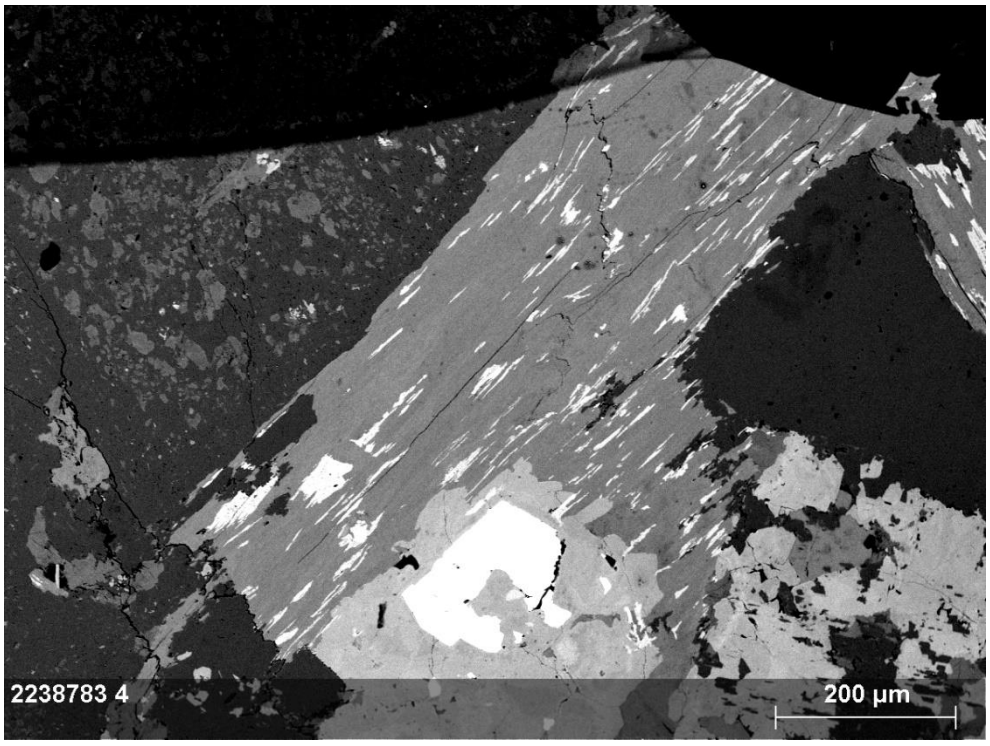
2238783 4
200 µm

2758647

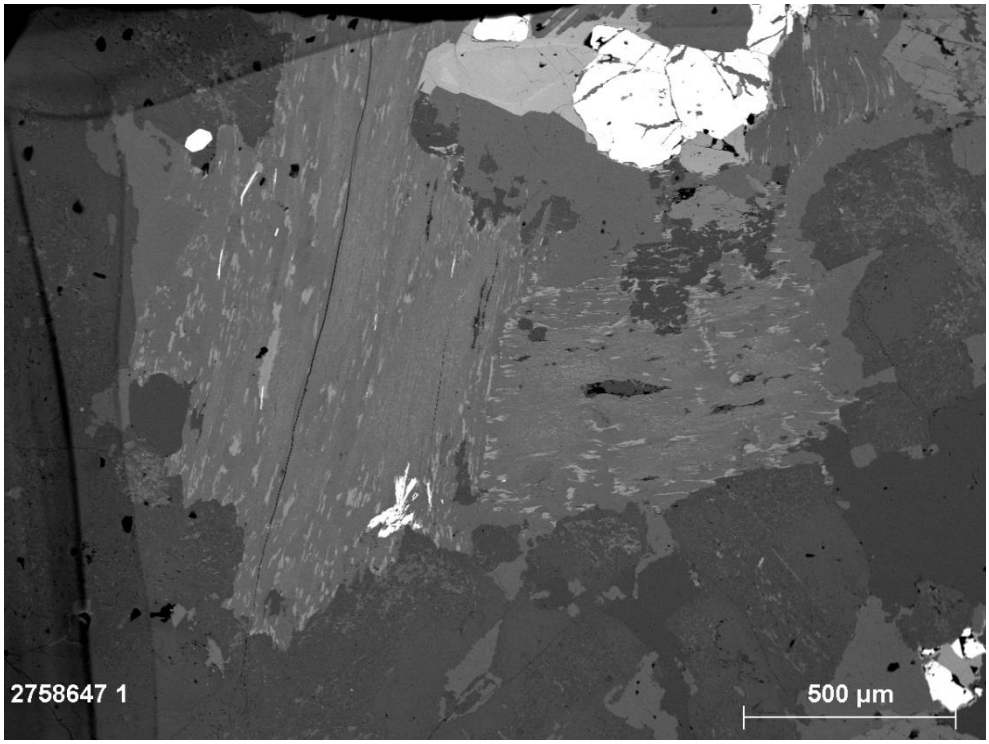

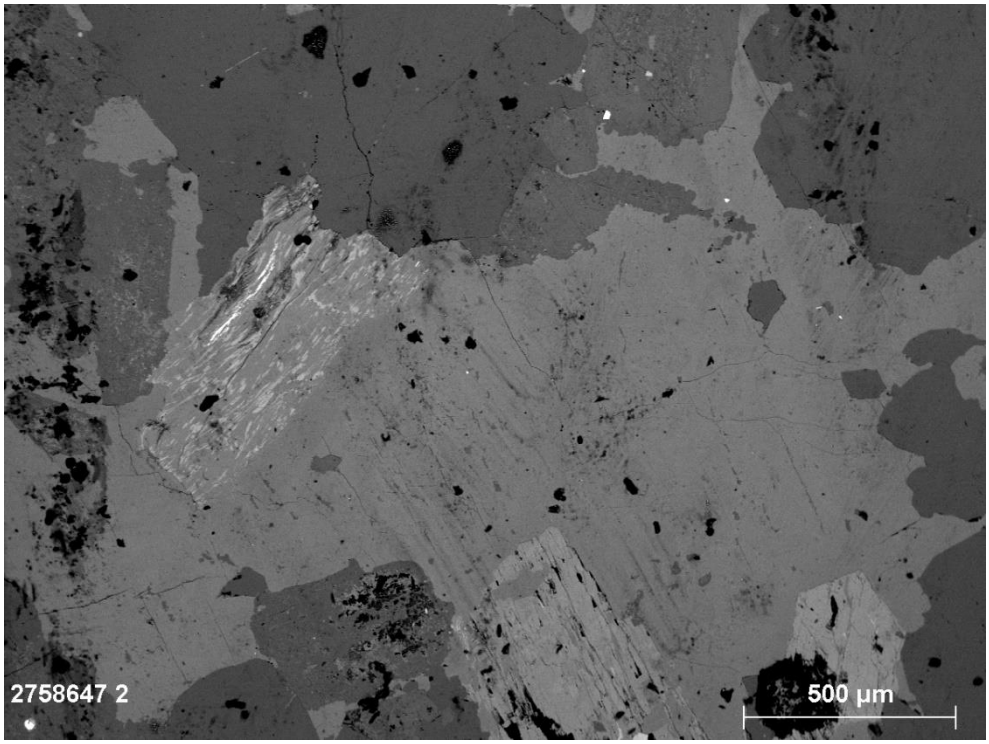

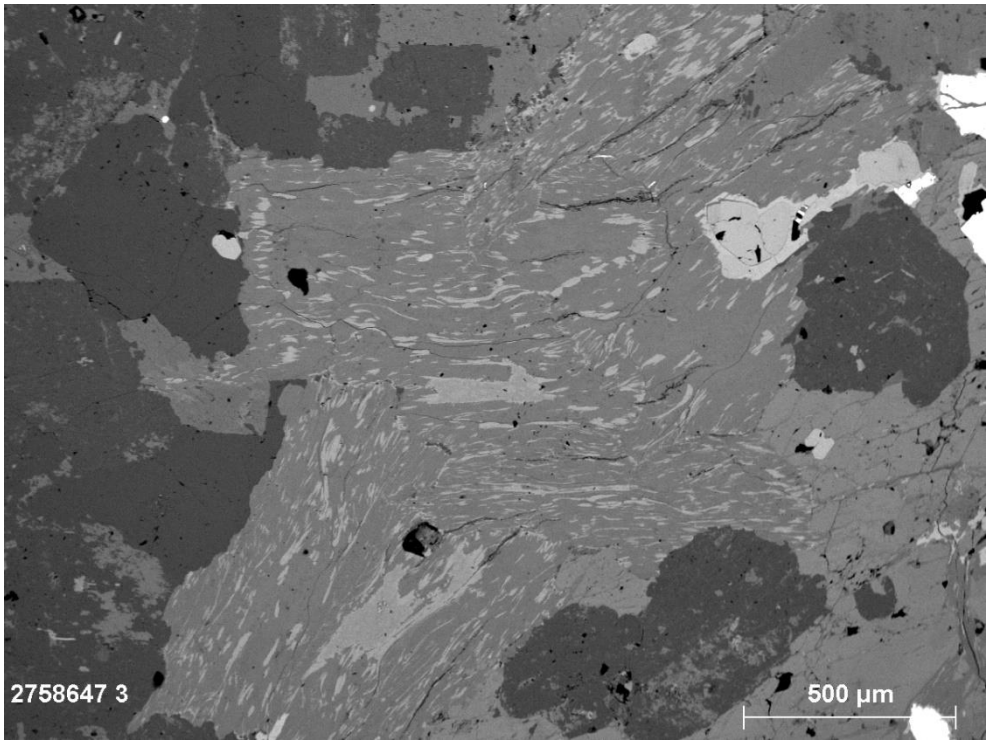
2758647 3
500 µm